1966

Hydrogen absorption and corrosion studies of zone-refined iron

Chang Don Kim

HYDROGEN ABSORPTION AND CORROSION STUDIES OF ZONE-REFINED IRON

A Dissertation

Presented to

the Faculty of the Graduate School

University of Missouri at Rolla

In Partial Fulfillment

of the Requirements for the Degree of

Doctor of Philosophy

---

by

Chang Don Kim

May 1966

ABSTRACT

The lattice constants of zone-refined iron filings and iron whiskers are 2.86623 and 2.86626 Å at 25°C respectively. Their thermal expansion coefficients are both the same, 12.1 x 10^{-6}/°C at temperatures 10 - 65°C.

The influence of hydrogen on the lattice constant of iron was investigated and it was found that hydrogen has no effect (within the limits of errors) on the lattice constant of iron at room temperature regardless of the charging methods. However, at elevated temperatures hydrogen expands the iron lattice due to increased solubility of the gas. The lattice constant of iron in vacuum and in a hydrogen atmosphere was determined at elevated temperatures and found to follow the empirical equations: in vacuum, $a = 2.86522 + 4.28 \times 10^{-5} t$ and in hydrogen (under conditions of the experiments), $a = 2.86554 + 2.45565 \times 10^{-5} t + 6.78828 \times 10^{-8} t^2 - 7.16922 \times 10^{-11} \times t^3 + 2.08773 \times 10^{-14} t^4$, where a is the lattice constant of alpha iron at temperatures between room and 910°C. The lattice constant of gamma iron in the range 910 - 1130°C is the same in vacuum and in hydrogen (under the conditions of the experiments) and follows the equation, $a = 3.5771 + 7.75 \times 10^{-5} t$, where a is the lattice constant at t°C. The thermal expansion coefficients of iron in vacuum are found to

stay at a nearly constant value of 14.8×10^{-6}/°C in the range 200 - 800°C. In a hydrogen atmosphere under the conditions of the experiments it is found to have a maximum (17.3×10^{-6} /°C) at about 450°C. The effect of hydrogen on the lattice constant of iron at elevated temperatures is discussed.

The influence of hydrogen on the density and electrical resistivity of pure iron was investigated and it was found that hydrogen has an effect neither on the density of pure iron nor on its electrical resistivity between 100 and 600°C.

The density of zone-refined iron was determined to be 7.8745 ± 0.0002 g/cm^3 at 25°C and the actual number of atoms per unit cell was calculated to be very close to the ideal number of two. Hence, the structure of zone-refined iron is sound or perfect.

The corrosion pattern of zone-refined iron in some acids (concentrated hydrochloric acid, 2 N sulfuric acid, 1.5 N nitric acid, 25 percent aqueous solution of aqua regia, and concentrated hydrofluoric acid) was studied and the following facts were found: (1) during corrosion of zone-refined iron, three main corrosion patterns develop on the surface and (2) all patterns consist of parallel steps and facets which are arranged in certain crystallographic orientations, and (3) the surface of these steps is mainly close to the

planes (110) and (122), (112) and (123).

An anodic dissolution study of zone-refined iron in hydrochloric and sulfuric acids showed no measurable amount of anodic disintegration.

TABLE OF CONTENTS

LIST OF TABLES

TABLE PAGE

TABLE PAGE

LIST OF FIGURES

FIGURE PAGE

FIGURE PAGE

FIGURE PAGE

I. INTRODUCTION

When a metal is in contact with hydrogen, there are four possible types of interaction:

(1) Hydrogen reacts to form salt-like hydrides with the alkali and alkaline-earth metals. These primary hydrides, which are ionic and generally crystalline, are analogous to the corresponding halides.

(2) The group IVB, VB and VIB metals form covalent hydrides which are gaseous at room-temperature. These compounds are analogous to the hydrocarbons.

(3) Many metals form true solid-solutions with hydrogen, as indicated by the facts that:

a. the hydrogen solubility varies with the square-root of the pressure (Sievert's law) and

b. the solubility increases as the temperature increases.

These metals are known as "endothermic occluders".

(4) Hydrogen forms "pseudo-hydrides" with the metals of IVA and VA together with the rare earths and the actinides. In this case the amount of gas absorbed by the metal decreases as the temperature increases. Hence, this type of metal is referred to as an "exdothermic occluder".

According to the above classification, iron belongs to the third class and takes up only small amounts of hydrogen even at elevated temperature.

Since Pfeil[1] reported, in 1926, that the presence of hydrogen in steel caused a considerable loss of ductility at room temperature under normal tensile condition, a large number of studies have been directed to the influence of hydrogen on the mechanical, physical, chemical and thermodynamic properties of hydrogen-metal system. In general, the introduction of hydrogen into metals is harmful, lowering particularly the ductility of the metals, which is one of the most desirable properties. Steel becomes brittle even in the presence of very small amounts of hydrogen. This phenomeon is known as "hydrogen embrittlement of steel". It is widely recognized, but the underlying causes are not well understood.

Although much effort has been made and many mechanisms have been proposed to explain this phenomenon, there is no agreement as to the mechanism involved. In order to study the mechanism, it is necessary to learn the nature and the properties of hydrogen-metal systems, and to understand the behavior of hydrogen in the metallic phase.

On the other hand, hydrogen is developed when iron is corroded by aqueous solutions or is dissolved in acids. This hydrogen may dissolve in iron and also cause its embrittlement. Therefore, it is very important to have a correct understanding of the mechanism of corrosion of iron, and the role of hydrogen in this process.

Iron and its alloys are most important in the present civilization, as the United States alone produces more than 75 million tons of iron and steel every year and it is estimated that due to the corrosion of these materials, an annual replacement of two percent of the total tonnage in use is required. Therefore, every new observation in the mechanism of corrosion and hydrogen absorption is of importance. Such an observation was made by Welch[2] who reported preferred attack on zone-refined iron surfaces during dissolution in acids. Furthermore he presented evidence of anodic disintegration of the surface of zone-refined iron during dissolution. This phenomenon of anodic disintegration has been reported to occur with other metal anodes, e.g. of Be, Mg, Ga, In, Al, and Zn[3]. Marsh and Schaschl[4] believed that about 50 percent of the observed corrosion rate of steel at pH 2 can be attributed to anodic disintegration.

In view of these beliefs and observations, the present investigation was divided into two main parts as follows:

Part I. The investigation of the influence of hydrogen on the physical properties of high purity iron, involving:

a) lattice constant measurements of pure and hydrogen-loaded iron at room and elevated temperatures,

b) the determination of densities of pure zone-refined iron and of the same supersaturated with hydrogen, and

c) measurements of the electrical resistivity of pure and hydrogen-loaded iron.

Part II. The dissolution studies of high purity iron in acids, involving:

a) observation and study of corrosion patterns developed on zone-refined iron as a result of preferred attack of the iron surface, and

b) surface disintegration studies of zone-refined iron in sulfuric and hydrochloric acids.

II. LITERATURE REVIEW

A. Hydrogen in Iron.

It is known that iron is one of the typical endothermic occluders which takes up hydrogen only in small quantities, even at elevated temperatures, where its solubility is greatest. This is in accordance with its positive temperature coefficient, resulting from a negative heat of absorption.

The results of earlier measurements of the solubility of hydrogen in iron are reviewed by Blake, Jordan and Dumphrey[5].

At room temperature the solubility of hydrogen in iron is very small but it slowly increases with increasing temperature. At 910°C, when transformation of the alpha phase to gamma occus, the solubility jumps and becomes almost twice as large. It then gradually increases still more until the gamma to delta transformation point is reached, where a marked decrease begins. Then, there is another gradual increase between the gamma to delta transformation point and its melting point, where a final big jump occurs again, since the solubility of hydrogen in liquid iron is much greater than in the solid.

In his monograph, Smith[6] derived the equations for the solubilities of hydrogen in alpha and gamma iron, using

the results of Sieverts[7] and Martin[8]:

$$\log S_{\alpha} = - 0.205 - \frac{1\,500}{T} + \tfrac{1}{2}\log p \qquad (1)$$

$$\log S_{\gamma} = + 0.018 - \frac{1\,630}{T} + \tfrac{1}{2}\log p \qquad (2)$$

where, S_{α} and S_{γ} are the solubilities of hydrogen in alpha- and gamma iron respectively, in cubic centimeters per gram of iron. T is the absolute temperature, and p the pressure of hydrogen in atmospheres.

Armbruster[9] recently measured the solubility of hydrogen in iron and steel under various hydrogen pressures ranging from 8.9 to 629 mm Hg at temperatures between 400 and 600°C and confirmed the square-root (Sievert's) law to hold in both iron and steel. She reported that the solubility of hydrogen in ferritic steel does not differ greatly from that in pure iron, whereas in an austenitic steel the solubility is four or five times as great. She also presented an equation for the solubility of hydrogen in pure alpha iron between 400 and 600°C as:

$$\log (S/p^{\frac{1}{2}}) = - \frac{1454}{T} + 1.946 \qquad (3)$$

where S is the solubility of hydrogen in micromoles per 100 grams of metal, p the pressure of hydrogen in mm Hg, and T the absolute temperature.

B. Lattice Constant of Iron.

Lattice constant determinations of iron were made throughout the whole temperature range up to its melting

point. In this range iron exists in two isometric allotropic crystal forms: (1) as alpha and delta iron with a body centered cubic structure, and (2) as gamma iron with a face centered cubic structure. The first form is stable below about 910°C and above 1400°C, where it is called delta iron. Gamma iron is stable at temperatures between these two ranges.

1. Lattice constants of pure iron at room temperature. The first determination of the lattice constant of pure alpha iron was made by Hull[10] in 1917, on electrolytic iron and iron powder (reduced from Fe_2O_3 in hydrogen) employing tungsten radiation. The structure of iron was determined by Davey[11] in 1924: the space group is $O_h^9 - I_{m3m}$ (tungsten-structure) with two iron atoms per unit cell. Since then, its lattice constant has been redetermined almost every year by a good number of authors. The results are summarized in Table I.

2. Lattice constants at high temperatures. Basinski et al.[32] have measured the lattice constants of pure iron (99.969 % Fe) from 20 to 1502°C, using a modified Unicam 19-cm-diameter high temperature camera. The thermocouple of the camera was calibrated against the melting points of antimony and silver, and the alpha-gamma transformation point of iron. At 916°C they found a = 2.9044 Å for alpha iron and a = 3.6468 Å for gamma iron, and at 1389°C, a =

TABLE I

Lattice constant of alpha iron

at room temperature (in Å)

Author	year	a	temp. (°C)	purity
Hull[10]	1917	2.86		electric Fe
Davey[11]	1924	2.861		chem. pure
Blake[12]	1925	2.8661		
Davey[13]	1926	2.865		
Mayer[14]	1929	2.8669		
Van Arkel & Burgers[15]	1931	2.8672		
Bradley & Jay[16]	1932	2.8663		
Esser & Muller[17]	1933	2.8669		
Owen & Yates[18]	1933	2.86675		
Jette & Foote[19]	1933	2.86624	25	(imp. 0.007 % C and 0.004 % each of Si, S and O)
Straumanis & Ievins[20]	1936	2.8664		
Montoro[21]	1937	2.86665		
Hanawalt, Rinn & Frevel[22]	1938	2.863		
Van Bergen[23]	1941	2.86651	20	99.96 % Fe
Lu & Chang[24]	1941	2.8663	20	99.96 % Fe
Troiano & McGuire[25]	1943	2.8665		
Thomas[26]	1948	2.8664_5	20	
Kochanovska[27]	1949	2.8667	25	
Swanson, Fuyat & Ugrinic[28]	1953	2.8664	25	99.9974% Fe
Grønvold et al.[29]	1954	2.8663	20	

(continued)

Author	year	a	temp. (°C)	purity
Owen & Williams[30]	1954	2.8662	18	99.98 % Fe
Sutton & Hume-Rothery[31]	1955	2.8662_1	20	99.969 % Fe
Basinski et al.[32]	1955	2.8662_8	20	99.969 % Fe

TABLE II

Thermal expansivity of iron (99.969 %)[32]

Temp. (°C)	a (Å)	Structure	Temp. (°C)	a (Å)	Structure
20	2.8663	b.c.c.	916	3.6468	f.c.c.
239.6	2.8750		923	3.6471	
350	2.8797		950	3.9496	
449	2.8839		1074	3.6598	
549	2.8882		1184	3.6696	
648	2.8927		1292	3.6792	
721	2.8961		1362	3.6844	
753	2.8976		]380	3.6868	
760	2.8977		1388	3.6869	
770	2.8980		1389	2.9315	b.c.c.
787	2.8989		1394	2.9322	
847	2.9011		1432	2.9347	
902	2.9038		1502	2.9393	
916	2.9044				

(All lattice constants are converted from Kx unit into Å using conversion factor of 1.00202)

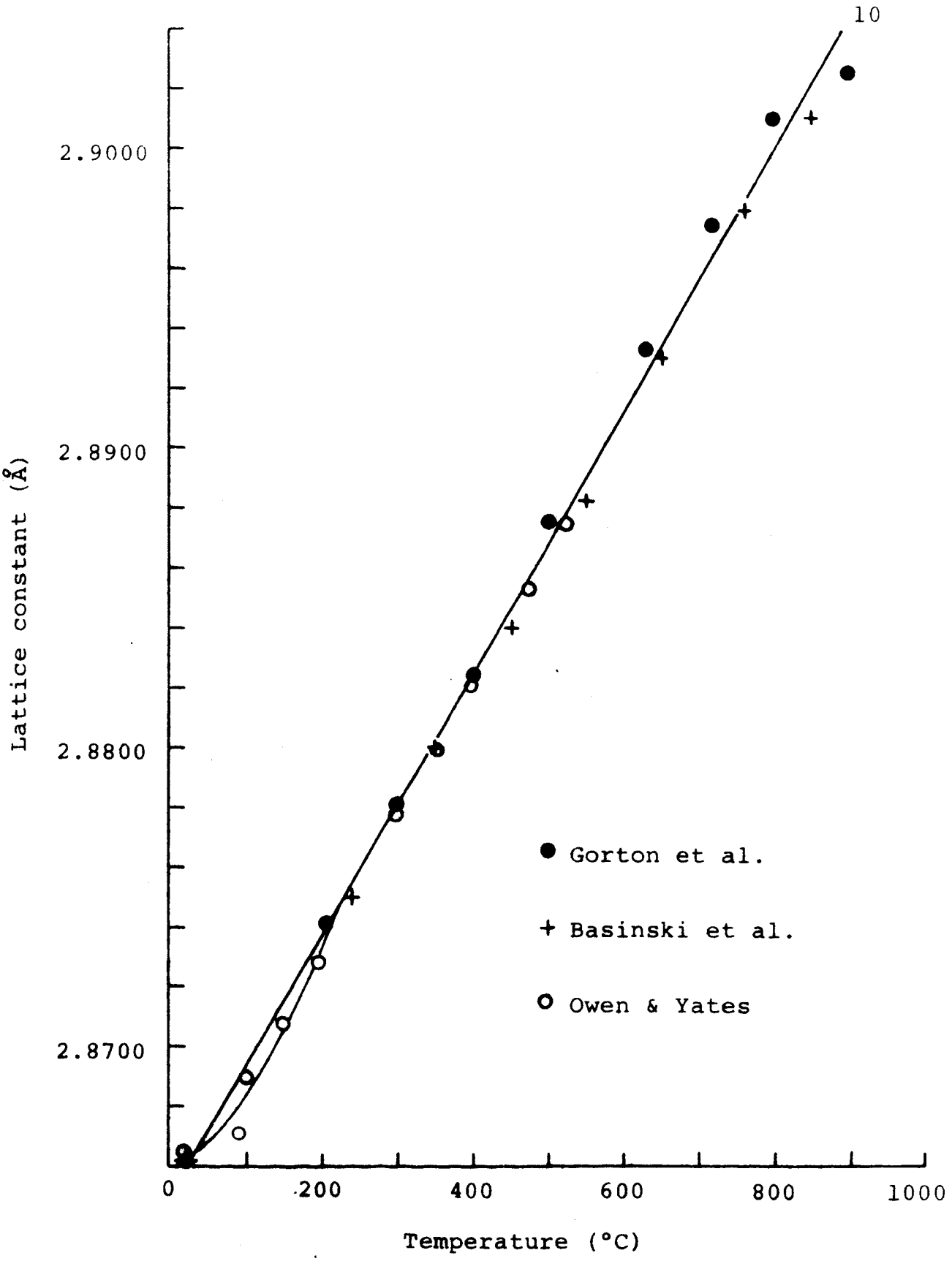

Figure 1. Lattice constant of pure iron at high temperature.

2.9315 Å for delta iron. Their results are tabulated in Table II and plotted in Figure 1.

Esser et al.[17] also measured the lattice constants of gamma iron between 900 and 1120°C and at 900°C they found an $a = 3.652$ Å.

Owen and Yates[18] determined the lattice constants of 99.969 % or 99.989 % pure iron filings, previously annealed at 500°C, from high temperature patterns taken with Co K α radiation at temperatures up to 640°C. In the camera, the filings were cemented to a "thermal plate" whose temperature could be determined with an accuracy of ± 1°C by a thermocouple. Their results are shown in Figure 1 together with the results of Basinski.

Gorton et al.[33] recently measured the thermal expansion of electrolytic iron powder of 99.67 % purity from 22 to 1070°C, using X-ray specimens which were vacuum sealed in thin-walled quartz capillary tubes. Their results are shown in Figure 1.

3. Low temperature measurements. Owen and Williams[30] examined the expansion of 99.9 % iron below room temperature from patterns obtained in a back-reflection camera, and presented an empirical equation for the lattice constants of pure iron between - 194 and 18°C:

$$a_t = 2.8598(1 + 11.9784 \times 10^{-6} t + 15.8447 \times 10^{-9} t^2 - 3.297 \times 10^{-12} t^3) \quad (4)$$

where a_t is the lattice constant of alpha iron in Å at t°K.

The lattice constant of iron at absolute zero was calculated by Heumann[34] as, $a = 2.854_1$ Kx (2.859_9 Å).

4. Lattice constant of hydrogen-containing iron. The influence of hydrogen on the lattice constants of iron was determined by Wever and Pfarr[35], using a 2 mm thick strip of mild steel. They observed an increase in the lattice constant from the initial value of 2.8609 Kx to 2.8614 Kx, i.e., about 0.017 percent, after prolonged charging by cathodically evolved hydrogen in the presence of hydrogen sulfide in 1 % sulfuric acid. The mean hydrogen content of specimens after charging was 30 cm^3/100 g metal, but the authors suggested that the concentration of hydrogen in the surface layer was probably much higher. During 15 days of standing at room temperature at atmospheric pressure, the hydrogen gradually escaped, and the lattice constant of the specimen decreased to a final value of 2.8611 Kx.

Baukloh and Stromburg[36] under similar conditions, charging for 24 hours in 10 % sulfuric acid solution in the presence of As_2O_3, observed a 0.03 percent increase in the lattice constant.

On the other hand, Portevin et al.[37] and more recently Andrews and Ubbelohde[38], and Tetelman et al.[39] found no detectable changes in the lattice constant of iron under the influence of cathodic charging.

Lihl[40] observed similar changes to those reported by Wever and Pfarr, but came to the conclusion that a correction of the values of Wever and Pfarr was indispensable, owing to high stresses arising in the surface layer of the specimens during pickling or electrolytic charging. According to Lihl, the true increase in the lattice constant from measurements of Wever and Pfarr was only 0.007 percent, i.e. below the limit of experimental error.

Rawdon et al.[41] observed a weakening of higher order diffraction lines due to electrolytic iron but found "nothing which would indicate a change in the atomic spacing attributable to hydrogen".

Plusquellec et al.[42] examined back reflection X-ray patterns of a single crystal and of a polycrystalline sample of Armco iron after electrolytic charging with hydrogen. They observed that the introduction of hydrogen caused broadening of all reflections from (110), (112), (222) and (123) planes, but that the (112) reflections were broadened more than the others. They also found that after heating the polycrystalline specimens for five minutes at 300°C the diffraction lines became sharp. Since this temperature was assumed to be below the recovery temperature of the iron, and since the (112) reflection was broadened most, they concluded that (i) hydrogen collected preferentially in the interstitial tetrahedral holes which lie in the (112) planes

and (ii) broadening of the reflections resulted from distortion produced by the presence of hydrogen in the holes.

Tetelman[43] studied the line broadening of the reflections from (110), (200), (112), (222), (400), (422) and (444), and reported that all lines investigated were broadened when hydrogen was electrolytically developed on pure iron at a current density of 0.1 amp./in^2 but X-rays offered no evidence for preferential location of hydrogen. Cathodic charging produced both distortion and anisotropic particle size broadening.

B. The Linear Thermal Expansion Coefficients of Iron.

The earliest measurement of the linear thermal expansion coefficient of iron was made by Hidnert[44]. Using a precision comparator type of apparatus, he measured the thermal expansions of 99.98 % purity iron between -130 and 900°C. Below 300°C measurements were made in air and above 300°C in helium. In spite of the helium, oxidation of iron by residual oxygen at higher temperatures made it difficult to measure the precise value of thermal expansion at these temperatures. Hidnerts' results are tabulated in Table III.

Later, Ebert[45] and Austin and Pierce[46] measured the thermal expansion coefficients, by means of an inter-

ferometer in vauum. Their results are shown in Figure 2. Austin and Pierce found the maximum of the thermal expansion coefficient between 400 and 500°C and the minimum at the Curie temperature (768°C), A_2 of pure iron. They also reported that below 600°C, thermal expansion coefficients of several samples are in reasonable agreement but above this temperature there are significant differences indicating that in this range the expansion of pure iron is sensitive to traces of impurities or depends on the previous treatment of the specimen.

Nix and MacNair[47] used a vacuum interferometric dilatometer for the same purpose. They worked at temperatures between -180° and 680°C and reported $\alpha_{20} = 11.7 \pm 0.2 \times 10^{-6}/°C$. Their low temperature results are in good agreement with those of previous workers'.

Lehr[48], recently measured true coefficients of expansion up to alpha-gamma transformation point with a differential dilatometer, using purified Armco iron heated at 980°C for two hours. He also found the maximum and minimum of the coefficients at about 500 and 760°C (Curie point). His results are given in Table III.

C. Density and Electrical Resistivity of Pure Iron.

The density of pure iron was found to depend to some extent upon its deformation state. A decrease of 0.004 g/cm^3

TABLE III

Mean coefficients of linear thermal expansion of high purity iron (millionths per °C).

Temperature interval (°C)		Hidnert	Lehr
-130	-100	8.7	
-100	-75	9.5	
- 75	-50	10.2	
- 50	-25	10.8	
- 25	0	11.1	
0	20	11.5_5	
20	100	12.3	
100	200	13.3	12.5
200	300	14.5	14.0
300	400	15.5	15.3
400	500	16.2	16.1
500	600	16.1_5	16.5
600	700	15.8	16.4
700	800	15.8	15.8
800	900	15.4	15.7

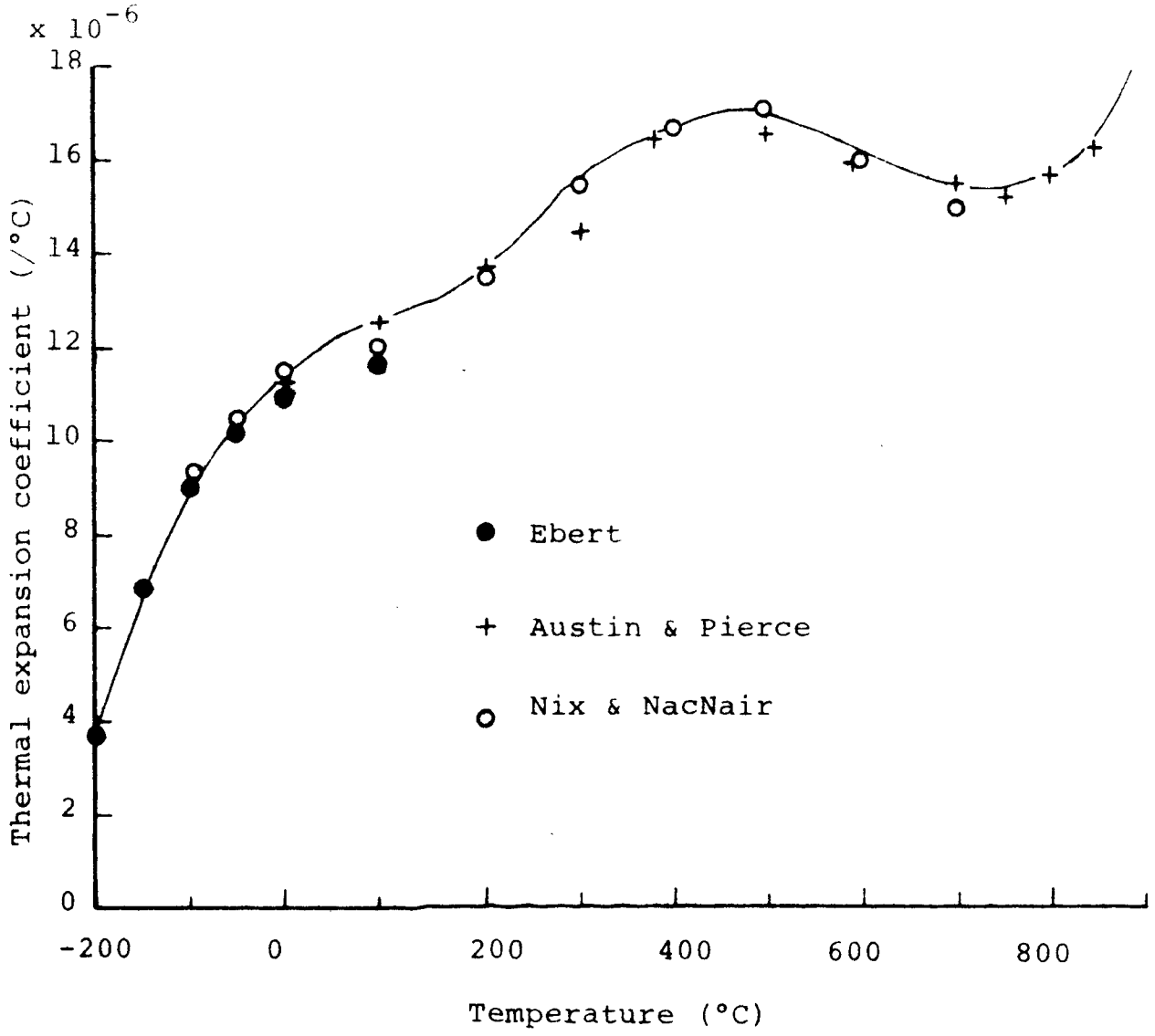

Figure 2. Linear thermal expansion coefficients of pure iron.

has been reported after severe cold working, but this is not always observed[49]. The density of electrolytic iron (0.08 % O_2, 0.007 % P), which was melted in vacuo, rolled down 80 percent and normalized at 1000°C, is 7.90 g/cm^3 at 20°C according to the International Critical Tables[50]. Adcock and Bristow[51] reported that the density of their high purity iron, in annealed condition after being cold worked, was 7.871±0.002 g/cm^3 at 19°C. Cleaves and Hiegel[52] remeasured the density of high purity iron (99.9917∿99.9871 % Fe) at room temperatures varying from 23 to 26°C and corrected it to 20°C by means of the coefficient of expansion. They reported 7.874±0.001 g/cm^3 which seems to be the best value of high purity iron.

The early measurements of the electrical resistivity of pure iron at elevated temperatures were made by Ribbeck[53], Adcock and Bristow[51], Jaeger[54] and Pallister[55]. Their results are tabulated in Table IV. Bäcklund[56] performed conductivity measurements of pure iron at 90 to 300°K and out of his results and Pallisters he derived an equation for the resistivity of pure iron at temperatures up to the Curie point of iron:

$$\rho = -2.4 + 3.65 \times 10^{-2} T + 0.64 \times 10^{-6} T^3 \qquad (5)$$

Data on the influence of hydrogen directly absorbed from the gas are conflicting. Belloc[57], Kleine[58] and Franzini[59] thought resistance increased, whereas Müller[60]

TABLE IV

Electrical resistivity of pure iron.

(in microohm per cm)

Temp.(°C)	Ribbeck	Adcock	Jaeger	Palister
0		8.8		8.86
20		9.88		9.81
50		11.5	10.8	11.54
100	14.6	14.5	13.5	14.53
150		17.8	17.2	17.85
200	22.2	21.5	21.3	21.55
250			25.6	25.65
300	31.0		30.2	30.2
350			35.3	35.3
400			41.0	40.95
450			47.1	47.0
500	53.6		53.7	53.7
550			60.8	60.9
600	68.1		68.6	68.7
650			76.8	76.85
700	85.5		86.6	86.9
750	96.0		96.1	96.0
760			97.4	98.5
800	105.6		101.1	104.9
850			104.0	108.7
900	113.6		106.0	111.6
950	115.3		107.0	113.9
1000				115.8

found no measurable effect up to 920°C.

For cathodic occlusion, Johnson[61] reported increases of resistance of 5.6 to 9.4 percent. However, he worked with so strongly an acidic electrolyte that his iron dissolved during the experiment. Kimura[62] who used a faintly acid electrolyte and determined the hydrogen content by weighing the wire at intervals, found the resistance first to increase and then to diminish—an indication of co-onduction by the occluded hydrogen. Harding and Smith[63] found an increase in resistance up to 5.8 percent during the charge from 2 normal sulfuric acid, where their wire parted. They also found an inverse response of resistance to current density. Grace[64] reported, without detail, an increase of resistance due to cathodic charging. Portevin, Chaudron, and Moreau[65] observed an increase of 1.7 percent, as the result of the occlusion of 100 cm^3/100 g in Armco iron. Van Ooijen and Fast[66] charged cathodically pure iron with hydrogen in sulfuric acid to supersaturation. They found that the hydrogen precipitate at the grainboundaries, building up high gas pressures, and reported no change in the resistance due to interstitial solution of hydrogen.

D. Dissolution of Iron in Acids.

Speller[67] states, in his monograph, that there is evidence of a potential difference between the crystalline

grains in some materials. Such a difference might give rise to a potential difference between grains that could initiate the dissolution of a high purity metal.

Engell[68] studied the current-voltage curves during anodic dissolution in acid and found that the rate of corrosion, as shown by the current density-voltage curve during dissolution of iron, in all cases investigated is independent of the orientation of the crystal surfaces at low current densities. At higher densities, on the other hand, the (111) and (110) surfaces are more readily attacked than the cube faces by a factor of two. The other orientations lie in their properties between these extremes.

Buck and Leidheiser[69] investigated the electrochemical properties of iron single crystal electrodes and found that the minor faces making small angles with the (111) face were etched most rapidly and the (100) face was etched most slowly in the following acids: citric, tartaric, oxalic, nital(5 % HNO_3 alcoholic solution) hydrochloric, sulfuric, phosphoric and acetic. They also found that the local cell action was more prone to occur on the (100) face than on the (321) face. Later they[70] investigated further the corrosion of iron single crystals and reported that the (100) face was cathodic to the (321) face as shown by potential measurements in 0.2 M citric acid in the presence and absence of air. The rates of corrosion

of the polycrystalline starting material from which the single crystals were prepared were several times greater than those of the single crystals. In the presence of 40 - 45 ppm of Sn(II) the rates of corrosion of the single crystals in 0.2 M citric acid at the boiling point were reduced greatly and no significant difference between the (100) and (321) faces was observed. Welch[2] also found preferential attack on sections of zone-refined iron during its issolution in sulfuric and hydrochloric acids.

Marsh and Schaschl[4] suggested that in acidc solutions there may be a change in the anodic reaction. They offer an explanation that below pH 5.5 corrosion proceeds by the removal of chunks of iron rather than by the removal of one atom at a time. Later, they[71] reported that the "chunk effect" (anodic disintegration) is most pronounced in steel under conditions which yield high corrosion rates. In their experiments, for example at pH 2, about 50 percent of the observed corrosion rate could be attributed to the "chunk effect" mechanism.

Welch[2] found anodic disintegration for steels dissolving in both, sulfuric and hydrochloric acids after a short period of exposure to the acid media. He also presented some evidence to postulate the formation of chunks of iron from the high purity metal.

PART I

INFLUENCE OF HYDROGEN ON SOME PHYSICAL PROPERTIES OF PURE IRON

III. EXPERIMENTAL

A. Materials.

1. Iron. High purity zone-refined iron was used for the present work. This iron was produced for the A.I.S.I. by the Battelle Memorial Institute. It was received in the form of a rod 1¼ inches in diameter, 6 inches long, weighing about 1.5 pounds.

The iron was prepared from a special electrolytic iron which was induction melted under vacuum, to achieve partial purification through the removal of gases. It was further refined by passing a molten zone through the bar. Since impurities are more soluble in a molten metal than in a solid metal they tend to collect near one end of the bar. This end may then be chopped off and discarded. The technique employed at Battelle is called "floating zone melting" and is carried out under an atmosphere of ultra-pure hydrogen. The results of an analysis of the original these impurities were reduced some what by the zone refining technique. Heffelfinger et al.(72) have described the methods employed at Battelle for determinning the impurity content of the high purity iron.

For the electrical resistivity measurements, pure iron wire was used, purchased from General Chemical Co., New York, N.Y.. Its minimum assay of iron is 99.85 % and

TABLE V

Analysis of high purity zone-refined iron

Impurity	in ppm	Impurity	in ppm
Al	15	Ni	20
Sb	5	P	9
As	5	Si	10
Bi	0.2	Sn	5
B	5	Ti	1
Cd	5	W	5
Ca	10	V	10
Cr	5	Zn	1
Co	5	Zr	1
Cu	7	H_2	0.2
Pb	1	S	5±3
Mg	5	O_2	1.7
Mn	0.5	C	9±4
Mo	5	N_2	0.2

maximum impurities are 0.02 % P, 0.02 % S, 0.02 % Si and 0.05 % Mn.

2. Iron whiskers. In order to use iron crystals free from defects, iron whiskers were grown by reducing ferrous chloride in a hydrogen stream[73, 74]. Ferrous chloride was prepared by dissolving zone-refined iron in chemically pure hydrochloric acid. Extreme care was paid in preparing and handling the chloride so as not to decrease its purity.

Reduction of ferrous chloride by hydrogen at 731°C was carried out in a hinged-type tube furnace. Approximately 20 grams of ferrous chloride were placed in a porcelain boat. This boat was then pushed into a Vycor tube (40 mm in diameter) and purged with helium at room temperature. The reaction tube was then slowly pushed into the furnace and preheated to 731°C. The salt dehydrated and melted at this temperature under a helium flow rate of 0.5 l/sec (STP). After the salt was molten, hydrogen was introduced into the system, and a flow rate of 1.1 l/sec (STP) was maintained until the end of the run. After two hours of reduction, the boat was cooled to room temperature in a hydrogen stream. Figure 3 shows some of the iron whiskers prepared in this way.

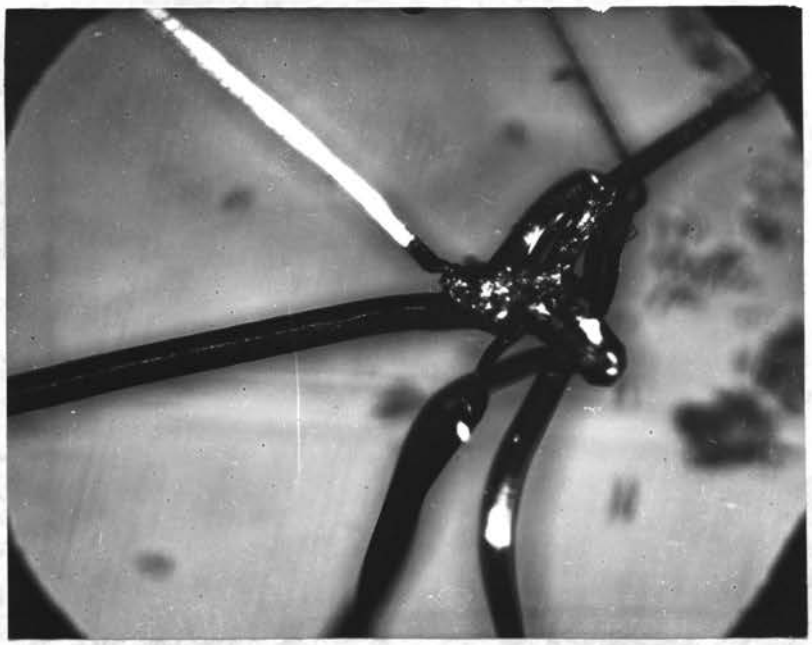

Figure 3. Iron whiskers prepared by reducing ferrous chloride in hydrogen stream at 731°C. x 150.

B. Hydrogen Charging.

As the purpose of hydrogen charging was to check its effect on the lattice constant of iron, powdered metal, convenient for making X-ray diffraction patterns, was used. The iron samples were charged with hydrogen in two ways, which will be described in detail below: (1) by heating the samples in a hydrogen atmosphere, and (2) by charging them cathodically in sulfuric acid.

1. Thermal charging. When iron is heated at high temperature in contact with hydrogen and cooled rapidly to room temperature, the gas can be retained in the metal in greater amounts than its solubility permits at room temperature.

Fresh iron filings were prepared from the inner part of a zone-refined iron chunk by filing away the skin layer and collecting the filings in a clean porcelain boat. This boat was then placed into a Vycor tube (25 mm in inner diameter) which was pushed into a tube furnace (Figure 4). Dry hydrogen was allowed to flow at approximately one atmosphere pressure for 30 minutes to flush out air. Then the furnace was heated to certain temperatures (500°C and 800°C) and held at one of these temperatures for two hours to allow an equilibration between iron and hydrogen. Then the tube was pulled out of the furnace in an opposite

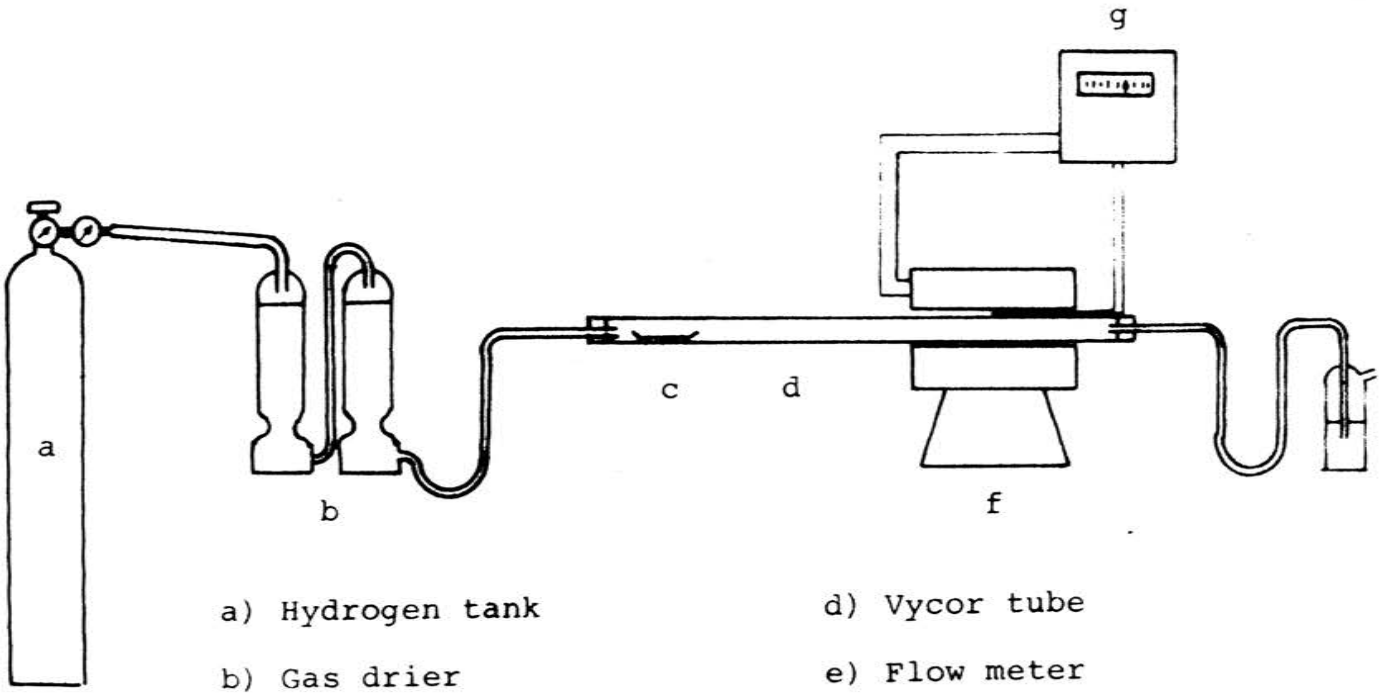

a) Hydrogen tank

b) Gas drier

c) Sample in a porcelain boat

d) Vycor tube

e) Flow meter

f) Tube furnace

g) Temperature controller

Figure 4. Apparatus for thermal charging of iron filings with hydrogen.

direction to gas flow and cooled to room temperature. For faster cooling the hydrogen flow rate was increased upon removal of the sample from the heating zone. Figure 4 shows the arrangement for hydrogen charging.

2. Cathodic charging. First, fresh zone-refined iron filings were placed into a pyrex glass tube (about 50 mm long and 8 mm in diameter), evacuated to less than 10^{-2} mm Hg, and sealed in vacuo. The samples were annealed at 500°C for 30 minutes, to remove the stress which would produce broad diffraction lines on the X-ray patterns and make difficult the precise measurement of lattice constant.

After annealing, the filings were pressed into the hole of a plastic mold electrode, where a platinum wire lead was inserted to make an electric contact with the filings (see Figure 5). The plastic mold electrode was connected to the negative terminal and the platinized platinum electrode to the positive terminal of a battery and both electrodes were placed into a beaker filled with 10 % sulfuric acid. The latter contained small amounts of HgCl for the purpose of promoting hydrogen absorption by poisoning the cathodic surface. A variable resistance and an ammeter were in the circuit. Since the cathode consisted of filings, it was impossible to estimate the cathodic surface area and hence, the current density. However, a current of about 500 mA was applied for one to ten hours. As soon as charging was

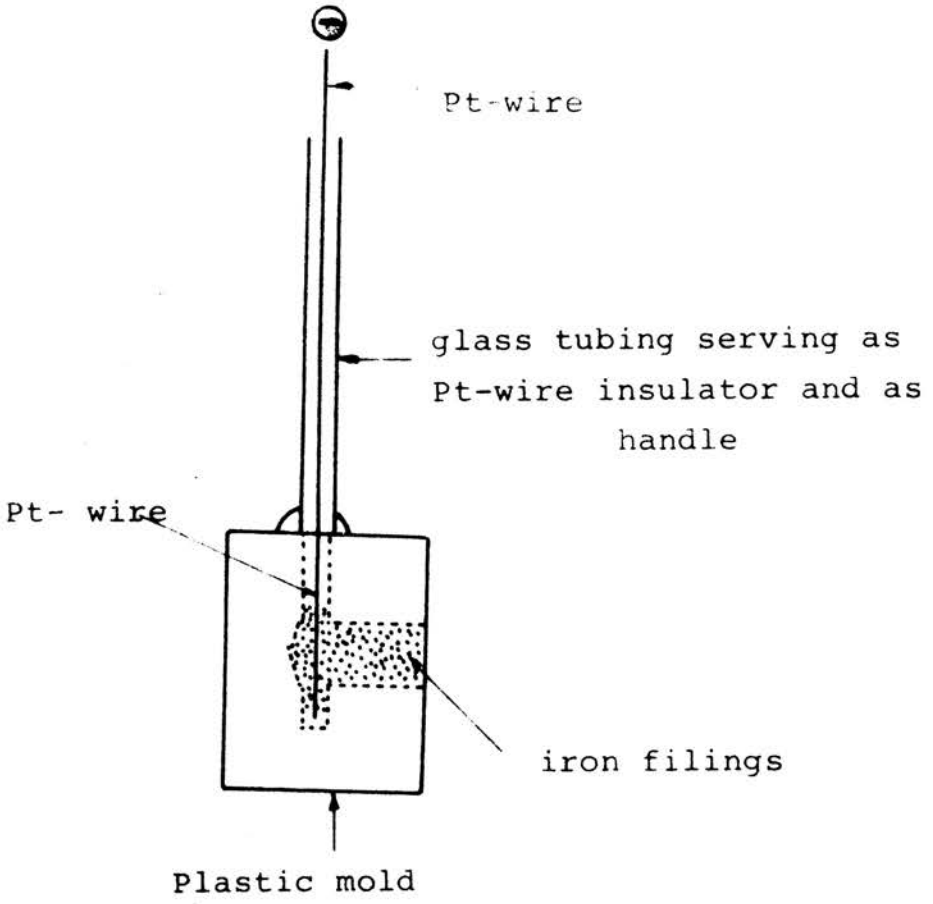

Figure 5. Plastic mold electrode for cathodic hydrogen charging of iron filings

finished, the plastic mold electrode was taken out of the electrolyte, the iron filings removed, washed with distilled water and acetone, and finally dried in a vacuum oven, pre-heated to 85°C. Special attention was paid to carry out the washing and drying operations in a short period of time. As soon as the samples were charged with hydrogen as described, the filings were screen, sample mounts were made for the X-ray determination. However, the largest part of the charged filings was used for hydrogen analysis.

C. Analysis of Hydrogen in Iron.

In any analytical procedure for the determination of gases in metals there are two distinct operations – the extraction of the gas from the metal and the analysis of the extracted gas. Several methods of extracting hydrogen from iron and steel have been developed, such as tin-fusion, graphite-fusion and hot vacuum extraction methods. Among these methods, the tin-fusion method is probably the most rapid one, as it requires about 10 minutes of extraction time. However, this method has the following disadvantages: it requires (1) a bake-out of the freshly charged tin for 2 hours after each day of operation regardless of the number of runs, and (2) frequent checks of blank rates are necessary. The graphite-fusion method has the disadvatage of using high temperatures to fuse the sample.

Martin et al.[75], recently made a thorough investi-

gation to evaluate the above mothods and reported that the hot vacuum extraction method is better than any other for determining hydrogen in steels. Therefore, this method was employed in the present study.

1. Hydrogen analyzer. A Leco Hydrogen Analyzer (No. 534-600), which works on the principle of hot vacuum extraction, was used. A schematic diagram is shown in Figure 6. This analyzer serves two functions, one is extracting the gases from a metallic sample by induction heating under vacuums of less than 10^{-3} mm Hg pressure, and the other is to determine the hydrogen amount by measureing its pressure. In Figure 6, the extracting part is shown on the left hand side and the analyzing part on the right. Total gases extracted are forced into the analyzing part by means of the diffusion pump in the analyzing part and pressure is measured on a McLeod guage. After passing all gases through the catalyzer (hot copper oxide) and anhydron, the hydrogen is removed by oxidyzing it to water in the catalyzer and being absorbed in anhydron, then the pressure is again read on the same guage, and the pressure difference between the two readings represents the hydrogen partial pressure in the total gases extracted.

Since the amount of adsorbed water on the iron surface is, sometimes, competitive with the amount of hydrogen absorbed and in this analyzer water can not be differentiated

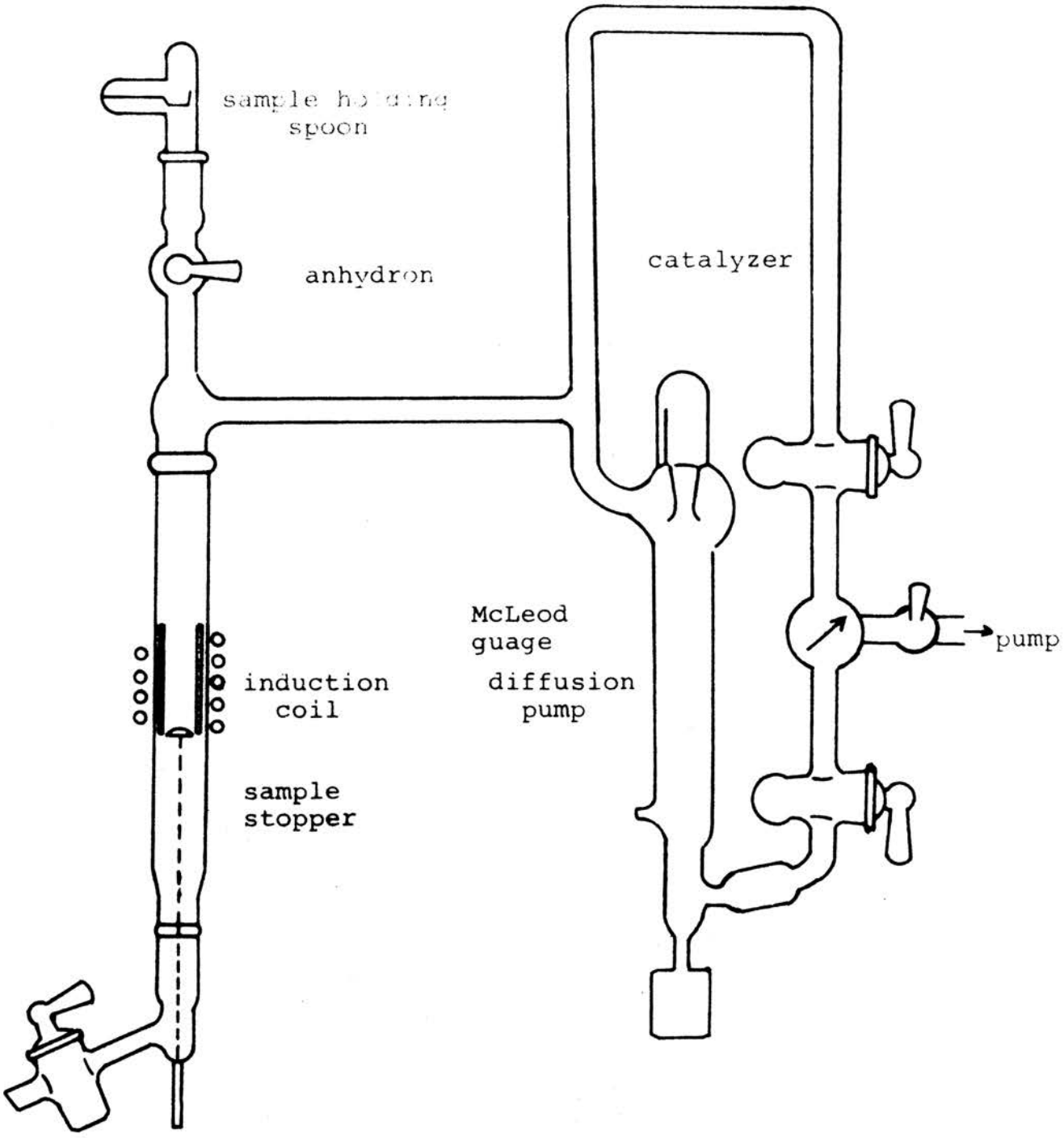

Figure 6. Schematic diagram of the Leco Hydrogen Analyzer

from hydrogen (as described above hydrogen is removed in the form of water and amount of gas removed is assumed as total hydrogen extracted), a slight modification was made to avoid the possibility of error arising from adsorbed water by introducing extra anhydron between the extracting and analyzing compartments as shown in Figure 6.

The volume of the system was calibrated at actual operating conditions by introducing a known amount of dry air into the system and measuring the pressure increase. In this way it was found that the system has a volume of 383 ± 4 cm^3 at operation conditions.

The temperature of the furnace could be adjusted by a manual control on the variable transformer. Temperature measurement of the sample was achieved with an optical pyrometer directed on the crucible within the induction coil. Thus, it was possible to correlate temperature with the dial reading on the variable transformer, assuming that temperature equilibrium had been reached.

2. Temperature and time of extraction. The extraction temperature was kept at approximately 850°C by setting the powerstat at the predetermined division where this temperature was measured by the optical pyrometer. 850°C is high enough to release not only the diffusible hydrogen but also the "residual" hydrogen[76,77].

Since the rate of evolution of hydrogen depends on such factors as sample size, composition, thermal history, and the extent of cold work, the extraction time should be determined by extracting gas from a blank. Preliminary runs for extracting hydrogen from iron filings showed that 15 minute extraction at 850°C is sufficient as there was no further pressure increase (no more gas extraction) beyond this period of time.

3. Determination of hydrogen in iron. As hydrogen was charged into iron filings, its analysis was made with the filings in a stainless crucible (6 mm in diameter and 20 mm in length) which was degassed before each run. The amount of hydrogen was calculated from the equation:

$$\text{Hydrogen in ppm} = \frac{P\ V\ M \times 1000}{R\ T\ W \times 760} \qquad (6)$$

where P is the corrected pressure from the McLeod guage in microns, V the precalibrated volume of the system (383 cm^3), M the molecular mass of hydrogen (2.016), R the gas constant (82.05 cm^3 atm./deg/mole), T the absolute temperature in degree Kelvin, and W the mass of the sample used in grams.

Mostly three to four determinations of each sample were made and the average hydrogen content was calculated.

D. Lattice Constants and Thermal Expansion Coefficients.

1. Preparation of the powder sample for X-ray diffration. For the lattice constant determination of uncharged zone-

refined iron, a fresh sample was prepared from the inner portion of the chunk by filing. The filings were annealed in vacuo at 500°C for 30 minutes in the manner described on page 30, to obtain sharp diffraction lines, which are indispensable for the determination of precise lattice constants. As the hydrogen-charged samples resulted from annealing in hydrogen, no further treatment was necessary. Only those filings which passed 300 mesh were used for production of X-ray diffraction patterns.

A lithium-boron glass fiber of about 0.05 mm in diameter was glued to the tip of the sample holder and so adjusted that the fiber rotated about the axis of the camera. A thin layer of oil was applied to the fiber the powder was uniformly spread over the coating such that the overall diameter did not exceed 0.2 mm. A thin layer of powder is essential to avoid the error due to absorption[78]. All of these operations were performed under a microscope.

2. Preparation of X-ray diffraction pattern and indexing of pattern. The asymmetric film loading method was used, which does not require the knowledge of the camera diameter for Bragg angle measurements. All exposures were made at constant temperatures by setting the whole camera in a thermostat capable of maintaining the temperature between 5 and 65°C with an accuracy of ± 0.05°C.

One of the requirements for precise lattice constant determination is the used of high back reflection lines (>75° [79]) sharp enough to be read with sufficient accuracy. To get the high back reflection lines, a proper X-radiation has to be used. The selection of this radiation was made by a graphical method, without experimenting with different targets[80], and Co Kα radiation was found to be appropriate. A powder diffraction pattern of iron is shown in Figure 7.

The alpha iron diffraction pattern was also indexed graphically[80], using a reciprocal lattice method. The indexing details and theory are given in the literature[80]. This method has a great advantage of finding the proper radiation by simply applying the different radii of the limiting circles for the respective radiations.

3. Lattice constants. Each set of some front and back reflection lines were measured with a comparator to a precision of 0.005 mm. From these measurements the effective film circumference, the conversion factor (from mm to degree) and the highest back reflection Bragg angle were calculated. The lattice constant of iron was then obtained from the equation which combines the Bragg and the interplanar spacing equations:

$$a = \lambda \sqrt{h^2 + k^2 + l^2} \; / \; 2 \sin \theta \qquad (7)$$

where λ is the wave length of the radiation used, θ the

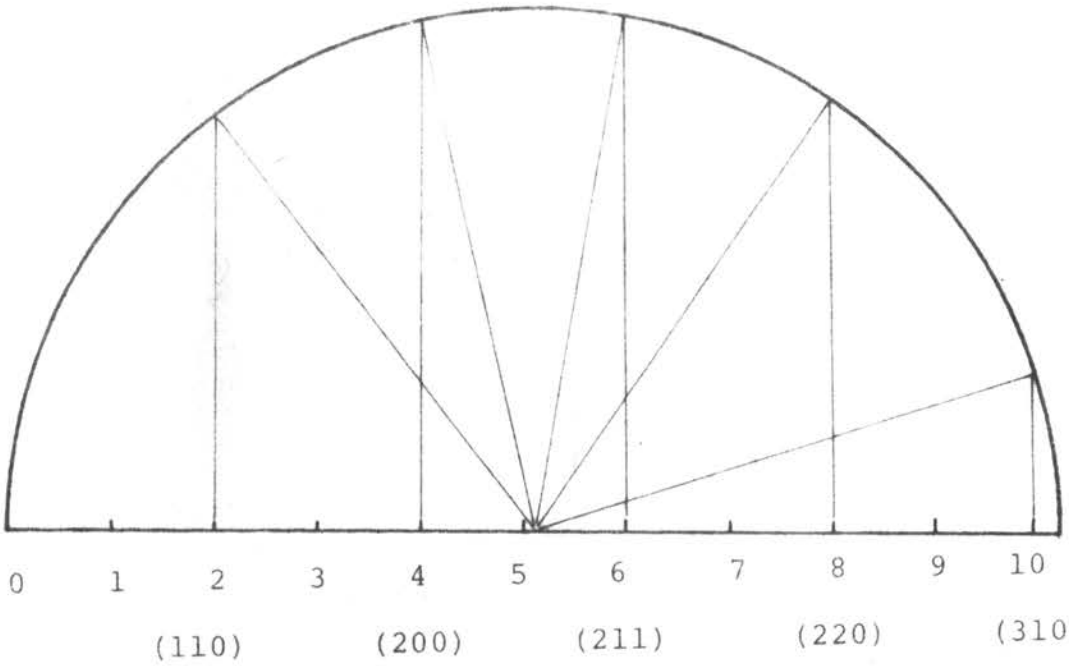

Figure 7. Graphical indexing of an alpha-iron asymmetric pattern shown below, obtained with Co-radiation.

reflection (Bragg) angle and h, k, l the Miller indices of the reflecting plane.

The wave lengths of the X-rays are altered when they pass from one medium to another. This refraction phenomenon causes a deviation from Bragg's law which leads to slightly smaller lattice constant values. Therefore, all precision lattice constants determined should be corrected for refraction. This correction was made using the equation:

$$a_{corr} = a + \frac{5.40\rho\ a^3 x\ 10^{-6}}{h^2 + k^2 + l^2} \qquad (8)$$

where a_{corr} is the constant, a corrected for refraction, and ρ is the density of the substance.

4. Coefficient of thermal expansion. Using the least squares adjustment method, the thermal expansion coefficients, α were determined from the average lattice constants obtained at different emperatures by the following equation:

$$\alpha = (\frac{da}{dt})_t / a_t \qquad (9)$$

where $(\frac{da}{dt})_t$ is the slope at t°C and a_t the lattice constant at t°C. The details of the least squares adjustment procedure are given in the literature[81].

In order to evaluate the precision of the lattice constant determination error calculations were necessary. The values of the lattice constants measured at different temperatures were reduced to 25°C, using the following

equation:

$$a_{25} = a_t[1 + \alpha(25 - t)] \qquad (10)$$

where α is the linear thermal expansion coefficient and a_t is the lattice constant at t°C. From the the deviations of these reduced constants from averages, the probable error was calculated at a 50 percent confidence limit, using the equation:

$$S' = 0.675\sqrt{\Sigma(dX)^2/(n - 1)} \qquad (11)$$

where S' is the probable error, $\Sigma(dX)^2$ the sum of the squares of the deviations, and n the number of measurements or degrees of freedom.

5. results.

a. Zone-refined iron. As shown in the previous section, Co $K\alpha_1$ radiation and the (310) line were used for the determination of the precise lattice constant of zone-refined iron. The $K\alpha_2$ line of (310) was disregarded, since the measurements were accompanied with a higher error due to the fuzziness of this line. Further experimental data are given in the Appendix. The average of two lattice constant determinations at a certain temperature is plotted against the temperature in Figure 8. The values of the lattice constants obtained at various temperatures are given in Table VI. Using the least square adjustment, the coefficient of thermal expansion was determined to be 12.1×10^{-6}

TABLE VI

Lattice constant of zone-refined iron with the refraction correction of 0.00010 Å added, Co $K\alpha_1$ radiation, (310) line.

Film No.	temp. (°C)	a_t (Å)	average a_t (Å)	a_{25} (Å)	
2536	10.7	2.86574			
2537	10.7	2.86576	2.86575	2.86624	
2532	20.0	2.86607			
2533	20.0	2.86605	2.86606	2.86622	
2610	30.0	2.86641			
2611	30.0	2.86645	2.86643	2.86626	
2612	40.0	2.86674			
2613	40.0	2.86675	2.86675	2.86623	
2614	50.0	2.86713			
2615	50.0	2.86701	2.86707	2.86620	
2534	59.6	2.86754			
2535	59.6	2.86735	2.86745	2.86625	
			average	2.86623	0.00002 Å

Thermal expansion = 3.46×10^{-5} Å/°C.

Thermal expansion coefficient = 12.1×10^{-6}/°C

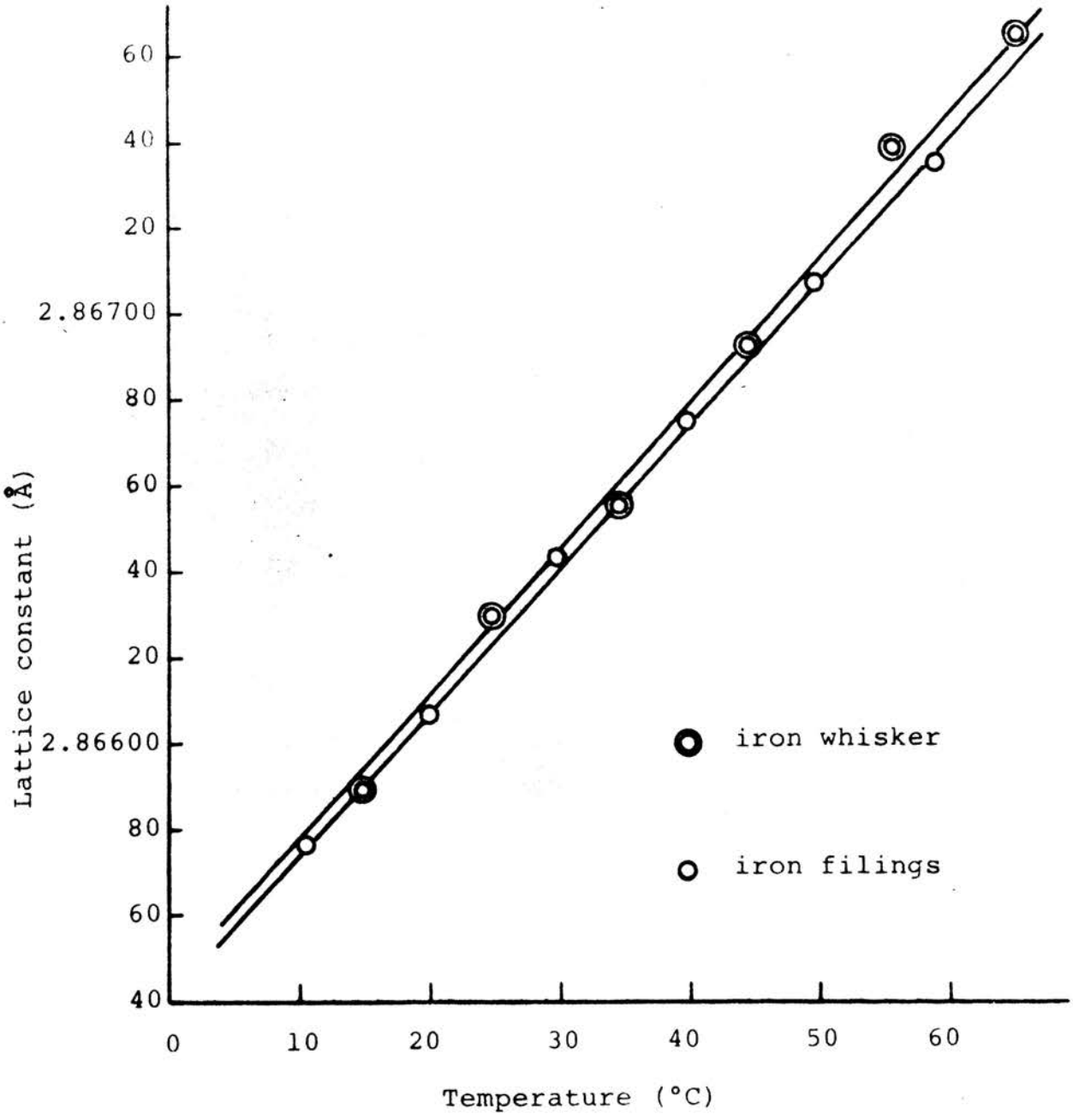

Figure 8. Lattice constant of zone-refined iron filings and whisker.

per degree at the temperature range between 10 and 60°C.

All the values obtained at various temperatures were reduced to 25°C and the lattice constant of zone-refined iron was found to be 2.86623 Å (refraction correction included). The probable error was 0.00002 Å.

b. Iron whisker. The rotating-crystal method was employed to measure the lattice constant of a well-shaped iron whisker of about 8 mm in length and 0.1 mm in diameter, mounted to the X-ray goniometer head. The direction of the whisker was so adjusted that the spot of the highest Bragg angle (310) reflection appeared on the equatorial line.

The same techique as used for the powder sample was also used for the determinations of the precise lattice constant of the iron whisker. Two or three pictures were taken at each temperature. The results are compiled in Table VII. The average values of the lattice constants are plotted in Figure 8. a_o at 25°C is 2.86626 Å, which is slightly higher than that determined for zone-refined iron powder. However, the coefficient of thermal expansion is the same in both cases (12.1×10^{-6} per degree between 15 and 65°C).

c. Lattice constants of iron charged with hydrogen.

TABLE VII

Lattice constant of iron whisker with the refraction correction of 0.00010 Å added, Co $K\alpha_1$ radiation, (310) line.

Film No.	Temp. (°C)	a_t (Å)	average a_t (Å)	a_{25} (Å)
2712	15.0	2.86585		
2713	15.0	2.86593	2.86589	2.86624
2713	24.7	2.86629		
2715	24.7	2.86632		
2716	24.7	2.86625	2.86629	2.86628
2717	34.8	2.86657		
2718	34.8	2.86657		
2719	34.8	2.86652	2.86655	2.86621
2720	45.2	2.86692		
2721	45.2	2.86688	2.86690	2.86620
2728	56.0	2.86740		
2729	56.0	2.86735		
2730	56.0	2.86741	2.86739	2.86632
2731	64.0	2.86763		
2732	64.0	2.86766	2.86765	2.86630

ave. a_{25} = 2.86626 ± 0.00004 Å

TABLE VIII

Lattice constants of zone-refined iron in comparison with those of hydrogen charged iron (in Å).

Sample	a_{25}	H_2(ppm)	Remarks
Pure zone-refined Fe	2.86623		
T-1	2.86627	10.1	at 500°C, p_{H_2} = 1 atm.
	(2.86631) 2.86623		
T-2	2.86626	10.5	at 700°C, p_{H_2} = 1 atm.
	(2.86626) 2.86625		
T-3	2.86621	10.1	at 800°C, p_{H_2} = 1 atm.
	(2.86623) 2.86618		
C-1	2.86625	13.4	10 % H_2SO_4, 2 hours
	(2.86627) 2.86623		
C-2	2.86621	17.7	10 % H_2SO_4 with HgCl,
	(2.86621) 2.86620		2 hours

Zone-refined iron filings were charged in two ways as already described. Upon completion of charging, the filings were screened through a 300 mesh sieve and for the X-ray samples, portions were used which passed the sieve. Hydrogen analyses were made of each of the batches. The results reported in Table VIII are the average values of each three determinations.

Sample T-1, T-2 and T-3 were charged by heating them in hydrogen at 500, 700 and 800°c, respectively. Nevertheless the amounts of hydrogen retained in each of the samples were all of the same magnitude (about 10 ppm) as showin in Table VIII.

Sample C-1 was cathodically charged in a 10 percent sulfuric acid solution for 2 hours and Sample C-2 was treated in the same way but in a solution containing a small amount of HgCl.

The precise lattice constant determinations were made for each sample at 25°C and the results are summarized in Table VIII. As shown in this table there is no measurable difference in the lattice constant of iron upon uptaking of hydrogen, regardless its manner of charging.

E. High Temperature Study

Austin and Pierce[46] suggested that the thermal expan-

sion of pure iron is sensitive to traces of impurities at high temperatures. Macroscopic measurements (mostly interferometric) of various investigators[44-48] showed that maxima and minima in expansivities appeared. However, they were not observed by Basinski[32] who measured the thermal expansion of pure iron by X-rays. Therefore, the intention of this investigation was to check whether or not hydrogen has an effect on the thermal expansivity of iron and whether X-ray measurements reveal the maxima and minima in its thermal expansivity curves.

Using a high temperature X-ray camera, the thermal expansivities of zone-refined iron filings and of iron whiskers were determined up to 1200°C.

1. High temperature X-ray camera. The high temperature camera used in this investigation was originally made by Dr. Seemann in Germany. This camera, which has platinum heating coils closely surrounding the sample, can be operated up to 1350°c, in either vacuum or controlled atmosphere. Some improvements of film loading and temperature control were made to insure more precise lattice constant determinations.

In order to maintain the sample temperature constant, the coils were fed a current of constant strength, predetermined for each of the temperatures used. The control was

achieved by passing a low current (about 0.1 amp.) through a "Capacitrol" superimposing a current of constant strength. In this way, the sample temperature could be kept constant within ± 2°C.

Although the camera was originally designed for symmetric film loading, the movable cassette was so changed that the film could be loaded asymmetrically, Five different exposures could be obtained on one film, shifting its position for each exposure by only 5 mm parallel to the cylinder axis. The details of the camera and its switchboard are shown in Figure 9.

2. Temperature calibration. The platinum platinum-rhodium thermocouple, whose tip is located close to the end of the powder sample inside the high temperature camera, was connected to the electronic controller to provide visual control of the temperature inside the camera. The thermal gradient inside was unavoidable due to the uneven heat produced by the coils. Because of this, the thermocouple did not necessarily measure the true temperature of the sample. However, it surely could be assumed that the exposed to the X-ray beam was uniform.

The calibration of the high temperature camera consists in establishing the relationship between the true temperature as shown by the controller. The true temperature of the

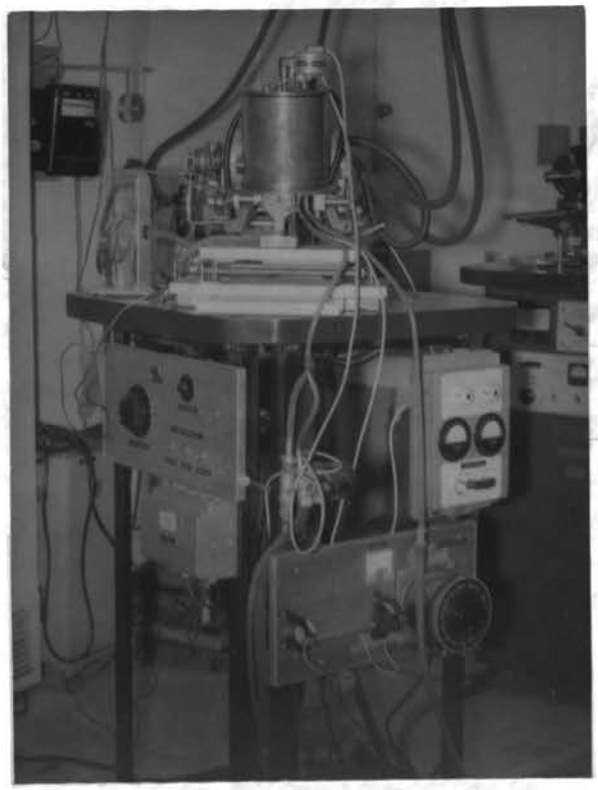

Figure 9. High temperature camera and temperature controlling switch board.

sample was established from the melting points of pure metals as follows: In-156.5, Bi-271, Zn-419, Sb-630.5, Ag-960.5 and Au-1063°C. The A_3 point of pure iron, 910°C, was also used for this purpose. The melting point determinations were made by preparing several diffraction patterns above and below the melting point of the metal in question. By marking the temperatures on the indicating instrument, where the metal passed from the crystalline to the liquid state as the latter gives no sharp diffraction lines, the true temperature of the sample was found. Most of the diffraction photographs were taken in 5° intervals. The results are shown in Table IX and plotted in Figure 10.

All the metals used for this purpose were 99.999 % pure and extreme care was paid to prevent contamination of the individual powder samples. Melting point determinations were always made with the powders enclosed in a small evacuated quartz tube of 0.3 mm diameter, with air inside the camera. When the atmosphere inside the camera is changed, the temperature gradients inside are also subjected to change because of the different heat transfer medium, and consequently another temperature calibration for this atmosphere should be furnished to measure the true sample temperature. For example, it was found that at about 600°C upon changing the atmosphere from air to hydrogen, the calibration made for air inside the camera showed about a 65° higher temperature

TABLE IX

Determination of the true sample temperature inside the high temperature camera (air inside camera)

Metal	Melting point (°C)	Indication instrument reading (°C)
In	156.5	70 ± 2.5
Bi	271	180 ± 2.5
Zn	419	338 ± 2.5
Sb	630.5	580 ± 3.0
$\alpha Fe \rightleftarrows \gamma Fe$	910	885 ± 5.0
Ag	960.5	933 ± 2.0
Au	1063	1040 ± 2.5

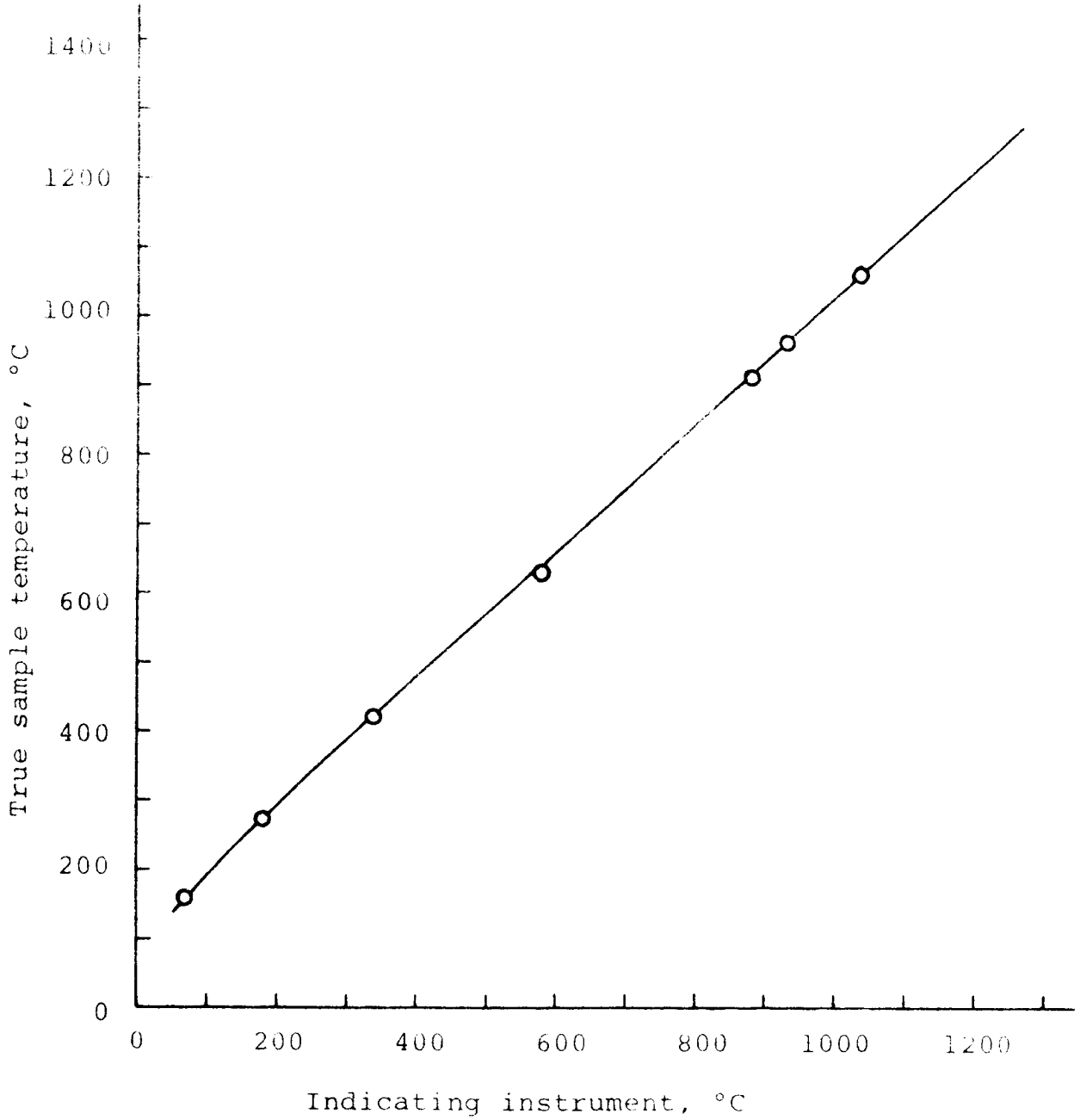

Figure 10. Temperature calibration inside the high temperature camera filled with air.

than the true sample temperature. Therefore, in this investigation all measurements were made under the same enviromental conditions as for the calibration, i.e. the air atmosphere was used.

3. Thermal expansion of alpha iron in vacuum. Diffraction patterns were made at various temperatures of the powder sample (zone-refined iron) enclosed in a vacuum-sealed thin-walled quartz capillary. The tiny iron whiskers were placed in quartz capillary, sealed under vacuum, and exposed to X-rays at various temperatures. The thermal expansivity of the iron whiskers was obtained from measurements of the lattice constant. The whisker diffraction lines were somewhat spotty, nevertheless, the lines could be measured with a sufficient accuracy.

The lattice constants of iron powder and whiskers were calculated from the highest indices (310) on patterns obtained with Co Kα radiation. They were then corrected for refraction and related to the corrected temperature of the sample as given in Table X. The relationship is primarily linear, except at 156°C (see Figure 11). The present results are in a good agreement with the previous study[32]. Using the least square adjustment method for the straight line portion of the curve (above 200°C), an empirical equation was derived to give the lattice constant, a_t of pure

TABLE X

Lattice constants (in Å) of zone-refined iron powders and iron whiskers in vacuum (corrected for refraction).

Temp. (°C)	a_p of powders	$a_{cal}^{(*)}$ calculated	$a_p - a_{cal}$	a_w of whiskers	$a_p - a_w$
22	2.86612	2.86616	-0.00004		
23	2.86632	2.86620	0.00012	2.86617	0.00015
156	2.87033	2.87190	-0.00157	2.87049	-0.00016
270	2.87653	2.87678	-0.00025	2.87546	0.00007
330	2.87876	2.87934	-0.00058	2.87924	-0.00048
400	2.88222	2.88234	-0.00012	2.88238	-0.00016
470	2.88531	2.88534	-0.00003		
472		2.88542		2.88572	
540	2.88874	2.88833	0.00041	2.88797	0.00077
610	2.89122	2.89133	-0.00011	2.89147	-0.00025
685		2.89454		2.89399	
690	2.89484	2.89475	0.00009		
750		2.89732		2.89753	
758	2.89776	2.89766	0.00010		
800		2.89946		2.89919	
830	2.90047	2.90072	-0.00025		
850		2.90160		2.90126	

(*) calculated from equation (12).

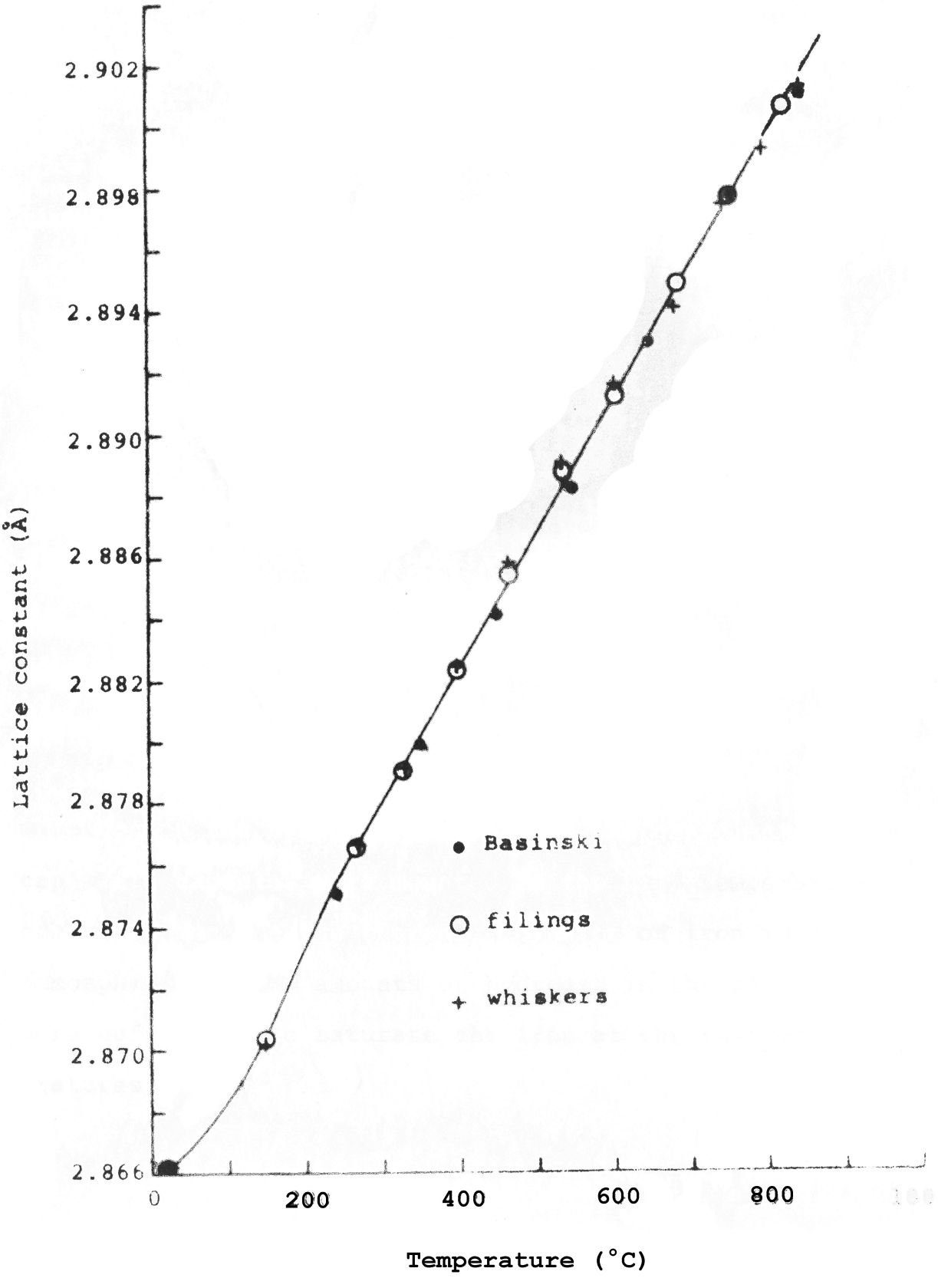

Figure 11. Lattice constant versus temperature of zone-refined iron and iron whiskers in vacuum.

iron at the temperatures between 200 and 910° in vacuum:

$$a_t = 2.86522 + 4.28 \times 10^{-5} t \qquad (12)$$

The coefficients of true linear thermal expansion of pure iron in vacuum were calculated from the following equation:

$$\alpha = \left(\frac{da}{dt}\right)_t / a_t \qquad (9)$$

The results are listed in Table XI.

4. Thermal expansion of alpha iron in hydrogen. Iron filings and tiny whiskers were enclosed in quartz capillaries which were evacuated and washed several times with hydrogen at approximately 750 mm Hg pressure at room temperature. Considering the hydrogen consumption due to its absorption into iron at high temperatures, the capillary capsules were made longer (about 40 mm in length and 0.3 mm in diameter) in order to minimize the effect of its consumption on the hydrogen pressure in the capsules. These capillary capsules were mounted in the high temperature camera to measure the thermal expansion of iron in a hydrogen atmosphere, as the amounts of hydrogen in the capillaries were sufficient to saturate the iron at the respective temperatures.

Due to the spottiness of the diffraction patterns of iron whiskers, the results obtained with whiskers were less

TABLE XI

Thermal expansion coefficient, α of iron in vacuum.

Temp. (°C)	200	300	400	500	600	700	800
$\alpha \times 10^6$ (/°C)	14.89	14.87	14.85	14.83	14.81	14.78	14.76

TABLE XII

Lattice constants (in Å) of zone-refined iron powders and iron whiskers in hydrogen (corrected for refraction).

Temp. (°C)	a_p of powders	a_{cal} (*) calculated	$a_p - a_{cal}$	a_w of whiskers	$a_p - a_w$
156	2.86981	2.87052	-0.00071	2.87088	-0.00007
270	2.87610	2.87601	0.00009	2.87702	-0.00092
350	2.88024	2.87969	0.00055	2.88087	-0.00063
450	2.88475	2.88466	0.00009	2.88561	-0.00086
550	2.89026	2.88956	0.00070	2.89041	-0.00015
650	2.89467	2.89422	0.00045	2.89428	0.00039
750	2.89849	2.89850	-0.00001	2.89809	0.00040
850	2.90232	2.890233	-0.00001	2.90218	0.00014

(*) calculated from equation (13).

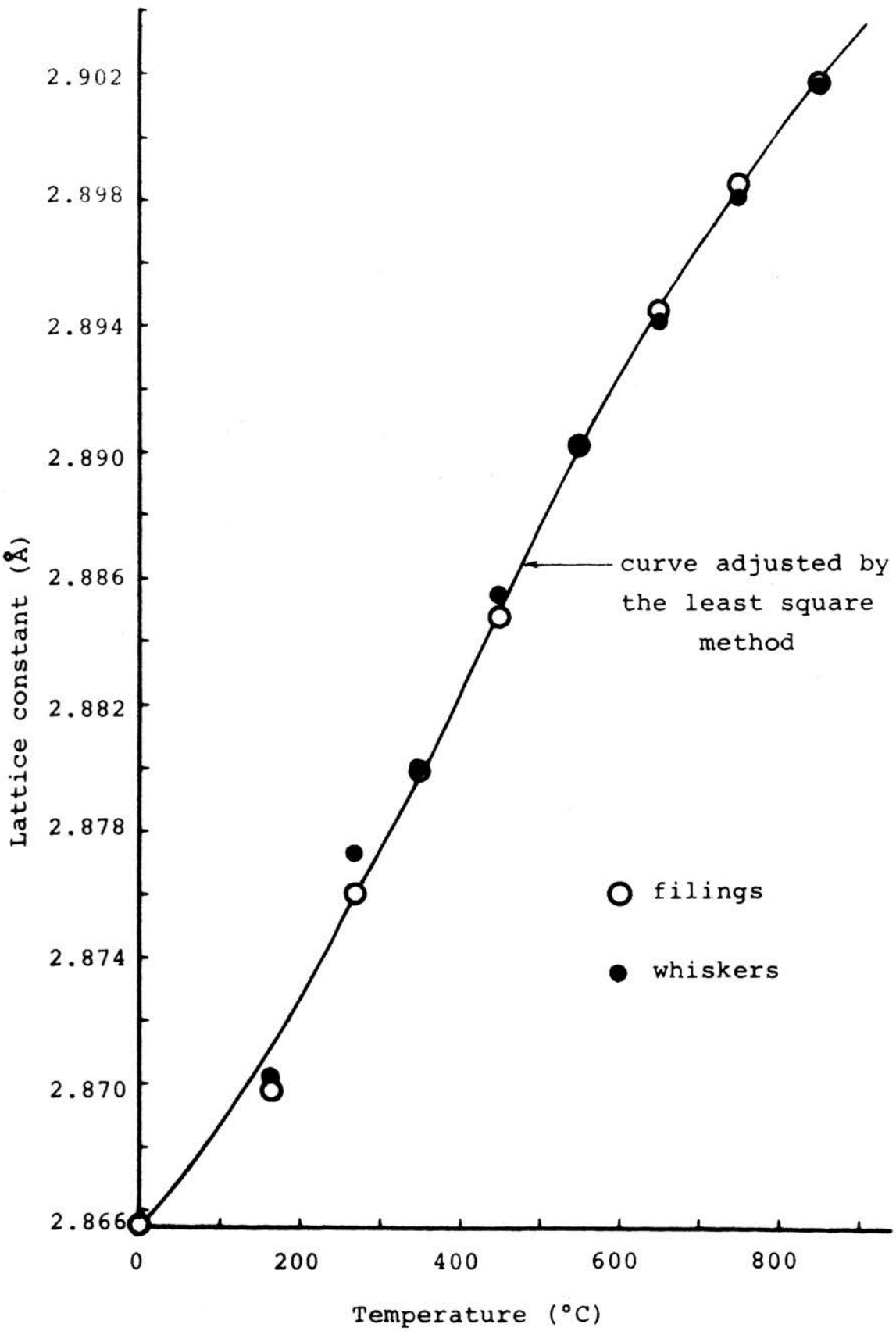

Figure 12. Lattice constant versus temperature of iron in hydrogen atmosphere.

reliable than those of pure iron filings. The results obtained with both samples are shown in Table XII. The lattice constants, when plotted against temperature (Figure 12), show a curved line instead of the straight line obtained in vacuum. The curve was found to follow a fourth order equation (between room temperature and about 900°C):

$$a_t = 2.86554 + 2.45565 \times 10^{-5} t + 6.78828 \times 10^{-8} t^2 - 7.16922 \times 10^{-11} t^3 + 2.08773 \times 10^{-14} t^4 \quad (13)$$

where a_t is the lattice constant of iron in Å in a hydrogen atmosphere at a temperature of t°C.

The coefficients of thermal expansion of iron in hydrogen were determined analytically by finding the slope of the curve at t°C and deviding them by the respective lattice constants. The results are given in Table XIII.

5. Thermal expansion of gamma iron. Zone-refined iron filings were first annealed at 500°C for an hour in vacuum. The filings were enclosed in a quartz capillary having a diameter of 0.3 mm and sealed under vacuum. For the same measurement in hydrogen the filings were again placed in a capillary, flushed several times with hydrogen and then sealed under a hydrogen pressure of approximately 750 mm Hg at room temperature.

Asymmetric powder patterns were made at different temperatures using Co Kα radiation. The last diffraction line

TABLE XIII

True thermal expansion coefficient of iron in hydrogen atmosphere.

Temp. (°C)	a_t (*) (Å)	$(\frac{da}{dt})_t \times 10^5$ (Å/°C)	$\alpha \times 10^6$ (/°C)
100	2.86860	3.6066	12.57
200	2.87263	4.3774	15.24
300	2.87725	4.8184	16.74
400	2.88217	4.9795	17.28
500	2.88713	4.9109	17.01
600	2.89193	4.6626	16.12
700	2.89641	4.2849	14.79
800	2.90048	3.8277	13.20

TABLE XIV

Lattice constants of gamma iron(zone-refined iron) in vacuum and in hydrogen, in Å (corrected for refraction).

Temp. (°C)	a_H in H_2	a_v in vacuum	$a_H - a_v$	a_{cal} (*) calculated	$a_H - a_{cal}$
905	3.64694	3.64706	-0.00012	3.6472	-0.0003
950	3.65039	3.65045	-0.00006	3.6507	-0.0003
1000	3.65463	3.65456	0.00007	3.6546	0.0000
1090	3.66109			3.6616	-0.0005
1100		3.66135		3.6624	
1130	3.66510	3.66550	-0.00040	3.6647	0.0004

(*) calculated from equation (14).

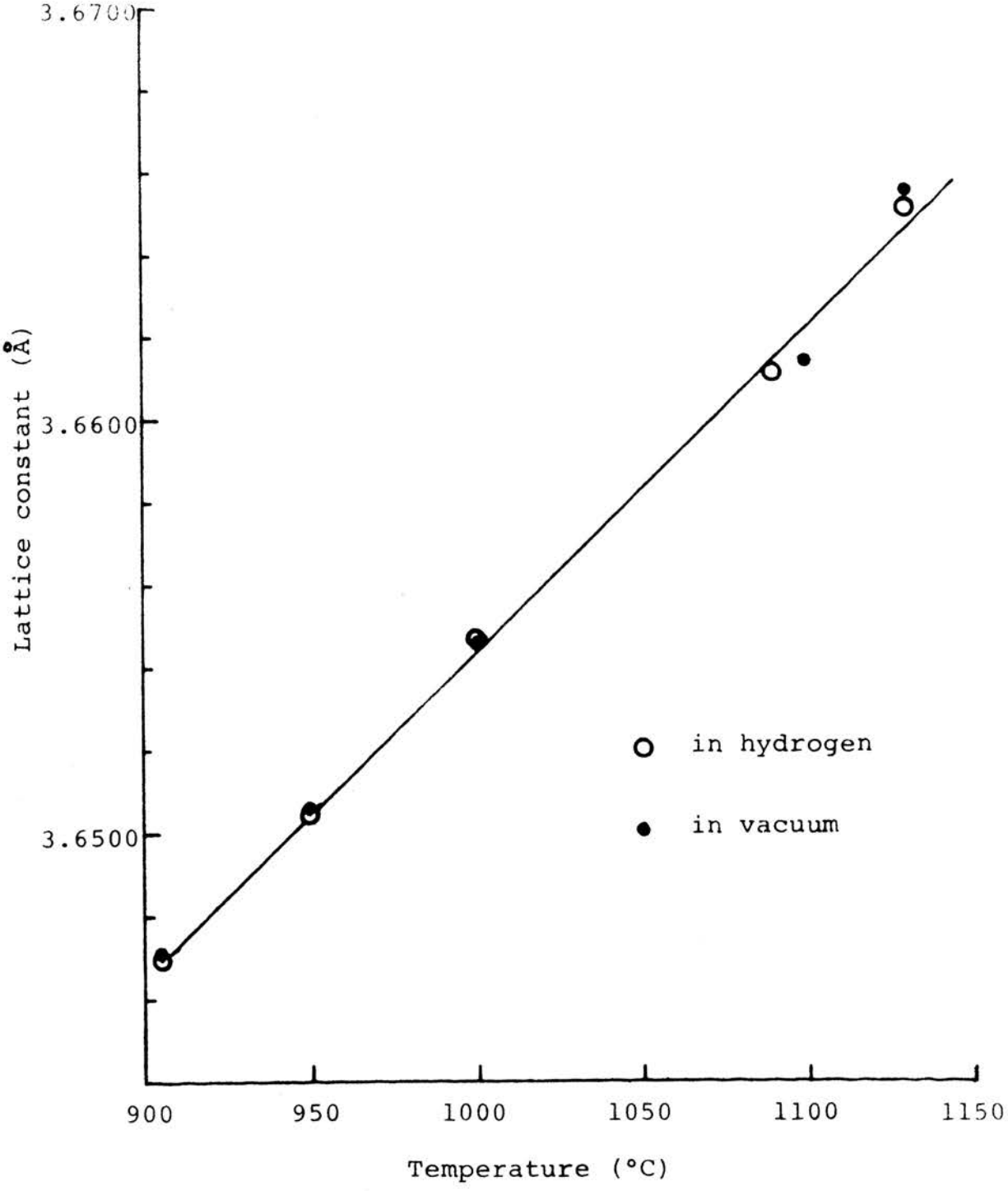

Figure 13. Lattice constant of gamma-iron in vacuum and in a hydrogen atmosphere.

(400) at about 78° was used for the lattice constant determination. Since gamma iron exists only above 910°C, the precise experimental density is not obtainable. For the refraction correction, the X-ray density of 8.15 g/cm^3 was, therefore, used. The correction for the constant calculated from the (400) diffraction line (Co Kα) was found to be 0.00013 A. This value was added to all lattice constants. The results are given in Table XIV and plotted in Figure 13. From the plot the following empirical equation was derived for the lattice constants of gamma iron (between 910 and 1130°C):

$$a_t = 3.5771 + 7.75 \times 10^{-5} t \qquad (14)$$

where a_t is the lattice constant of gamma iron at temperature t°C.

F. Electrical Resistivity Measurements

Using an ohmmeter, the effect of hydrogen on the electrical resistivity of iron was investigated by comparing the resistivities of hydrogen-charged and -uncharged samples.

1. Experimental apparatus. The samples were prepared by winding the exact length (100 cm) of an iron wire (99.85 % Fe), 0.228 mm in diameter around a porcelain tube. Both ends of the wire were then connected to copper lead wires. The sample was charged with hydrogen in the measuring chamber (see Figure 14) by heating it in a hydrogen atmosphere, and the amount of hydrogen absorbed was estimated from Arumbruster's

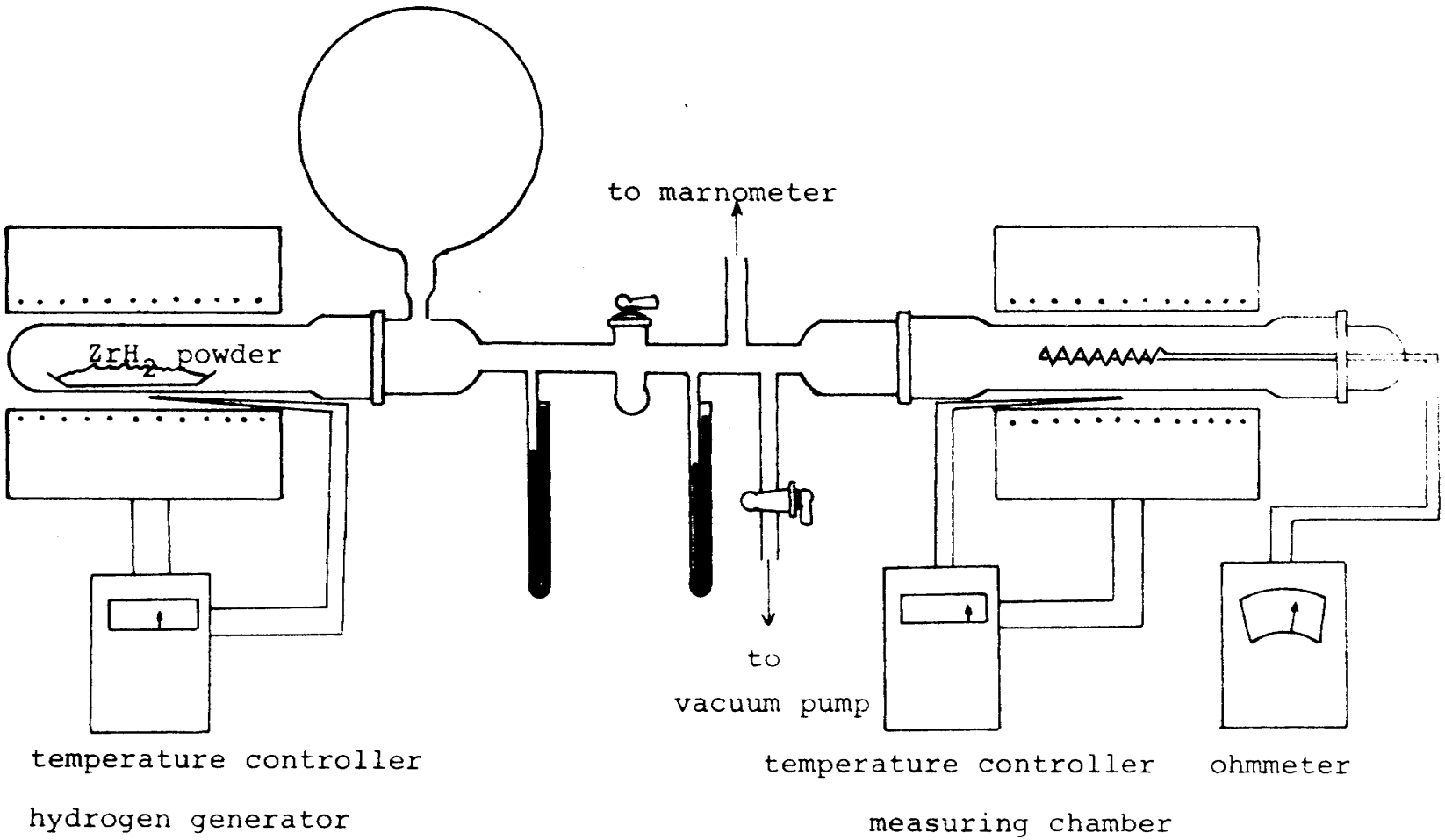

Figure 14. Apparatus for electrical resistivity measurements of iron wire in a hydrogen atmosphere.

equation (equ. 3).

The resistivity measurements were made in an apparatus showin in Figure 14. It consists of three main parts: the hydrogen generator, the measuring chamber, and the vacuum pumping system.

Hydrogen was generated by thermal decomposition of zirconium hydride in the hydrogen generator and the amount of hydrogen was controlled roughly by the decomposition temperature, which was maintained by the temperature controller of the furnace. The sample was placed into the measuring chamber, which was evacuated to 1 micron Hg pressure. The sample was then washed several times with hydrogen by admitting hydrogen from the generator. Before making the measurements, the sample was annealed at 850°C for two hours in vacuum.

The measurements were made at the temperatures from 100 to 600°C at various hydrogen pressures for the purpose of varying the amount of hydrogen absorbed by the sample. All measurements were performed after equilibrating the sample for two hours with the surroundings at specific conditions of temperature and hydrogen pressure.

2. Resistivity of iron in vacuum and hydrogen. For the purpose of comparison, the resistivities of the sample

at different temperatures were measured. Then hydrogen was absorbed and the same measurements repeated. The amounts of absorbed hydrogen were varied by changing its pressure.

The iron wire, of 100 cm in length and 0.228 mm in diameter, was first degassed by heating for two hours at 850°C in vacuum. Then its resistivity at different temperatures was measured in vacuum. The resistivity was calculated from the following equation:

$$\text{Resistivity} = (A/l)R \qquad (15)$$

where A is the cross sectional area of sample, l the length and R the measured resistance.

In order to control the amount of hydrogen absorbed by the sample, the hydrogen pressure in the measuring chamber was varied from 62 to 725 mm Hg, and at each set of temperature and pressure the resistivities of the hydrogen absorbed sample were determined. Both results, in vacuum and in hydrogen, are listed in Table XV and plotted against temperature in Figure 15.

The results of the present work are generally slightly higher than those of previous work with the difference increasing with increasing temperature (see Figure 15). The present higher values are considered to result from im-

TABLE XV

Electrical resistivities, ρ of iron wire in vacuum and in hydrogen atmosphere (ohm/cm).

Temp. (°C)	Hydrogen pressure (mm Hg)	$\rho \times 10^6$	Temp. (°C)	Hydrogen pressure (mm Hg)	$\rho \times 10^6$
100	vacuum	1.489	400	vacuum	4.248
	725	1.489		720	4.256
	548	1.502		563	4.248
	253	1.506		452	4.236
				360	4.248
200	vacuum	2.195	500	vacuum	5.693
	738	2.175		702	5.693
	525	2.195		533	5.623
	430	2.199		400	5.672
	193	2.179		152	5.693
	62	2.199		80	5.713
300	vacuum	3.301	600	vacuum	7.182
	695	3.305		708	7.182
	472	3.289		587	7.156
	227	3.309		158	7.182

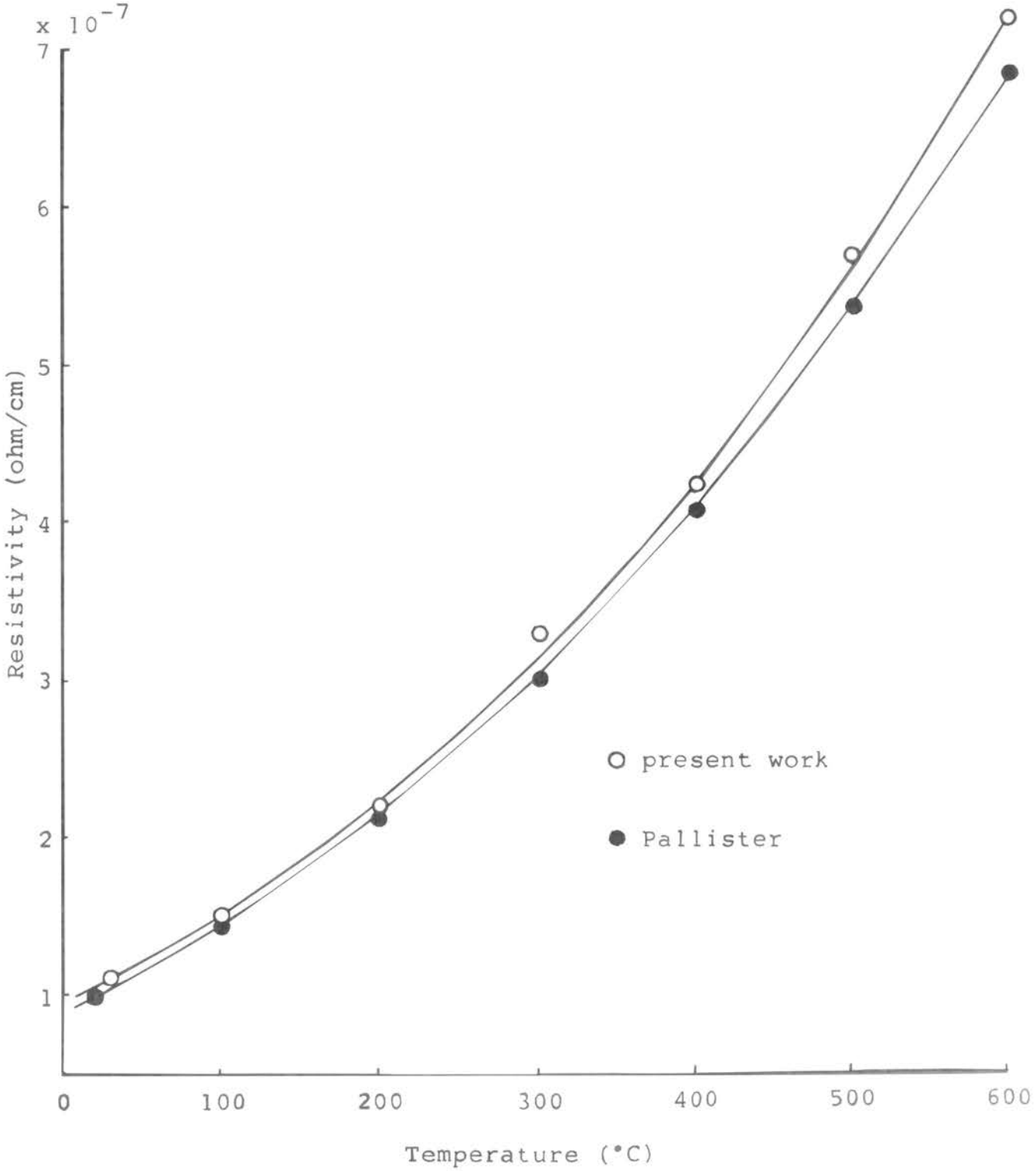

Figure 15. Electrical resistivity versus temperature of pure iron.

purities, as given in page 24. The purity of the sample used in this work is only 99.85 % Fe as compared with 99.9917 % Fe of previous workers. However, this investigation shows that there is no measurable resistivity change of iron with uptake of hydrogen.

G. Density Measurements

Most of the recent mechanisms proposed for hydrogen embrittlement of steel assume a heterogeneous distribution of hydrogen in the metal and that hydrogen forms lattice defects of one sort or another. The form of these imperfections varies from author to author: the term rift, void, Griffith-crack and dislocation pile-up have all been used. Morlet, Johnson and Troiano[82] prefer generally to refer to the term "voids". The assumption is that these voids are large when compared with the volume of a unit cell of the lattice.

If there are really such voids in iron supersaturated with hydrogen, the density of such a metal should decrease. In order to evaluate this, precise density measurements were made with hydrogen-charged and -uncharged specimens.

1. Determination of the density of xylene. The hydrostatic weighing method, which is based on the "principle of Archimeds", was employed for the presise density determina-

tions of zone-refined iron specimens charged with hydrogen and uncharged. This method involves weighing the sample in air, and in a liquid of know density. The liquid must have a low surface tension to assure deep penetration into the sample from its surface. Liquid xylene was chosen for this purpose because of its low surface tension and inertness to iron.

"Natural Histological Xylene" liquid was supplied by Fisher Scientific Company. The density of this liquid was determined at temperatures ranging from 20 to 36°C, using a thermostatically controlled pycnometer and triply distilled water. The experimental details can be found in the literature[83].

The measured densities were all reduced to absolute density (density in vacuo) at each temperature. The results are given in Table XVI and plotted against temperature in Figure 16.

2. Sample preparation. A zone-refined iron chunk was sliced into small pieces weighing 8 to 19 grams. Each of the pieces was ploished on metallographic papers and washed with distilled water and acetone, then dried in hot air. All specimens were stored in a dessicator before the density measurements.

Table XVI

Densities of xylene at different temperatures

Temp. (°C)	Wt. of xylene (g)	vol. of pycnometer (cm^3)	density of xylen (g/cm^3)
20.0	21.7362	25.10856	0.86569
20.0	21.7331	25.10997	0.86552
24.0	21.6507	25.11593	0.86203
24.0	21.6515	25.11533	0.86208
28.0	21.5641	25.11904	0.85848
28.0	21.5664	25.11834	0.85855
32.0	21.4792	25.12234	0.85498
32.0	21.4786	25.11953	0.85506
36.0	21.3955	25.12564	0.85154
36.0	21.3965	25.12364	0.85165

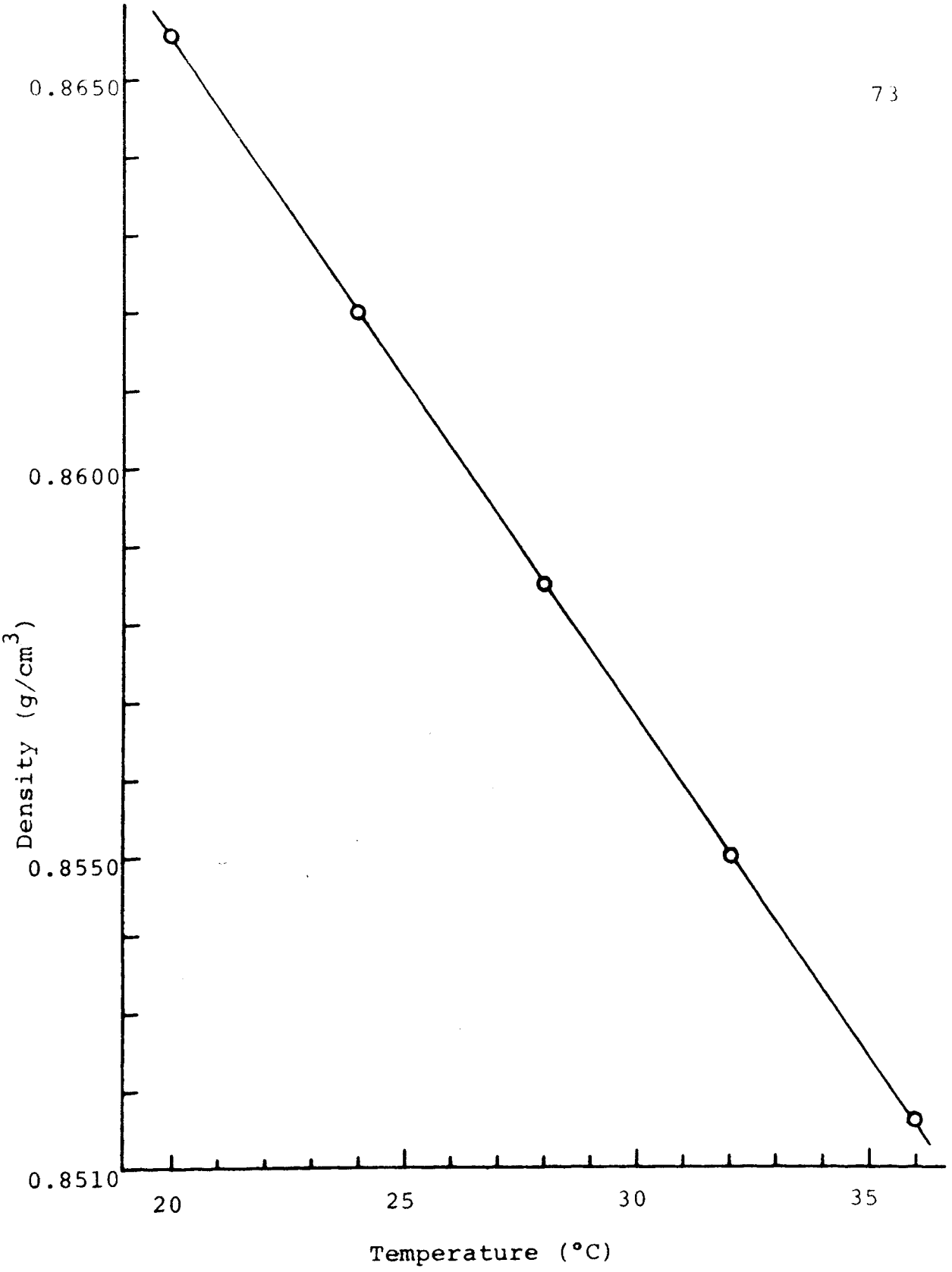

Figure 16. Density of xylene (reduced to vacuo) versus temperature.

Prior to the density measurements each of the uncharged specimens was heated at 850°C in vacuo for the purposes of stress relieving and degassing.

The specimens were charged with hydrogen by heating them in a hydrogen atmosphere at 500 and 800°C, and cooling rapidly to room temperature. Hydrogen charging was performed in the same apparatus as shown in Figure 14.

3. Method of measuring the bulk density. A Sartorius semimicro balance was used to weigh the specimens in air and in xylene. This balance was enclosed in a plexiglass housing to minimize the temperature effect of the surrounding, by passing constant temperature water through the copper tube coils inside the housing and by circulating the air inside the housing. Loading, unloading and weighing operations were made by means of levers extended to the outside of the housing without opening it.

The temperature of the liquid was determined, by accurate reading of the scale of a thermometer suspended in the liquid. Such a reading of the temperature of the liquid is essential for the precise density measurement, as the difference in density which arises from slight temperature changes affects significantly the density of the solid under investigation. Equilibration of temperature between the

specimen and the liquid is also important because of the same reason. Therefore, all weighing operations were made after waiting a sufficiently long time (normally about 30 minutes). For the reduction of the density obtained to vacuum, corrections for the density of air should be made. Therefore, the temperature and barometric pressure were recorded at the time of weighing. The temperature of the liquid was assumed to be that of the air, since the air density varies only very little for the few degrees difference. This change is small and is within the limit of error of the xylene density measurements.

The weight of the sample in liquid was obtained while suspending it from a fine tungsten wire attached to the balance pan holder. A correction was made by subtracting from the sample weight the weight of the wire alone when immersed in the liquid under the same conditions.

The density of the specimen was then calculated from the following formula:

$$d_s = (d_l - d_g)\left[\frac{\text{weight of sample in air}}{\text{weight loss of sample in liq.}}\right] + d_g \quad (16)$$

where d_s is the density of the sample at the temperature of measurement, d_l and d_g are the densities of xylene and air, respectively, at the temperature of the sample and the respective air pressure.

All the densities obtained were then reduced to 25°C using the following formula:

$$d_{25} = d_t[1 - 3\alpha(t - 25)] \qquad (17)$$

where d_t is the density of the specimen at the temperature t°C and α is the linear thermal expansion coefficient of the specimen (12.1×10^{-6}/°C).

4. Results. The densities of five different specimens were measured in an uncharged and hydrogen-charged condition. Six to thirteen measurements were made of each specimen and the densities were reduced to 25°C.

Specimen 1 was charged with hydrogen at 500°C for 22 hours and Specimens II, III, IV and V were charged with hydrogen at 800°C for four to 22 hours respectively.
Their measured densities are shown in Tables XVII, XVII, XIX, XX and XXI.

TABLE XVII

Densities of zone refined iron, Specimen I

before and after charging with hydrogen

(in g/cm^3)

Before charging			After charging at 500°C		
Temp. (°C)	d_t	d_{25}	Temp. (°C)	d_t	d_{25}
22.6	7.87152	7.87081	23.7	7.87054	7.87017
22.7	7.87094	7.87031	23.8	7.87056	7.87022
22.8	7.87089	7.87026	23.9	7.87074	7.87043
23.0	7.87167	7.87112	24.0	7.87068	7.87042
23.2	7.87152	7.87101	24.2	7.87086	7.87063
23.55	7.87152	7.87111	24.2	7.87061	7.87038
23.8	7.87126	7.87092	24.3	7.87021	7.87001
23.9	7.87118	7.87086	24.4	7.87039	7.87022
24.0	7.87193	7.87163	24.7	7.87100	7.87091
24.2	7.87205	7.87188	25.8	7.87058	7.87064
Average d_{25}= 7.87088±0.00035			Average d_{25}= 7.87040±0.00018		

TABLE XVIII

Densities of zone-refined iron, Specime II before and after charging with hydrogen (in g/cm^3)

Before charging			After charging at 800°C		
Temp. (°C)	d_t	d_{25}	Temp. (°C)	d_t	d_{25}
26.5	7.87427	7.87470	24.5	7.87435	7.87423
26.6	7.87430	7.87476	24.45	7.87438	7.87426
26.3	7.87399	7.87437	23.6	7.87500	7.87460
26.5	7.87427	7.87470	23.75	7.87458	7.87420
26.25	7.87437	7.87473	24.6	7.87495	7.87485
26.20	7.87456	7.87490	23.75	7.87458	7.87420
Average d_{25}=7.87470±0.00008			Average d_{25}=7.87440±0.00058		

TABLE XIX

Densities of zone-refined iron, Specimen III before and after charging with hydrogen

Before charging			After charging at 800°C		
Temp. (°C)	d_t		Temp. (°C)	d_t	d_{25}
25.0	7.87484	7.87484	23.8	7.87502	7.87469
25.1	7.87469	7.87472	23.9	7.87485	7.87454
25.1	7.87471	7.87474	23.9	7.87500	7.87469
25.1	7.87471	7.87474	24.0	7.87465	7.87435
24.45	7.87487	7.87471	24.0	7.87464	7.87435
25.75	7.87425	7.87446	24.0	7.87453	7.87424
25.25	7.87462	7.87469,	24.2	7.87490	7.87467
25.3	7.87441	7.87450	24.6	7.87511	7.87498
Average d_{25}=7.87475±0.00032			25.6	7.87439	7.87460
			Average d_{25}=7.87457±0.00049		

TABLE XX

Densities of zone-refined iron, Specimen IV before and after charging with hydrogen (in g/cm^3)

Before charging			After charging at 800°C		
Temp. (°C)	d_t	d_{25}	Temp. (°C)	d_t	d_{25}
20.2	7.87633	7.87496	19.6	7.87635	7.87481
20.9	7.87584	7.87467	19.6	7.87626	7.87472
20.9	7.87636	7.87519	19.6	7.87648	7.87488
21.0	7.87641	7.87524	19.7	7.87651	7.87499
21.4	7.87499	7.87396	19.8	7.87626	7.87477
21.5	7.87555	7.87455	20.4	7.87621	7.87489
21.6	7.87564	7.87467	20.4	7.87626	7.87494
20.9	7.87580	7.87463	20.5	7.87596	7.87467
20.9	7.87571	7.87454	20.5	7.87587	7.87458
20.9	7.87593	7.87476	20.5	7.87579	7.87450
21.0	7.87572	7.87458			
21.0	7.87563	7.87449			
21.0	7.87602	7.87488			
Average $d_{25}=7.87470\pm0.00024$			Average $d_{25}=7.87478\pm0.00011$		

TABLE XXI

Densities of zone-refined iron, Specimen V
before and after charging with hydrogen
(in g/cm^3)

Before charging			After charging at 800°C		
Temp. (°C)	d_t	d_{25}	Temp. (°C)	d_t	d_{25}
22.6	7.87458	7.87389	22.4	7.87473	7.87399
22.6	7.87480	7.87411	22.4	7.87458	7.87384
22.7	7.87478	7.87412	22.0	7.87484	7.87390
22.7	7.87482	7.87416	22.0	7.87480	7.87386
22.7	7.87452	7.87386	22.0	7.87510	7.87416
22.6	7.87484	7.87415	22.0	7.87506	7.87412
20.3	7.87520	7.87386	22.0	7.87458	7.87364
20.4	7.87486	7.87355	22.0	7.87455	7.87361
20.4	7.87486	7.87355	22.0	7.87450	7.87356
20.4	7.87494	7.87363	22.0	7.87452	7.87358
20.5	7.87477	7.87348	21.8	7.87458	7.87367
20.5	7.87484	7.87355			
Average d_{25}=7.87383±0.00018			Average d_{25}=7.87381±0.00016		

VI. DISCUSSION

The lattice constant of zone-refined iron determined in this investigation(a_{25}=2.86623 Å) is slightly lower than that of pure iron determined by previous workers (see Table XXII). Yet, the differences between the present value and previous ones are less than 0.0003 Å, which barely exceeds the limit of experimental errors.

TABLE XXII

Lattice constant, a of pure iron at 25°C

(in Å)

Author	a	Purity
present work	2.86623	zone-refined Fe
Swanson et al.[28]	2.8664	99.9974 % Fe
Grønvold et al.[29]	2.8664_7(*)	
Owen & Williams[30]	2.8664	99.98 % Fe
Sutton & Hume-Rohtery[31]	2.8663_6	99.969 % Fe
Basinski et al.[32]	2.8664	99.969 % Fe

(*) Temperature was held constant, ±2°C.

The slightly lower lattice constant of this study is considered due to extreme purity of the zone-refined iron. However, the lattice constant of iron determined by Swanson was obtained as an average from five last lines. The averaging of the values from different planes is based on the assump-

tion that a-calculations from different planes have the same extent of precision independently of the Bragg angle. But this is not true; the precision of the measured lattice constant increases with increasing Bragg angle, as can be shown easily. Therefore, averaging the values determined from different planes does not lead to the correct lattice constant as obtained from the highest indexed plane.

The lattice constant of iron whiskers is accompanied by a slightly higher error, because of broad spots instead of fine lines. There is, however, no measurable difference between the lattice constant of an iron whisker and zone-refined iron powder. This suggests that the lattice defects, such as point defects or dislocations till present in zone-refined iron powder after annealing, do not influence the lattice constant of iron, within error limits, because it is assumed that iron whiskers are without defects, except for a few screw dislocations.

The literature review revealed that the question whether or not occluded hydrogen in iron has an effect on its lattice constant has been open for a long time. The present investigation shows clearly that hydrogen has no such effect at room temperature, regardless of the charging methods (cathodically or thermally), as shown in Table VIII. However, differences do develop at elevated temperatures.

The present measurements at elevated temperatures in vacuum agree well with previous measurements[32] (see Figure 17). Although above approximately 200°C the thermal expansivity of zone-refined iron in vacuum is linear with respect to temperature, nevertheless, in the range between 25 and 200° C, the dependence seems to follow a curved rather than a straight line. A similar relationship was observed by previous workers[32,33]. This might be due to the difficulties in equilibration of sample temperature or to an unknown transition point in this range.

Even though hydrogen has no effect on the lattice constant of iron at room temperature, it does increase the thermal expansion of iron at elevated temperatures. This effect begins at about 400°C and gradually increases up to its maximum between 600 and 700°C, and then diminishes slowly with increasing temperature (see Figure 17). In order to check whether this phenomenon of decrease was not due to hydrogen escape through the quartz capillary wall (which would result in a decrease of hydrogen concentration in the iron powder), samples were prepared in same way as previously, sealing the capillary after filling it with hydrogen at 750 mm Hg at room temperature. The lattice constant of such an iron sample was then measured at 740°C, as soon as this temperature was reached, then again after keeping 5 hours and finally after

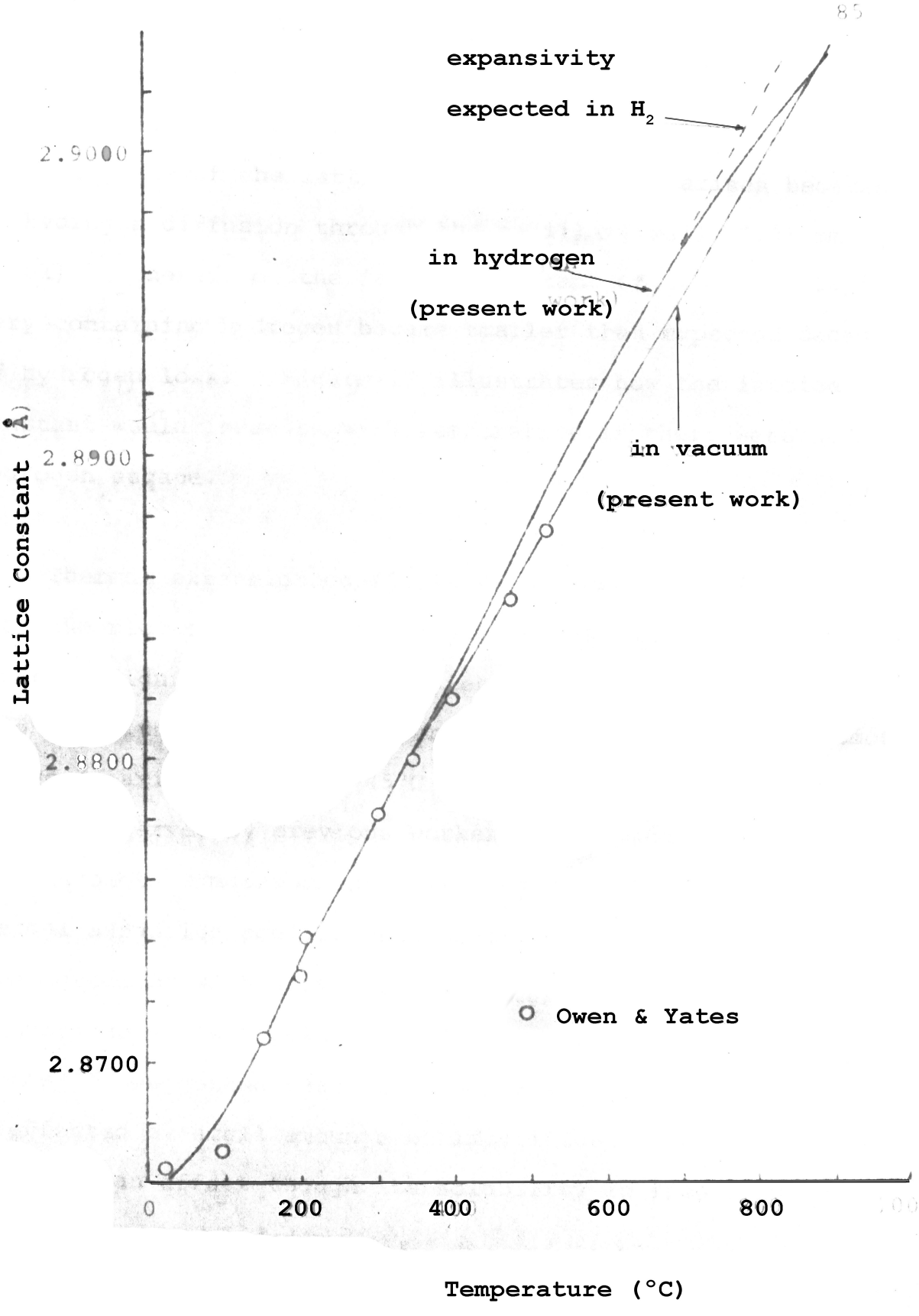

Figure 17. Lattice constant of pare iron in vacuum in hydrogen.

holding the sample for 18 hours at this temperature. The results were 2.89803, 2.89792 and 2.89659 Å respectively. The constant in vacuum at the same temperature was 2.89675 Å. This decrease of the lattice constant of iron arises because of hydrogen diffusion through the capillary wall (0.01 mm thick). Therefore, the lattice constant of iron in a capillary containing hydrogen became smaller than expected because of hydrogen loss. Figure 17 illustrates how the lattice constant would increase with temperature if there were no hydrogen escape.

Thermal expansion coefficients of iron were determined from the plot of lattice constants versus temperature. As shown in Figure 18, the coefficient decreases in vacuum slightly with increasing temperature, but in a hydrogen atmosphere a maximum at about 45°C is found. This maximum was already observed by previous workers[45,46] who used the interferometric measurements (see Figure 2). The present thermal expansion coefficients of iron in hydrogen are in a good agreement with previous macroscopic measurements, particularly the maximum point at about 450°C. Austin and Pierce[46] suggested that the thermal expansivity of pure iron is affected by small amounts of impurities. Thus, hydrogen must have an effect though its solubility in iron is very small.

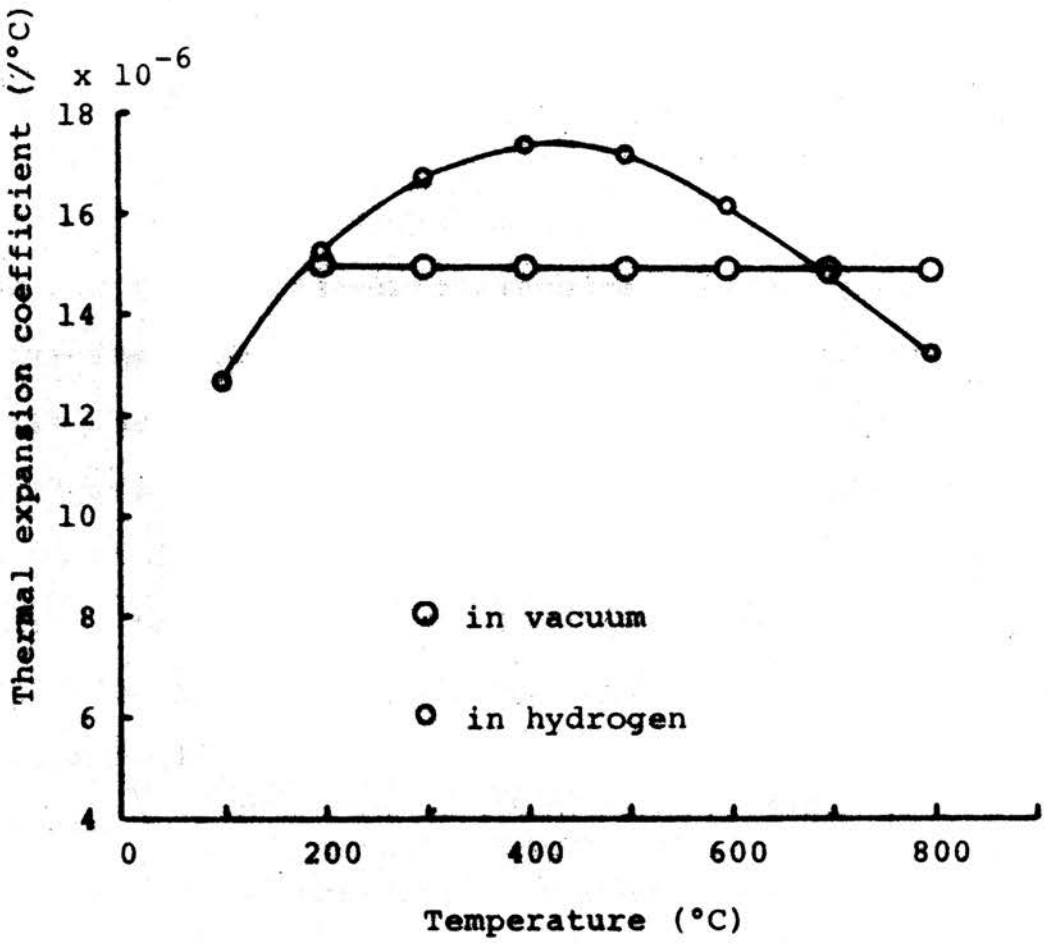

Figure 18. Thermal expansion coefficients of pure iron in vacuum and in hydrogen.

Although the effect of hydrogen on the thermal expansivity of iron is evident, there is still a question as to how such an effect can be produced by such small quantities of hydrogen.

In a b.c.c. lattice there are two kind of interstitial positions for foreign atoms: tetrahedral and octahedral. If spheres are inscribed in the respective holes, the radius ratios with the surrounding iron atoms are 0.291 and 0.154, respectively. In the case of alpha iron, the radii of the spheres, which fit in these voids without distortion, are 0.361 for the tetrahedral and 0.191 Å for the octahedral voids. The calculation was made on the assumption that the radius of an iron atom is 1.24 Å. If the radius of a hydrogen atom is assumed to be 0.48 Å, as suggested by Pauling[84], its atom is larger than any of the voids mentioned, and it becomes concievable that the iron lattice will dilate upon dissolving hydrogen atoms. The dilation of iron lattice due to dissolved hydrogen may be calculated from physical data reported for hydrogen solubility and iron. The hydrogen concentration at the conditions of lattice constant measurements can be estimated from Arumbruster's equation (equ. 3). As the iron samples were enclosed in a quartz capillary at a hydrogen pressure of 750 mm Hg at room temperature, the pressure inside the capillary must increase upon heating. Therefore, the hydrogen concentrations in iron at each of the elevated temp-

eratures can be computed using the calculated pressures. Now, the magnitude of lattice dilation due to hydrogen dissolution in each of the voids can be evaluated from the following equations:

for octahedral void,

$$\Delta a_t = 2(R_H - R_V)(C_t/n) \quad (18)$$

and for tetrahedral void,

$$\Delta a_t = 2(R_H - R_V)\cos 32°(C_t/n) \quad (19)$$

where Δa_t is the lattice dilation due to hydrogen absorption by the voids at the temperature t, R_H and R_V the radii of hydrogen and of the sphere which fits exactly in the respective void, n the number of voids per iron atom (one in an octahedral and two in a tetrahedral void). The above equations are derived assuming that a hydrogen atom in each such a void causes an uniform average dilation of the lattice, depending upon the hydrogen concentration. The dilations due to hydrogen in tetrahedral and octahedral voids are calculated for different temperatures and summarized in Table XXIII. As shown in Table XXIII, actually observed iron lattice dilations upon hydrogen dissolution are much greater than those calculated. This suggests that the iron lattice dilation is not simply due to the hydrogen present in the interstitial positions but a more complicated phenomenon.

How perfect is the structure of zone-refined iron ? This question can be answered by determination of the number

TABLE XXIII

Comparison of the observed lattice dilations due to hydrogen dissolved in iron and the calculated values assuming preferential location of hydrogen.

Temp. (°C)	Lattice constant (A) in hydrogen	Lattice constant (A) in vacuum	Hydrogen concentration (H/Fe)
350	2.88024	2.88020	0.000018
450	2.88466	2.88448	0.000042
550	2.88956	2.88876	0.000076
650	2.89422	2.89304	0.000125
750	2.89850	2.89732	0.000188
850	2.90232	2.90160	0.000262

Temp. (°C)	Observed lattice dilation due to H $(a_H - a_V)$ (A)	Calculated lattice dilation assuming hydrogen in Tetrahedral voids (A)	Calculated lattice dilation assuming hydrogen in Octahedral voids (A)
350	0.00004	0.000001	0.000010
450	0.00018	0.000002	0.000024
550	0.00080	0.000004	0.000044
650	0.00118	0.000007	0.000072
750	0.00118	0.000011	0.000110
850	0.00072	0.000015	0.000162

of atoms, n', per unit cell, using density and lattice constant measurements. As mentioned in the experimental part, the precise density measurement requires a correct knowledge of the density and the equilibrated temperature of the liquid at the time of weighing and, of course, the correct weight of the specimen. Actually, in attaining precision, the error in liquid density, arising from misreading the temperature of the liquid, is the most serious, particularly for specimens of higher density. Other factors, such as the density of air and the weight of the specimen in air are of lesser influence. Of course, voids in the specimen produce the worst systematic error, producing low values. Voids can mostly be eliminated using single crystals or samples consisting of only a few grains, which minimize greatly the possibility of such defects (fissures, microcracks, holes, etc.). Taking all possible precautions to avoid the above mentioned pitfalls, the present density determination of zone-refined iron showed an error about ten times smaller than any of the previous results, and consequently one more significant number in the results can be reported (see Table XXIV).

The actual number, n' of atoms or molecules per unit cell can be calculated from

$$n' = V\, d\, N_o / M \qquad (20)$$

where V is the volume of the unit cell, d the experimental

density of the crystalline substance, M the atomic or molecular weight, and N_o Avogadro's number. The measurements

TABLE XXIV

Density of pure iron (g/cm^3)

Author	Density	Temp. (°C)	Composition
Present work	7.87450	25.0	zone-refined iron
International Critical Table	7.90	20.0	0.08 % O_2, 0.007 % P
Adcock & Bristow	7.871	19.0	
Cleaves & Hiegel	7.874	20.0	99.9917∿99.9871 % Fe

of V and d must be made at the same temperature or reduced to the same temperature. n' was determined for five samples of zone-refined iron(uncharged), and the results are summarized in Table XXV.

However, conclusions concerning the presence of defects in solids from n' calculations can be drawn only if

$$|n' - n| > |\Delta n'| \qquad (21)$$

That is, if the difference $|n' - n|$ is larger than the error $\Delta n'$ by which the n' determinations are affected. n is the ideal number of atoms per unit cell. If this difference is equal or smaller than $\Delta n'$, the propagated error, no conclusion can be made concerning the presence of imperfections and

the structure of solid is in all probability perfect or sound. The propagated error, $\Delta n'$ can be calculated from equation 22, adjusted for the cubic system:

$$\Delta n' = n'[(3f_1\frac{\partial a}{a})^2 + (f_2\frac{\partial d}{d})^2 + (f_3\frac{\partial N}{N_o})^2 + (f_4\frac{\partial M}{M})^2]^{1/2} \quad (22)$$

where $\partial a/a$, $\partial d/d$, etc. are the relative errors of the a, d and M measurements, and ∂a, ∂d, etc. are the probable deviations (errors) of the same measurements. f_1, f_2, etc. are the weighing factors which will allow for the unknown systematic errors. Using one for each of f_1, f_2, f_3 and f_4, and M = 55.847±0.003 and $N_o = 6.024\pm0.0005 \times 10^{23}$, n' calculated for the five specimens is listed in Table XXV (third column).

TABLE XXV

Calculation of $\Delta n'$, the propagated error of n'.

determinations.

Sample	d_{25}	Δd	n'	$\lvert n' - n \rvert$	$\Delta n'$	n'(*)
[I	7.87040	±0.00018	1.99901	0.00099	±0.00012	1.99873]**
II	7.87470	±0.00008	2.00010	0.00010	±0.00012	1.99982
III	7.87475	±0.00032	2.00012	0.00012	±0.00013	1.99983
IV	7.87470	±0.00022	2.00010	0.00010	±0.00012	1.99982
V	7.87383	±0.00018	1.99988	0.00012	±0.00012	1.99960
Ave.@	7.87450	±0.00020	2.00005	0.00011	±0.00012	1.99974

(*) These n's were calculated using the new conversion factor, 1.002056 Å/kX and new $N_o = 6.02252 \times 10^{23}$.

(**) Sample I was excluded, it evidently contained voids or micropores.

(@) All averages were made excluding the value of sample I.

As shown in the above table, all zone-refined iron specimens, except specimen I, show n' values very close to the ideal number 2.00000, and the difference $|n' - n|$ is equal or smaller than the propagated error, $\Delta n'$, except for specimen I, which was excluded. Therefore, the conclusion is that the zone-refined iron is sound, except specimen I which contains some kind of defects, possibly micropores.

The n' is also calculated using the new conversion factor (Λ = 1.002056 Å/kX and the new Avogadro's number 6.02252×10^{23})[96]. These results are also given in Table XXV (seventh column). This time, all n' values show a slightly lower value than the ideal number of two and the difference $|n' - n|$ is, in all cases, just outside of the propagated error limit, $\Delta n'$. Thus, from this point of view the old values of Λ = 1.00202 and of $N_o = 6.0240 \times 10^{23}$ should, evidently, be preferred in crystallographic measurements. $\Lambda^3 N_o$ as calculated from the present measured value of a and ρ, was 6060.43×10^{20}. Comparing the previous $\Lambda^3 N_o$ measurement, the present result is slightly higher than that of Bearden[85] (6059.72×10^{20}) but is in better agreement with former results (see Table XXVI).

TABLE XXVI

Data on $\Lambda^3 N_o$ (86)

Crystal	Value of $\Lambda^3 N_o$	Weight w_i	Author
(Mo $K\alpha_1$, 707.831 X-units)			
KCl	6058.23	4	Yuching Tu
Calcite	6059.60	20	G. Brogen
Diamond	6059.60	21	Yuching Tu
Calcite	6059.60	20	J.A. Bearden
Diamond	6059.81	23	Yuching Tu
Calcite	6059.98	35	Yuching Tu
Quartz	6060.06	3	G. Brogen
Rocksalt	6060.11	5	Yuching Tu
Weighted average value $\Lambda^3 N_o$ = 60.59.72±0.10			
(Cu K_1, 1537.396 X-units)			
Silicon	6059.90	23	Smakula et al.
CaF_2	6060.05	10	Smakula et al.
CsI	6060.08	2	Smakula et al.
TlCl	6060.14	5	Smakula et al.
Aluminum	6060.17	28	Smakula et al.
TlBr	6060.28	5	Smakula et al.
Germanium	6060.42	3	Smakula et al.
LiF	6060.81	12	Straumanis et al.
Weighted average value $\Lambda^3 N_o$ = 6060.18±0.11			

V. SUMMARY

1. The lattice constants of iron at 25°C are

   $a = 2.86623 \pm 0.00002$ Å for zone-refined iron, and

   $a = 2.86626 \pm 0.00004$ Å for an iron whisker.

2. The lattice constants of iron in vacuum at temperatures between 200 and 910°C can be represented by an empirical equation:

   $$a_t = 2.86522 + 4.28 \times 10^{-5} t$$

   where a_t is the lattice constant in Å at temperature t°C.

3. Hydrogen has no effect (within the limits of error) on the lattice constant of iron at room temperature regardless of the charging methods (charging cathodically or thermally).

4. However, hydrogen increases the lattice constant at elevated temperatures. The lattice constant of iron within a capillary filled with hydrogen can be calculated from an empirical equation:

   $$a_t = 2.86554 + 2.45565 \times 10^{-5} t + 6.78828 \times 10^{-8} t^2 - 7.16922 \times 10^{-11} t^3 + 2.08773 \times 10^{-14} t^4$$

   where a_t is the lattice constant of iron in Å in the hydrogen atmosphere of the capillary at a temperature of t°C.

5. The lattice constant of gamma iron is the same both in vacuum and in hydrogen (under the conditions of the present measurements) between 910 and 1130°C. The equation is

$a_t = 3.5771 + 7.75 \times 10^{-5} t$

where a_t is the lattice constant of gamma iron in either vacuum or hydrogen atmosphere at temperature t°C.

6. Hydrogen has no effect on the density of pure iron or on the electrical resistivity of iron at temperatures between 100 and 600°C.

7. The density of zone-refined iron at 25°C is as follows:

[Specimen I 7.87040 ± 0.00018 g/cm^3]

Specimen II 7.87470 ± 0.00008 g/cm^3

Specimen III 7.87475 ± 0.00032 g/cm^3

Specimen IV 7.87470 ± 0.00022 g/cm^3 and

Specimen V 7.87383 ± 0.00020 g/cm^3.

Average d_{25} = 7.87450 ± 0.00020 g/cm^3.

Specimen I is believed to have some voids or microcracks. Therefore, neglecting this value, the best value for the density of zone-refined iron is the average value of the four remaining specimens: 7.87450 0.00020 g/cm^3.

8. The actual number of atoms, n' per unit cell of zone-

refined iron is

[Specimen I	1.99901	± 0.00012]
Specimen II	2.00010	± 0.00012
Specimen III	2.00012	± 0.00013
Specimen IV	2.00010	± 0.00012
Specimen V	1.99988	± 0.00012
Average(*) =	2.00005	± 0.00012

(*) Average of four specimens excluding Specimen I.

9. The present calculation of $\Lambda^3 N_o$ is 6060.43 x 10^{20}.

PART II

DISSOLUTION STUDIES OF ZONE-REFINED IRON IN SOME ACIDS

VI. EXPERIMENTAL

A. Orientation Studies of Corrosion Patterns of Iron Obtained in Some Acids.

During dissolution studies of zone-refined iron in sulfuric and hydrochloric acids, a preferred attack of the surface was observed[2]. A further investigation of the preferred attack of iron was made in the present study, using various acids as etchants and examining the facets developed by means of microscopic, X-ray diffraction and goniometric measurements.

1. The attack of iron by acids. When zone-refined iron is attacked by acid, a preferred attack of the surface always takes place according to a certain crystallographic orientation and this preferred attack causes the development of small facets arranged along certain crystallographic direction within a grain. Figure 19 shows the effect of preferred attack on the surface of a piece of zone-refined iron by concentrated hydrochloric acid. As shown in Figure 19, all the small facets developed within each grain are arranged according to a certain orientation, and all facets within each grain have a similar shape.

2. Optical goniometer. The Stoe small two-circle optical goniometer, mode E (made in Heidelberg, West Germany) was used in this investigation to adjust the specimens for

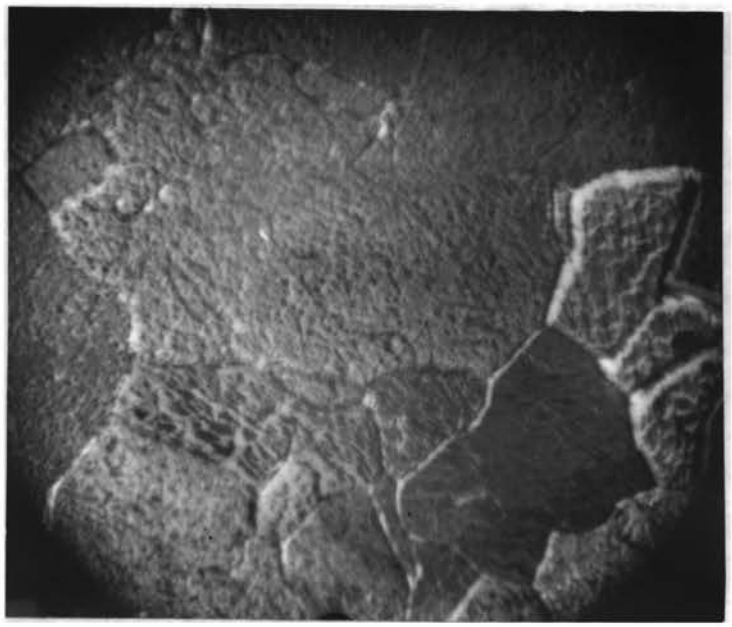

Figure 19. Corroded surface of zone-refined iron, attacked by conc. HCl, x 7. Note large grain size and corrosion patterns on various grains.

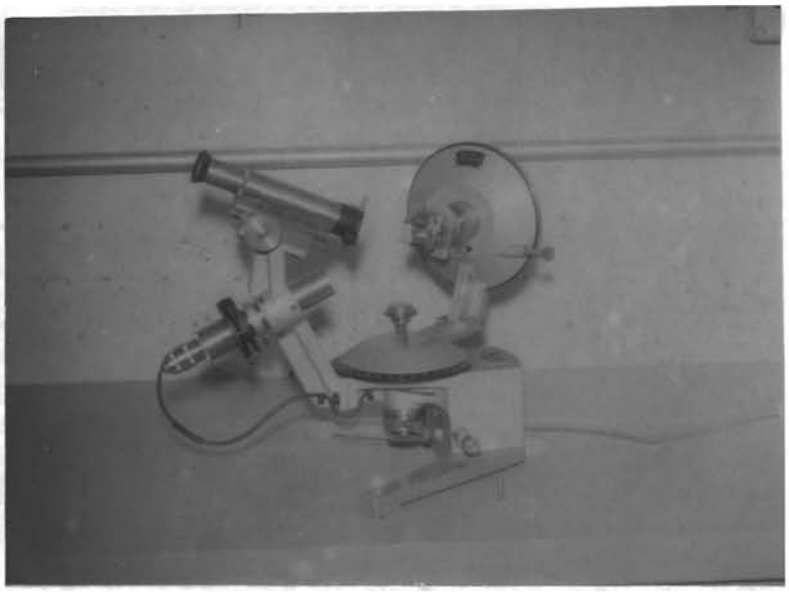

Figure 20. Two-circle optical goniometer. X-ray goniometer head with sample mounted on it is arranged on two-circle optical goniometer.

making Laue patterns and to measure the angles between the facets developed during corrosion.

Figure 20 shows the two-circle goniometer. A solid base casting supports the optical and mechanical parts and contains the transformer for the light source. The bronze bearing for the vertical axle is mounted in the base casting. The horizontal circle and the support for the arm which carries the vertical circle are mounted on the vertical axle. The arm with the collimator and telescoped is also attached to the base. The vertical circle is completely enclosed and is exposed only where a small window permits direct observation and reading of the scale. Both circles are divided in full degrees, which can be read to 1/10° by means of verniers and are equipped with fine adjustments. The goniometer head with the sample is screwed into the horizontal axle of the vertical circle. A motion along this axis is provided so that the crystal can be centered regardless of size. The center of the instrument is at the intersection of the two axles. The telescope receives the light beam which originates in the collimator and is reflected from the crystal surface after passing through the Websky diaphragm (signal).

3. Sample preparation. The specimens were shaped into small pieces with a thickness of about 5 mm. The surface of

each specimen was ground and polished on the metallographic paper in order to assure a uniform surface. These specimens were then exposed to the action of various acids, which at first removed the surface layer deformed during the slicing operation. The acid attack slowly progressed in depth. The solutions used were concentrated hydrochlric acid, 1.5 normal nitric acid, 2 normal sulfuric acid, 25 % aqeous solution of aqua regia, and concentrated (48 %) hydrofluoric acid. The duration of the attack differe from acid to acid. For instance, it took only a few hours to produce an etch pattern in concentrated hydrochloric acid, while a few days were required to get the same pattern in a 2 normal sulfuric acid. However, the attack of all specimens was continued until the grain boundaries were clearly revealed. After the reaction, each specimen was washed thoroughly with distilled water, dried, and then examined microscopically.

4.Determination of orientation.

a. Preparation of Laue pattern. After microscopic examination, those grains which were large enough to be exposed to the X-ray beam (0.5 mm in diameter) were selected and then all grains except that one under observation were covered with masking tape in order to adjust conveniently the steps of one grain on the optical goniometer and to bring the X-ray beam onto this particular grain. The specimen

was then mounted on an X-ray goniometer head, which fitted to both the optical goniometer and the Laue camera set-up. Next, the X-ray goniometer head with the sample on it was first remounted on an optical tow circle, as shown in Figure 20. The whole grain was shifted so that the spots on it, upon rotation of vertical circle of the optical goniometer, reflected the light beam with a maximum intensity. This adjustment was made in a series of operations. By repeating these operations several times, the maximum reflected light intensity was finally obtained through the telescope: at such a moment, the steps with larger areas are perpendicular to the axis of the vertical circle which, in turn, is parallel to the X-ray beam of the Laue camera set-up.

The goniometer head was then carefully removed from the optical goniometer without disturbing the setting of the specimen and mounted on the back reflection Laue camera set-up in such a way that the surface of the steps was perpendicular to the primary X-ray beam. The X-ray beam was then centered on the chosen grain by sliding the goniometer head along the plane perpendicular to the beam. A narrow piece of fluorescent screen (about 2mm wide) was used to locate the beam on the grain.

Back reflection Laue photographs were made of every grain. In this way the crystallographic orientation of

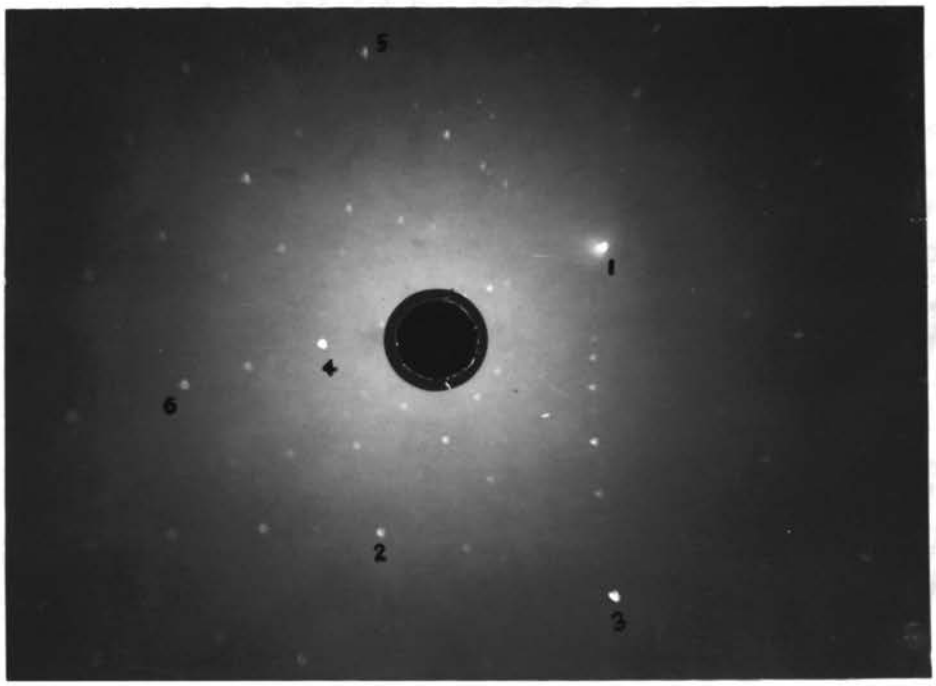

Figure 21. Back reflection Laue pattern of iron, iron radiation, 40 KV, 6 mA, 1.5 hours exposure, 3 cm specimen-to-film distance.

the steps having larger areas developed during corrosion was determined. All pictures were taken with iron radiation at 40 Kv and 6 mA for one and half hours. Sample-to-film distance was kept as close as 3 cm. One of the back reflection Laue patterns is shown in Figure 21.

b. Indexing the Laue pattern. The purpose of indexing a Laue pattern is to determine the crystallographic orientaion of the plane, perpendicular to the X-ray beam. This can be done by finding the correct Miller indices of the spots on the Laue pattern. Actually a plane can be determined correctly from three Laue spots, which have to be indexed. In this investigation, more than three spots are indexed for correctness.

The indexing method used is the classical trial and error method in which tentative indices are assigned to spots until the assumed orientations meet the correct angular relationships between each of the pairs. The symmetry consideration, which can be obtained through careful examination of the pattern, is very helpful in assigning correct indices to the major spots. For example, in a cubic system, [100], [110] and [111] have four-, two- and three-fold rotation axes, respectively. Therefore, when a four-fold rational symmetry is found around a spot, it could be [100], when a two-fold, [110] and if three-fold, [111] is possible. A demonstration of indexing is made below for a Laue back re-

flection pattern showin in Figure 21.

First, with the aid of a Greninger-Bond net (for a 3 cm sample-to-film distance), the locations of all strong reflections were read and plotted in Wulf's stereonet (see Figure 22). With the aid of this net, great circles were drawn through the various sets of spots corresponding to the various hyperbolas of spots on the film. These great circles connect planes of a single zone. Planes lying at their intersections are generally of low indices. Such poles are the points 1,2,3,4 and 5 in this pattern, and P_A, P_B, P_C and P_D are the main poles found at the intersections of great circles which do not appeared on the film. A careful examination of point 1 revealed that it represents a two-fold symmetryaxis, which leads to the index [011] for the axis. P_A, P_B, P_C, and P_D are equally spaced by an angle of 45°, and , hence point 1 includes an angle of 45°, with P_B. As the angle between (110) and (100) is 45°, P_B was assumed to be [001], P_C [$\bar{1}$01], and P_D [$\bar{1}$00]. A closer examination of point 2 revealed a three-fold rotational axis. As this point is separated 35° approximately from point 1 and P_C, it should have the index[$\bar{1}$11], because the theoretical angle between (110) and (111) is 35.3°. Next, the angles between each pair of points 1 to 6 and P_A to P_D were measured with the aid of Wulff's net and summarized in Table XXVII. Comparing these measured angles with theoretical values shows that all

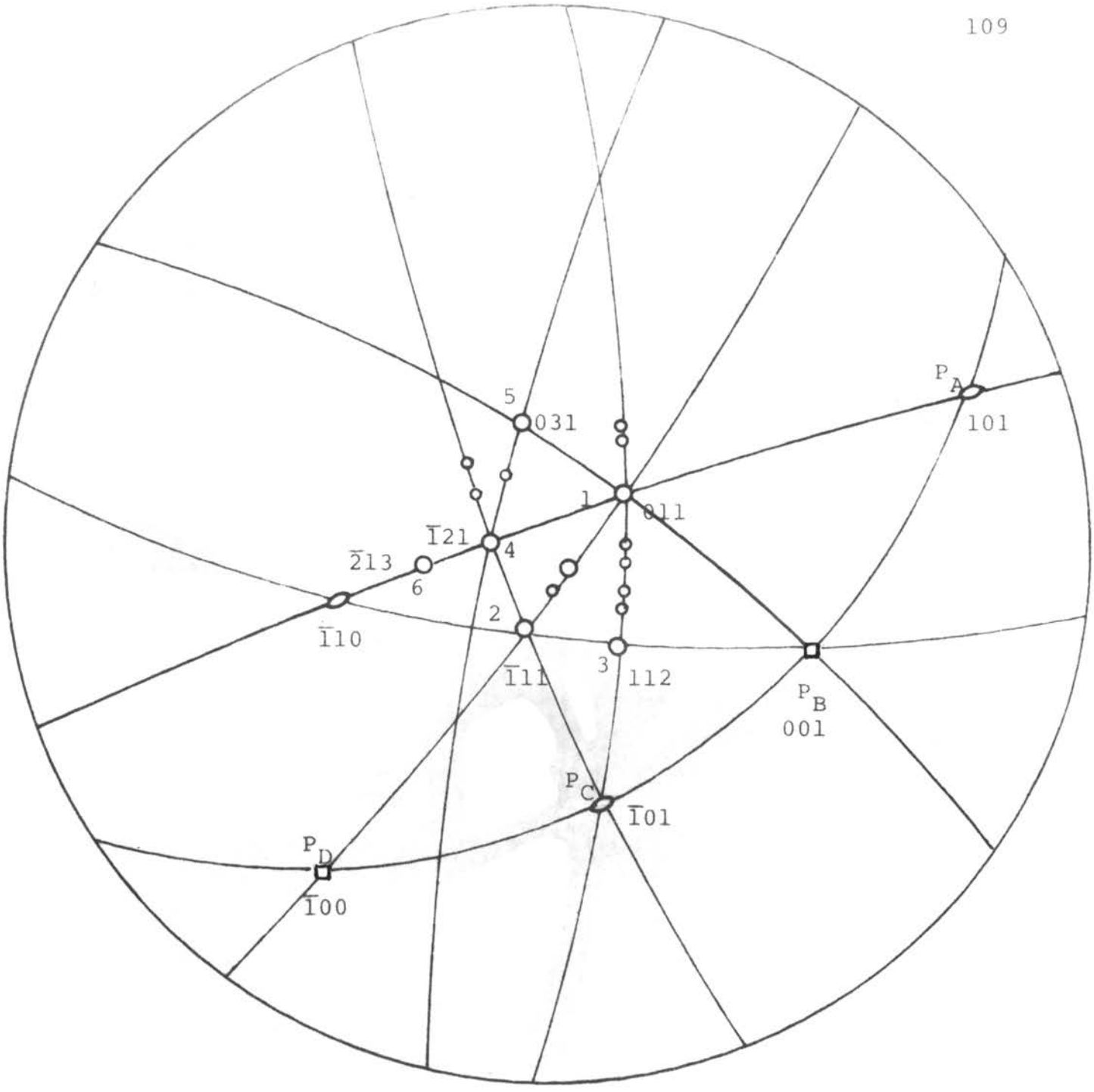

Figure 22. Indexing of a back reflection Laue pattern shown in Figure 21.

TABLE XXVII

Angles measured between pairs of six strong reflections and four poles found at the intersections of zones drawn (in angular degrees) in comparison with the theoretical values (in parenthesis).

Point	1	2	3	4	5	6	P_A	P_B	P_C	P_C
1		35 (35.3)	30 (30)	30 (30)	27 (26.6)		60 (60)	45 (45)	60 (60)	
2			20 (19.5)	20 (19.5)	43 (43.1)			55 (54.7)	36 (35.3)	
3				34 (33.6)	50 (49.8)	40 (40.2)				
4					25.5 (25.4)	11 (10.9)				
5						32 (32.3)				
P_A								45 (45)	90 (90)	
P_B							45 (45)		45 (45)	90 (90)
P_C								45 (45)		
(hkl)	011	$\bar{1}11$	112	$\bar{1}21$	031	$\bar{2}13$	101	001	$\bar{1}01$	$\bar{1}00$

the indices are correctly assigned.

Actually, the stereonet projection is somewhat unecessary because direct angular measurements between spots on the film and symmetry examinations around major spots provided almost sufficient information for correctly indexing the pattern. Let us neglect P_A, P_B, P_C and P_D which are found as intersections of zones drawin the net. Symmetry examinations still lead to assign ment of points 1 and 2 as (011) and (111), because of their two-fold and three-fold symmetry respectively. With this assumption, all other points should be indexed as listed in Table XXVII, and the angles between the pairs of points should agree with the theoretical values.

5. Corrosion patterns of iron.

a. Grain orientation distribution on sample of zone-refined iron. The orientation distribution of zone-refined iron was examined by taking Laue patterns of each grain. For this examination, a piece of zone-refined iron was sliced and etched for a short time (about 2 minutes) with aqua regia to reveal only the grain boundaries. The surface orientation of of eight large grains was examined by indexing each pattern in the manner previously described, and the results are plotted in a standard (001) projection as shown in Figure XXVIII. This projection shows a random distribution of surface orientation of grains of zone-refined iron.

b. Corrosion patterns of zone-refined iron in acids. After prolonged reaction of the samples with various acids, they were washed with distilled water and acetone, then dried in hot air. The structures of the corroded surface of each specimen were examined under a Reichert optical microscope.

The surface of the specimens attacked by concentrated hydrochloric acid was very clean and had a shining metallic luster, while those treated with sulfuric and hydrofluoric acids were covered with whitish-gray salts. Those treated in 1.5 normal nitric acid and 25 % aqueous solution of aqua regia were partly covered with a black or brown film, probably iron oxides.

Because of the corrosion products on the surfaces of the specimens, the microscopic examination was some what difficult in the last two cases. Nevertheless the results of microscopic examinations showed that the surface structures of all specimens treated in various acids are generally similar: i.e., all grain surfaces consisted of small parallel steps arranged in a certain crystallographic direction.

It is concluded from the microscopic examinations that there are generally three major corrosion patterns on the surface of the specimens. Patterns were obtained where (1) a parallel set of grooves running nearly parallel to the sur-

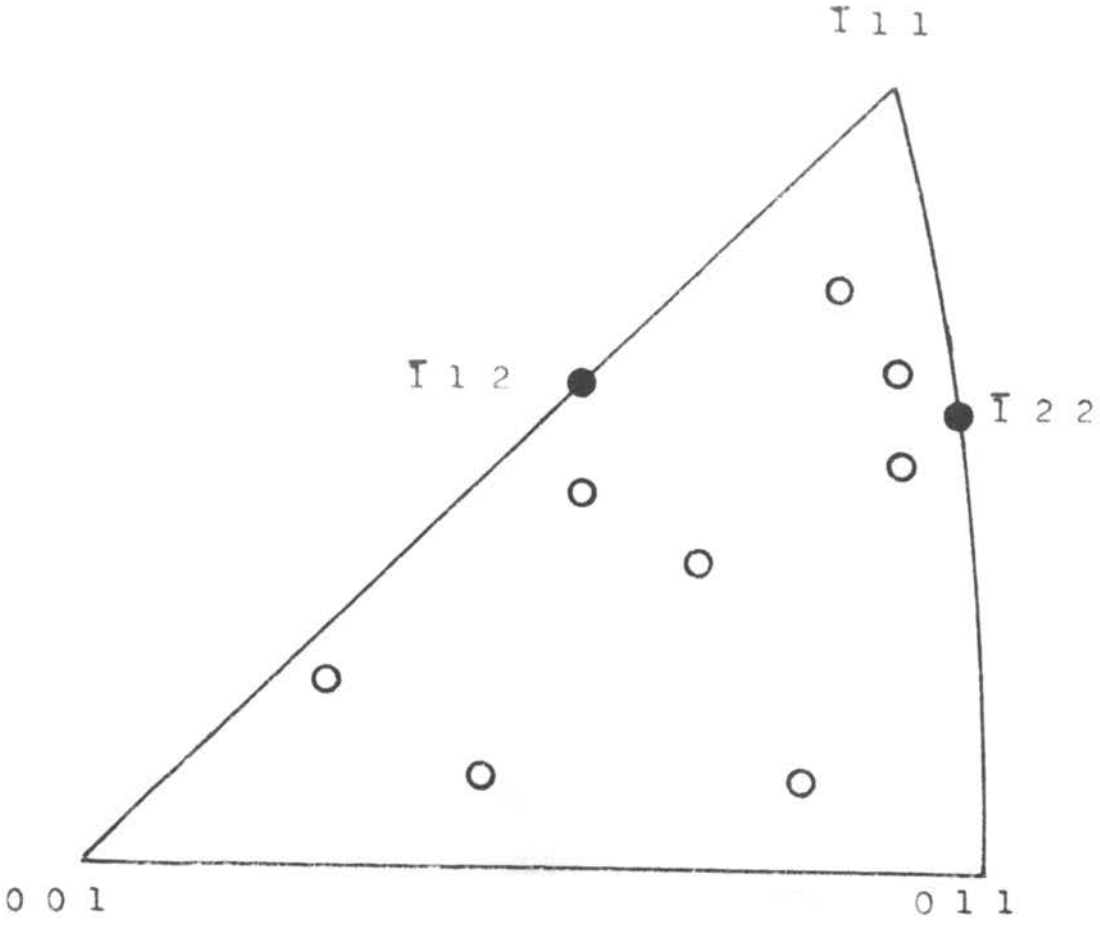

Figure 23. Surface orientations of large grained zone refined iron specimen.

face of the specimens is present (Figure 24), (2) an array of small pyramids appears on the grains (Figure 25) and (3) a set of parallel, somewhat irregularly shaped steps making a certain angle with the specimen surface appears (Figure 26).

c. Orientation of planes and steps developed during corrosion. In order to determined the crystallographic planes of the facets developed during corrosion, Laue back reflection pictures were taken, adjusting the reflecting planes with the aid of the two circle optical goniometer, perpendicular to the X-ray beam.

(1) Orientations determined by the X-ray method. All of the Laue patterns obtained from the larger area facets of different grains, attacked by various acids were indexed. The orientations of these facets are shown in Figures 27, 28, 29 and 30.

It was found for the specimen, treated in concentrated hydrochloric acid, that among eleven different grains giving the strongest reflections, six were close to the (011) plane, four to $(\bar{1}22)$, and one to $(\bar{1}23)$. The specimen treated in 25 % aqua regia produced seven different grains of which six had steps close to (011) and one to $(\bar{1}22)$. Dilute sulfuric acid caused steps on grains close to the (011) plane. In

Figure 24. Corroded surface of zone-refined iron, attacked in conc. HCl for 12 hours, x 320. Note a parallel set of grooves

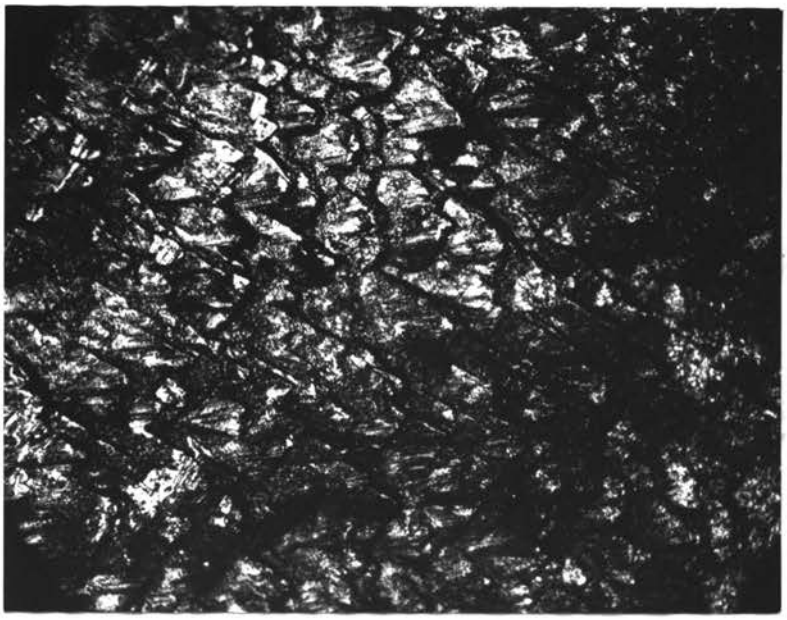

Figure 25. Corroded surface of zone-refined iron, attacked in conc. HCl for 12 hours, x 320. Note a parallel set of dark lines within the triangular facets.

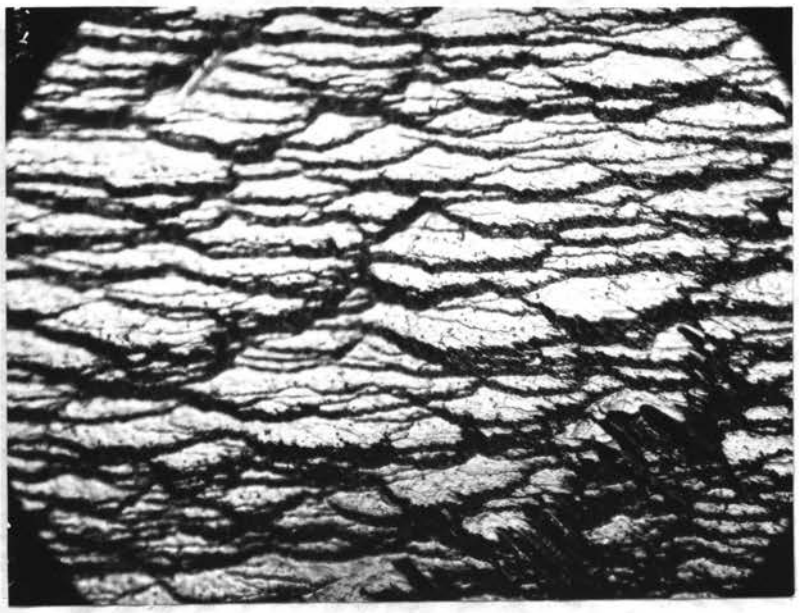

Figure 26. Corroded surface of zone-refined iron, attacked in conc. HCl for 12 hours, x 320. Note the irregular steps parallel to each other.

1.5 normal nitric acid out of seven facets examined, five developed steps close to (011) and two to $(\bar{1}22)$. In hydrofluoric acid, because of the corrosion products formed, the facets developed were too difficult to adjust in the optical goniometer. Therefore, no attempts were made to study such specimens.

As shown in the results of the orientation studies, the steps developed on the grains during corrosion in acids are most likely to be parallel to (011) and (122) planes.

The angles between the original specimen surface and the steps on the grains examined by Laue patterns were all within 30°, and it was almost impossible to examine the narrow side steps (beside the larger area steps), because of limitaions in the geometry of the experimental set-up.

(2) Orientations determined by goniometric measurements. Though the crystallographic planes developed (with large area) on the grains were determined by X-ray techniques, there were still some other faces which remained unknown constituting the sides of the steps with larger area. As mentioned before, the geometry of the specimen surface and of the Laue camera set-up made it impossible to determine the crystallographic planes of such side faces. Here the two-circle optical goniometer was a useful tool in attacking this

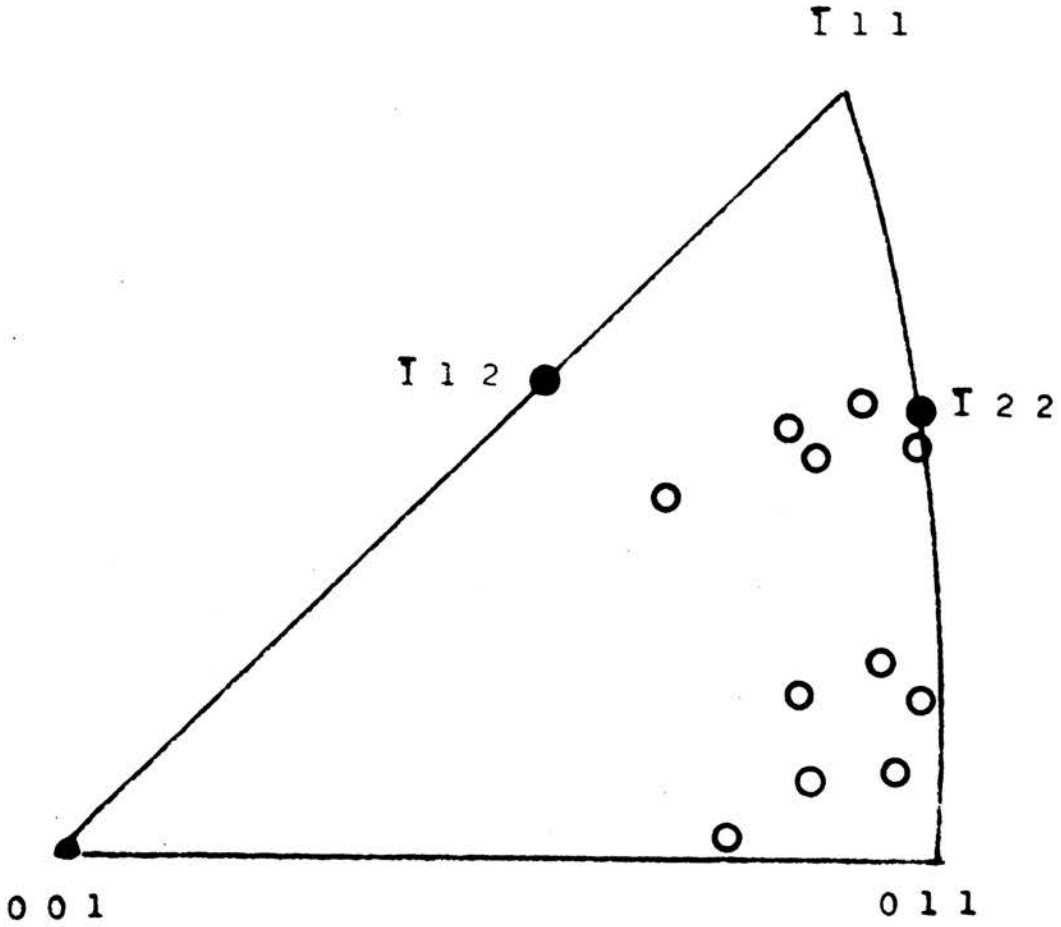

Figure 27. Orientations of the best-defined facets in each of tengrains in specimen treated in concentrated hydrochloric acid.

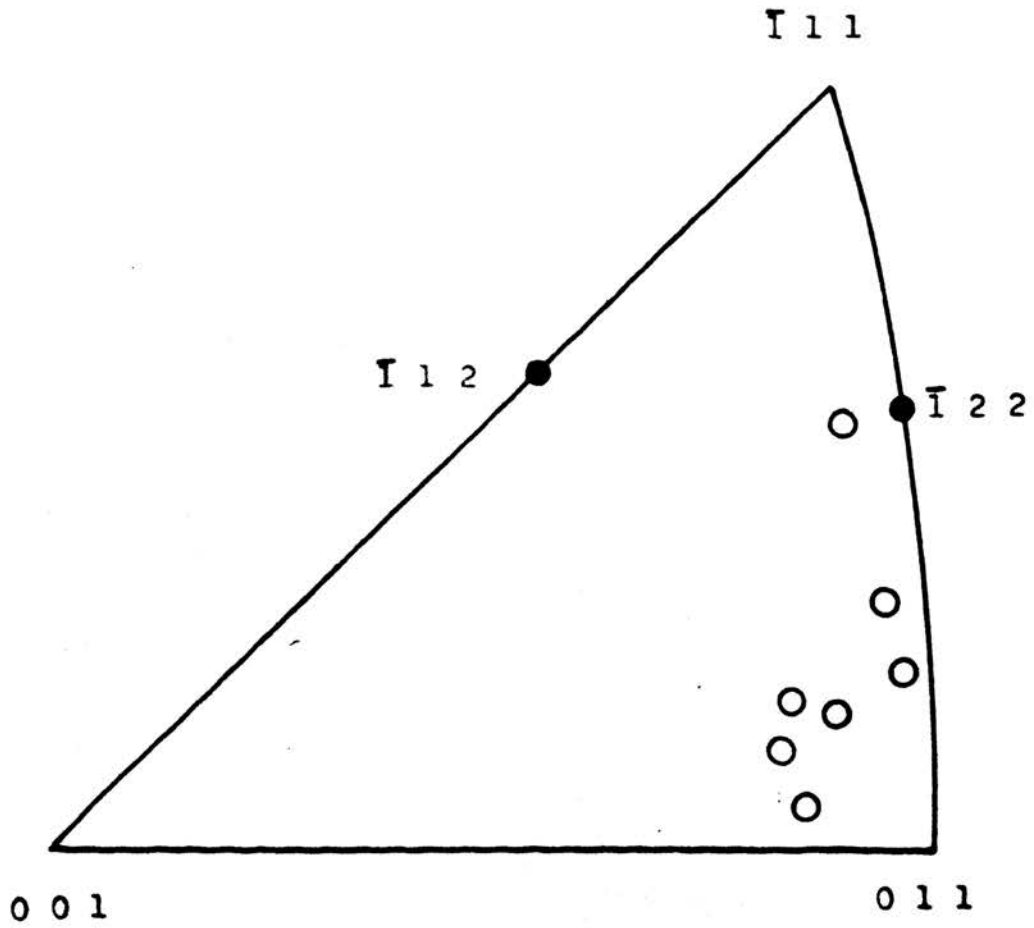

Figure 28. **Orientations of facets of zone refined iron treated in 25 % aquaregia**

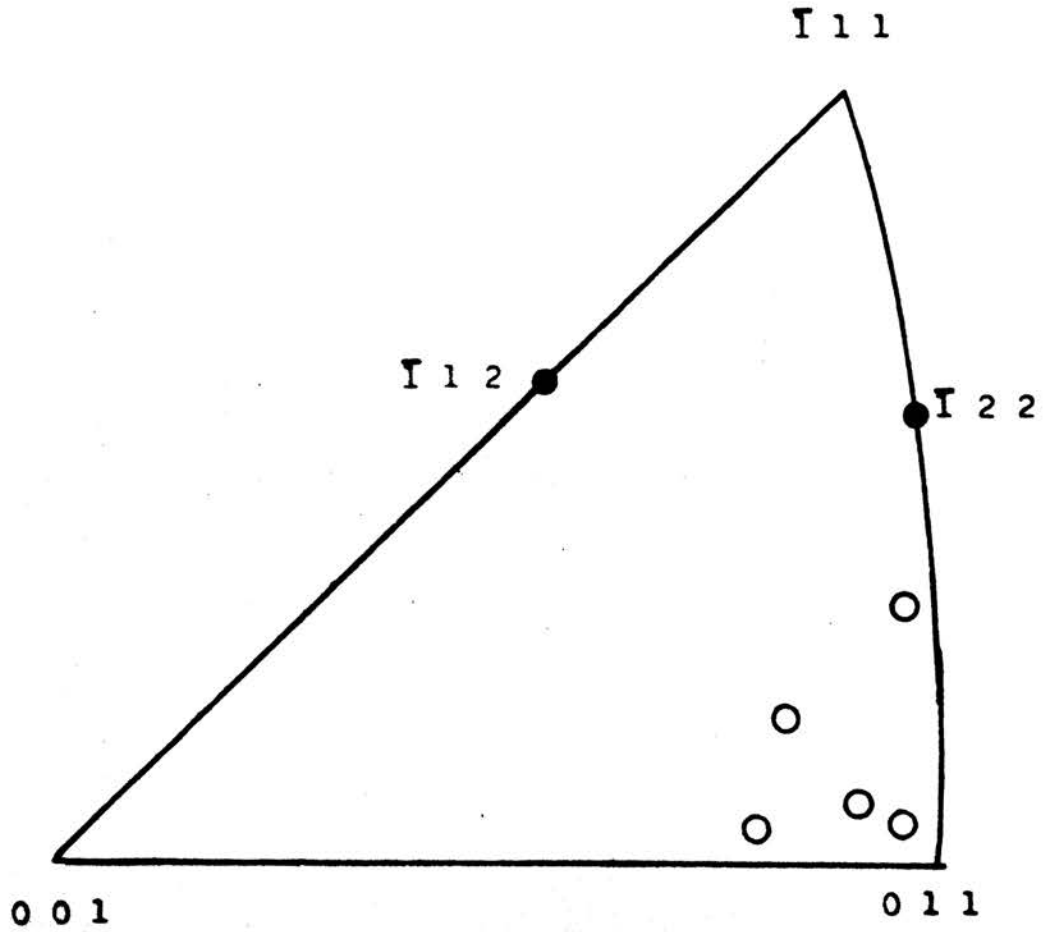

Figure 29. **Orientations of facets of zone refined iron treated in diluted sulfuric acid.**

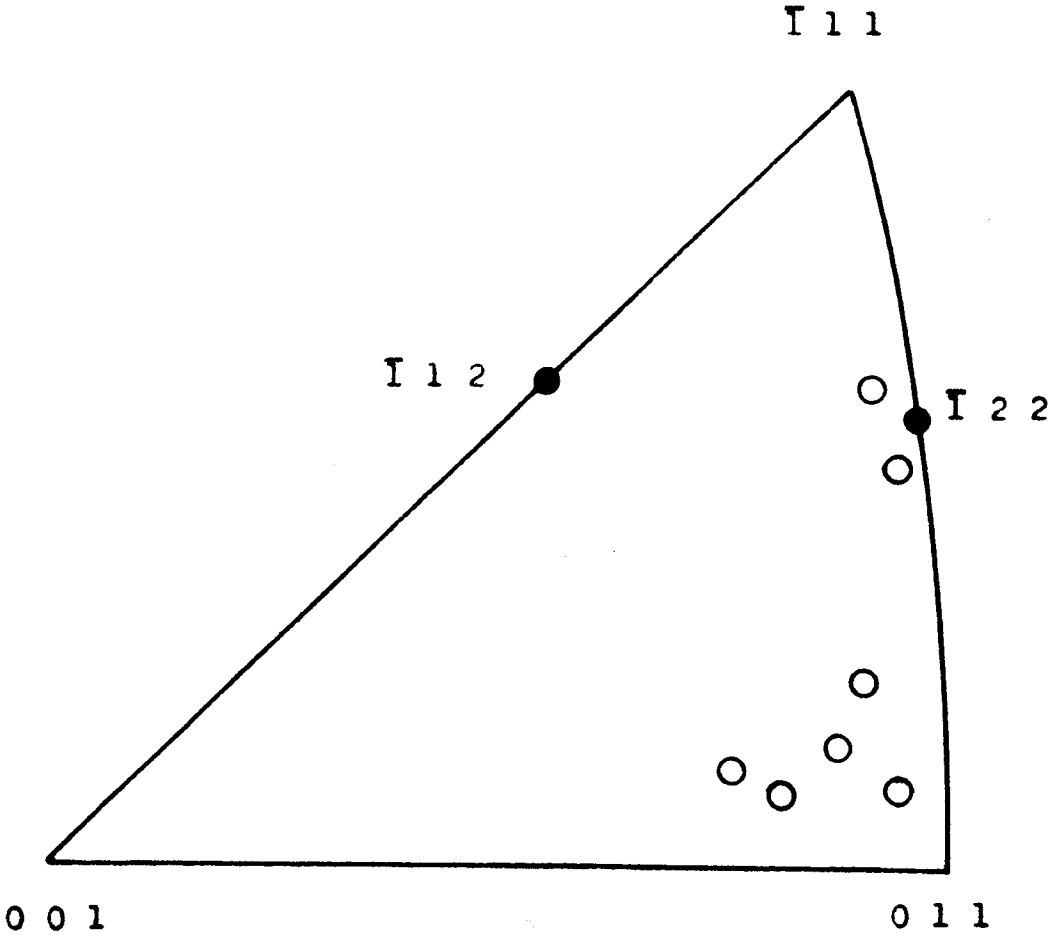

Figure 30. Orientations of facets of zone refined iron treated in 10 % nitric acid.

problem, knowing the reference direction and plane.

On each pattern, the straight lines on the surface (actually grooves formed during corrosion) and the planes with maximum reflectivity served as references. Such references were always the (011) planes, known from previous studies, and the grooves having the $[\bar{0}11]$ direction.

Knowing the reference direction and plane, the crystallographic planes of the side faces in each of the three major patterns could be determined on the two-circle optical goniometer as shown below.

Pattern 1. The specimen was mounted on the optical goniometer head in such a way that the horizontal circle would rotate around the reference axis of one of the grains, and the maximum reflection would be observed at the zero point of the horizontal circle. Then, sending a light signal, the horizontal circle was rotated slowly. Each angle where reflection was observed was recorded noting its relative intensity: i.e., at about +20° a weak reflection, at about -20° a medium intensity reflection, and at about +55° a very weak reflection, in addition to very strong reflection at the zero point. Since these reflections are all from planes parallel to the $[0\bar{1}1]$ direction, they all belong to the $[0\bar{1}1]$ zone. Now, the angles at which the reflections were observed were

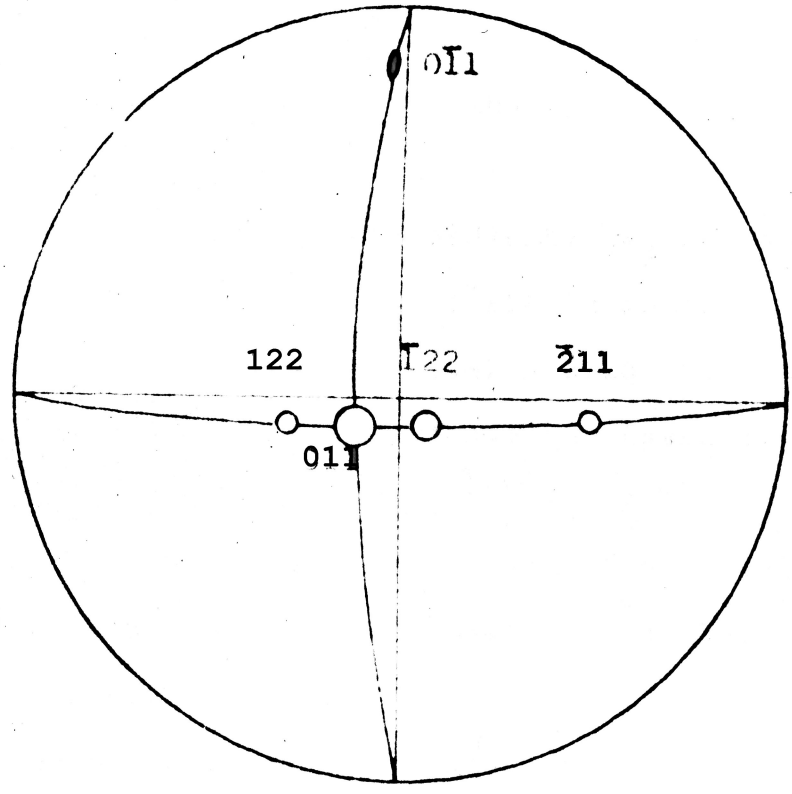

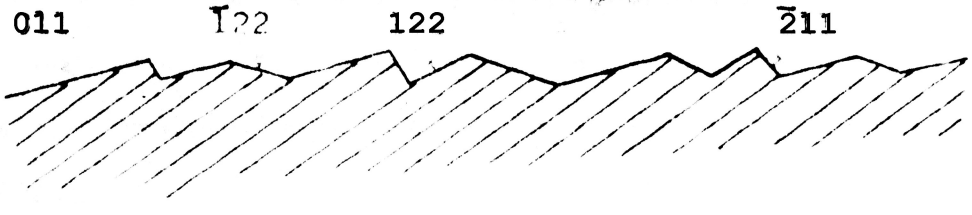

Figure 31. Results of goniometric measurements for patter 1 (shown in Figure 24) and indesing of the reflecting planes (above). A schematic diagram of the vertical section running perpendicular to grooves (beolow).

plotted on the [0$\bar{1}$1] circle of the (011) standard projection and the indices of the planes giving these reflections were found by comparing their angles with those of the theoretical positions of the planes on the projection (see Figure 31). The results are (122), ($\bar{1}$22 and ($\bar{2}$11) in addition to (011). A schematic diagram of the vertical section running at right angle with the grooves is also shown in Figure 31.

Pattern 2. This pattern on some of the grains is characterized by the appearance of small triangular planes in a certain orientation, evidently belonging to pyramids whose one face is developed into a larger area while the others are very narrow. When the faces with larger area were examined under higher magnification, sets of fine straight grooves were found on the surface. Laue patterns of this grain showed that the triangular planes and the set of fine straight grooves on them correspond to the crystallographic plane and direction of the pattern, i.e., (011) plane and [0$\bar{1}$1] direction. These facets and grooves were, therefore, used as reference plane and direction.

First, the specimen was mounted on an optical goniometer in the same way as for pattern 1. Rotating around the reference axis of [0$\bar{1}$1], three reflections were observed: i.e., a very strong reflection set at the zero point, a strong one at about -20° and weak one at about +20°.

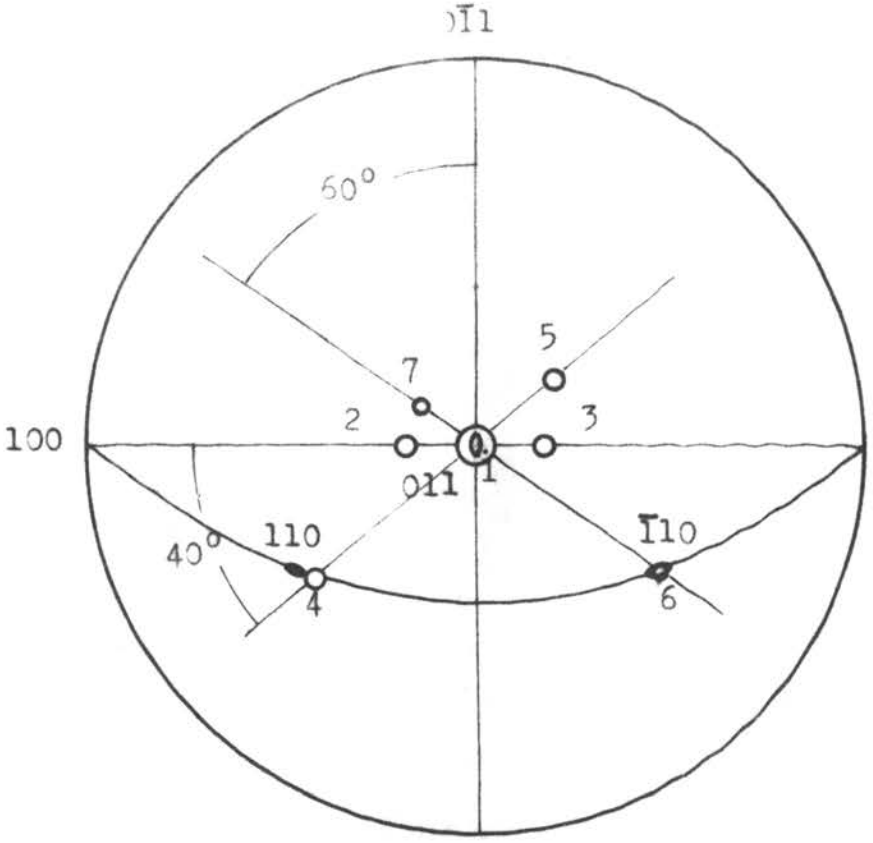

Point 1 ... very strong ... (011)

Point 2 ... strong...(122) Point 3 ... weak ...($\bar{1}$22)

Point 4 ... medium...(110) Point 5 ....weak ...($\bar{1}$12)

Point 6 ... medium...($\bar{1}$10) Point 7 ... weak ...(123)

Figure 32. Results of goniometric measurements for pattern 2 (shown in Figure 25) and indexing of the reflecting planes.

Next, at each 5° of rotation of the vertical circle, the horizontal circle was rotated to observe the reflections. At 40° (clockwise) rotation of vertical circle, there were two additional reflections, beside the very strong reflection at zero point: a medium intensity reflection at -56° and a weak one at +30°. Two more reflections were observed, when the vertical circle was rotated by 60° (counterclockwise); a medium intensity reflection at +60° and a weak one at -20°. All observed reflecting angles were plotted on the (011) standard projection and indexed as shown in Figure 32.

Pattern 3. The reference axis and plane were determined from Laue patterns for grains showing the microscopic pattern 3. Here again the reference plane (011) and reference axis [0$\bar{1}$1] could be found. The latter was drawn on the grain surface with a pencil: this axis runs almost parallel to one set of arrays of the facet edges as shown in Figure 26. The goniometric measurements were made in same way as for pattern 2 and reflections were observed at the following angles: during rotation of the horizontal circle around the reference axis, a very strong reflection set at the zero point appeared and a weak one at about +20°. After rotating the reference axis 60° counterclockwise, a weak reflection appeared at about +60° on horizontal circle. These observed angles were plotted on a (011) standard projection and indexed. Figure 33 shows the results.

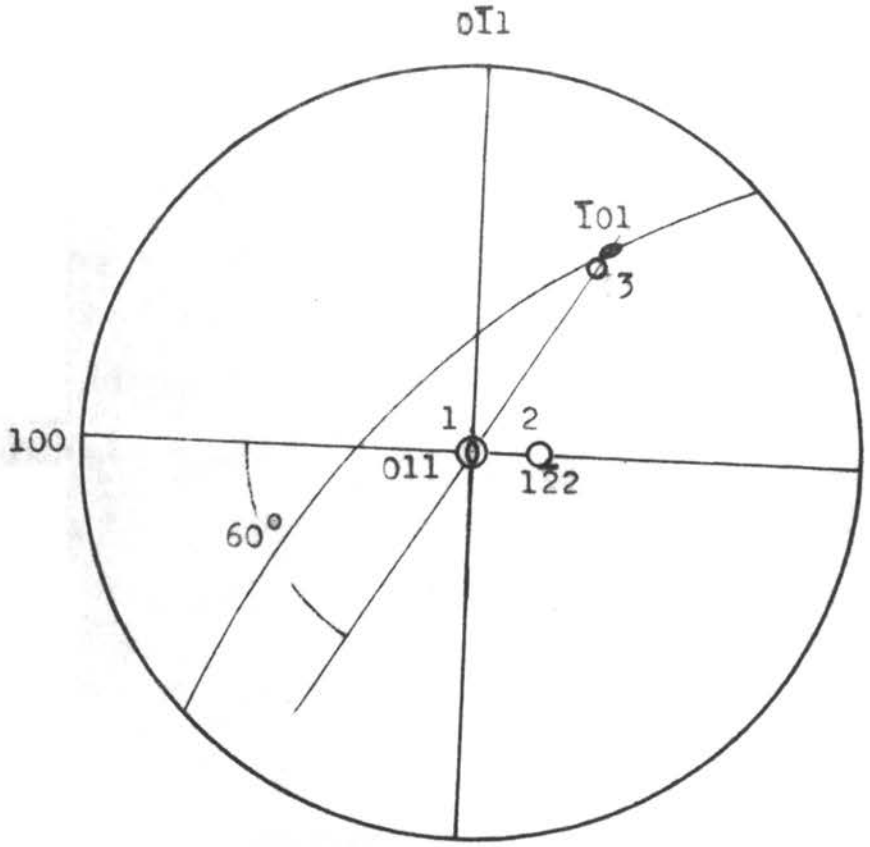

Point 1 ... very strong ... (011)

Point 2 ... weak ..... (Ī22)

Point 3 ... weak .....(Ī01)

Figure 33. Results of goniometric measurements for pattern 3 (shown in Figure 26) and indexing of the reflecting planes.

From the above orientation determinations of the corrosion patterns of iron, (110) and (122) planes were found by X-ray diffraction and goniometric measurements showed planes such as (112), (122) (123) and (110). This means the corroded surface of the zone-refined iron consist of several specific crystallographic planes as listed above.

However, it should not forgotten that the X-ray determinations were possible only for the facets which gave the strongest light reflections and that the relative intensities of reflected light do correspond to the relative areas of the facets on which the light reflected.

B. Anodic Dissolution Studies.

The literature review revealed that several workers had already reported on the anodic disintegration of steel and Welch presented evidence of formation of metallic particles upon dissolution of iron and of high purity iron in sulfuric acid. A further investigation was made to determine the degree of disintegration of high purity iron under conditions of dissolution.

1. Qualitative study. Qualitative runs were made in sulfuric and hydrochloric acids of various concentrations as follows: A rectangular shaped, zone-refined iron piece was made the anode of an electrolytic cell by connecting it

to the positive terminal of a battery and a platinized platinum electrode as cathode. A variable resistance and an ammeter were also placed in the circuit to control and measure the current. The electrodes were placed in a stand and approximately 50 ml of a certain electrolyte was poured into a clean beaker. The electrodes were then dipped into the electrolyte and current passed for a certain time. Visual examination, employing a magnifying glass, was used to check for particle formation. Special attention was given to the observation of the anode surface, gas bubble formation and disintegration. After some period of time the electrode was removed, rinsed and dried for the next experiment.

An attempt was made to collect any particles which might have fallen from the anodic surface by placing carbon tetrachloride under the electrolyte (in the case of sulfuric acid) to collect the particles before they were dissolved by the electrolyte. This attempt was, however, unsuccessful. The reason could be, either there was no disintegration at all or that the particles were too small and light to penetrate into the carbon tetrachloride. In order to differentiate between these two possibilities, a quantitative study was necessary.

2. Quantitative study. For the quantitative study of

disintegration a cell was set up as shown in Figure 34. The anode was constructed of a rectangularly shaped, zone-refined iron piece whose surface was ground and polishes on metallographic paper. The surface area was measured to determine the current density. Electrodes were made by soldering a copper wire to one end of each specimen. The wire was enclosed in a glass tube and the soldered portion was covered with hard wax. A platinized platinum electrode was used as a cathode.

The anode was accurately weighed on an analytical balance before each run. An one ohm shunt was introduced into the circuit to measure the current with a Honeywell Electronik 18 Potentiometer (see Figure 34). The time and current were automatically recorded and simultaneously the time was checked with a stop watch. All factor except the variable being investigated, were held constant in the successive runs.

After each run, the anode was washed with distilled water which was collected and joined with the original electrolyte for further titration. The anode was then dried in hot air, and weighed again. The total weight loss was found by subtracting the final weight from the original. This loss is due to anodic dissolution, self-dissolution and possibly disintegration. Since the amount of electrolytic and self-dissolution can be calculated from current, time, rate

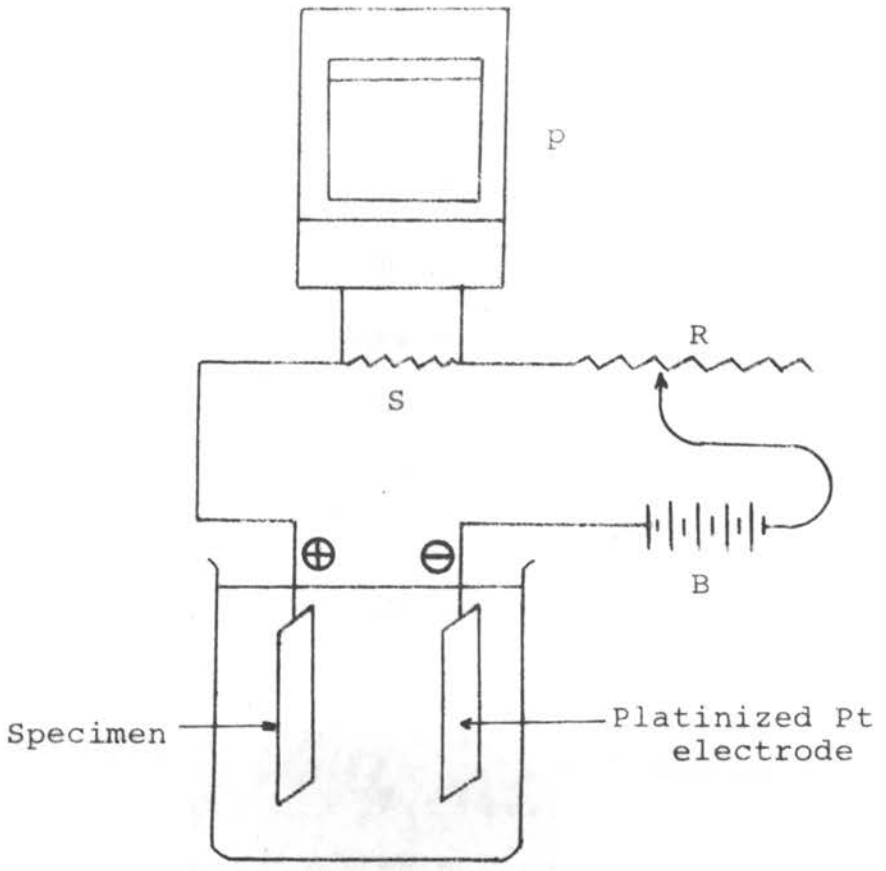

p Honeywell Electronik 18 Potentiometer

S 1 ohm shumt

R Variable resistance

B Battery (12 volt D.C.)

Figure 34. Experimental set-up for a quantitative disintegration study.

of self-dissolution, and surface area, the amount of disintegration can be evaluated.

For the determination of the dissolved iron, the electrolyte was titrated with 0.1 N $K_2Cr_2O_7$ solution using a 0.2 % aqueous solution of sodium diphenylamine sulfonate as indicator. Titration was made always after reducing iron (Fe^{++}) with tin chloride solution. The details of the titration are given in the Appendix. This titration confirmed that the weight loss of the iron sample went all into solution.

The amount of self-dissolution was calculated from the measured surface area, time and the dissolution rate of the same material found by Welch. The calculated values of this self-dissolution were subtracted from the total weight loss, and the remainder was compared with the amounts found from Faraday's law from the amount of coulmbs which passed through the cell. From this the percent of disintegration was calculated by:

$$\% \text{ disintegration} = \frac{\left(\begin{matrix}\text{Total}\\ \text{weight}\\ \text{loss}\end{matrix}\right) - \left(\begin{matrix}\text{Self-}\\ \text{dissol-}\\ \text{ution}\end{matrix}\right) - \left(\begin{matrix}\text{Weight cal-}\\ \text{culated by}\\ \text{Faraday's law}\end{matrix}\right)}{(\text{Total weight loss}) - (\text{Self-dissolution})} \qquad (23)$$

The disintegration percentage was investigated at various concentration of sulfuric and hydrochloric acids and at various current densities.

3. Experimental results. Special attention was paid to observations of the anodic surface, the behavior of gas bubbles on it, and any metal particles scattering from the anode. No metallic particles could be observed on the bottom of the beaker, except in the case of one specimen whic was cold worked and recrystallized (see the section of discussion). The anodic surface was always clean at lower current densities, but at higher ones close observation was difficult because of vigorous gas evolution over the entire anodic surface. Most of the gas bubbles moved upwards as soon as they left the surface, however a few shiny small bubbles moved downwards from the surface and their size increased slightly during downward movement. They, then moved upwards again before reaching the bottom of the beaker.

The results of quantitative studies in hydrochloric and sulfuric acids are listed in Table XXVIII to XXXII.

TABLE XXVIII

Results of quantitative disintegration studies of pure iron in 1 N hydrochloric acid.

Current density (mA/cm^2)	Total weight loss (g)	Weight loss due to electrolytic dissolution (g)	Weight loss due to self-dissolution (g)	Disintegration (in %)
100	0.0729	0.0729	0.000014	0.00
	0.0737	0.0729	0.000014	1.14
	0.0652	0.0659	0.000014	-1.07
	0.0661	0.0660	0.000014	0.15
			average	0.04
500	0.1712	0.1702	0.000007	0.59
	0.1703	0.1702	0.000007	0.06
	0.1733	0.1736	0.000007	-0.18
			average	0.16
740	0.5142	0.5140	0.000014	0.04
	0.5140	0.5140	0.000014	0.00
	0.4929	0.4920	0.000014	0.18
			average	0.07

TABLE XXIX

Results of quantitative disintegration studies of pure iron in 3 N hydrochloric acid.

Current density (mA/cm^2)	Total weight loss (g)	Weight loss due to electrolytic dissolution (g)	Weight loss due to self-dissolution (g)		Disintegration (%)
50	0.0348	0.0342	0.0003		0.86
	0.0345	0.0339	0.0003		0.87
	0.0338	0.0339	0.0003		-1.18
	0.0363	0.0356	0.0003		1.10
	0.0338	0.0337	0.0003		-0.59
				average	0.51
100	0.1043	0.1042	0.0005		-0.39
	0.1084	0.1078	0.0005		0.09
	0.1036	0.1029	0.0005		0.19
				average	-0.04
200	0.1440	0.1424	0.0003		0.90
	0.1070	0.1068	0.0002		0.00
	0.1078	0.1078	0.0002		-0.19
				average	0.36
500	0.1294	0.1289	0.0002		0.23
	0.1252	0.1250	0.0002		0.00
	0.1277	0.1276	0.0002		-0.08
	0.1369	0.1367	0.0003		-0.07
				average	0.02

TABLE XXX

Results of quantitative disintegration studies of pure iron in 5 N hydrochloric acid.

Current density (mA/cm^2)	Total weight loss (g)	Weitht loss due to electrolytic dissolution (g)	Weitht loss due to self-dissolution (g)	Disintegration (%)
150	0.1692	0.1667	0.0033	-0.47
	0.1287	0.1250	0.0025	0.93
	0.0826	0.0807	0.0017	0.24
	0.1245	0.1211	0.0025	0.72
			average	0.35
250	0.1305	0.1289	0.0017	-0.08
	0.1721	0.1702	0.0022	-0.17
	0.1348	0.1341	0.0017	-0.74
			average	-0.33
500	0.0924	0.0903	0.0006	1.62
	0.1374	0.1354	0.0008	0.87
	0.1336	0.1328	0.0008	0.00
			average	0.083

TABLE XXXI

Results of quantitative disintegration studies of pure iron in 1 N sulfuric acid.

Current density (mA/cm^2)	Total weight loss (g)	Weight loss due to electrolytic dissolution (g)	Weight loss due to self-dissolution (g)	Disintegration (%)
100	0.0239	0.0234	0.00002	2.00
	0.0246	0.0252	0.00002	-2.52
	0.0315	0.0313	0.00003	0.54
	0.0279	0.0278	0.00003	0.25
			average	0.07
200	0.1328	0.1302	0.00003	1.26
	0.1205	0.1198	0.00003	0.56
	0.1265	0.1268	0.00003	-0.26
	0.1265	0.1268	0.00003	-0.26
	0.1229	0.1233	0.00003	-0.35
			average	0.19
500	0.2695	0.2691	0.00003	0.14
	0.2673	0.2674	0.00003	-0.05
	0.2636	0.2639	0.00003	-0.13
	0.2608	0.2599	0.00003	0.34
			average	0.08

TABLE XXXII

Results of quantitative disintegration studies of pure iron in 4 N sulfuric acid.

Current density (mA/cm^2)	Total weight loss (g)	Weight loss due to electrolytic dissolution (g)	Weight loss due to self-dissolution (g)	Disintegration (%)
100	0.1014	0.1007	0.0032	-1.48
	0.0969	0.0955	0.0032	-1.86
	0.1188	0.1146	0.0032	0.84
	0.0896	0.0886	0.0024	-0.44
			average	-0.73
250	0.3395	0.3369	0.0024	0.06
	0.2544	0.2439	0.0024	-0.75
	0.2564	0.2527	0.0024	0.51
			average	-0.18
500	0.1681	0.1667	0.0011	0.18
	0.5252	0.5244	0.0032	-0.46
	0.2539	0.2526	0.0016	-0.12
	0.2534	0.2526	0.0016	-0.39
			average	-0.20

VII. DISCUSSION

1. Corrosion patterns of pure iron. As the microscopic examinations revealed, when a piece of pure iron is corroded by acids, regardless of the acids used and their concentration, steps and small facets parallel to certain crystallographic planes develop on the surface of each grain. In general, the shape of these steps and facets within a single grain belong to one of three major patterns mentioned previously, depending upon the angle the cubic axis makes with the surface of the sample. The crystallographic indices of these steps are close to (110) or some times to (112), (122) and (123), as determined by X-ray and goniometric measurements. However, most of the X-ray determinations showed the plane close to (110), except for the specimen treated in concentrated hydrochloric acid where (122) plane was found almost as often as (110). As mentioned before, X-ray determinations were made for the faces giving the most intense light reflections which means the faces are larger compared with the areas of others and cleaner. Thus the planes determined by X-rays can be considered as those having clean larger areas than others. Such a plane is (110). Therefore, it can be concluded that when iron dissolves in acid, the (110) plane dissolves most evenly. Goniometric measurements revealed other planes such as (112), (122) and (123) besides (110). These determinations were made of planes which make

larger angles (more than 20°) with the original specimen surface. It is impossible to determine these planes by X-ray diffraction because of the geometry of the specimen arrangement.

It can be easily understood that the (110) plane corrodes mostly evenly and hence form the steps, ledges or facets of the corrosion patterns. In all probability the behavior of the (110) plane is due to the fact that a b.c.c. structure has the highest atomic density of surface atoms on this plane, (110), where one has six nearest neighbor atoms, i.e., the coordination number is six. Then, why do not (100) and (111) planes appear as the facets, as they have higher atomic densities than those of (112), (122) and (123) which, nevertheless, developed during corrosion. This question may be answered by considering further the geometry of surface atoms. When an atom is coordinated by more atoms, it should be harder to take away this atom, because of the stronger bonding. Therefore, the coordination number is also important as well as the packing density on the surface plane. The coordination numbers of the surface atoms on various planes and the relative atomic densities of these planes are given in Table XXXIII. According to Table XXXIII the (122) plane has the lowest coordination number of a surface atom and the least atomic density, consequently the conclusion is that the surface atoms on the (122) plane can be removed readily.

TABLE XXXIII

Coordination numbers of surface atoms on various planes and atomic densities of such planes in a b.c.c. lattice.

(h k l)	Coordination No. of surface atom	Relative atomic density
(1 0 0)	4	1.000
(1 1 0)	6	1.520
(1 1 1)	4	0.577
(1 1 2)	5	0.408
(1 2 2)	4	0.334
(1 2 3)	5	0.535

Next, the (112) and (123) planes have also lower atomic densities although the the coordination numbers are five. Indeed the three planes, (122), (112) and (123) were found from goniometric measurements; even X-ray determinations showed these three planes occasionally. On the goniometer, these planes produced a medium or weak reflected light, while the reference plane, (110) reflected very strongly, meaning that the former three planes did not have such a large and even surface as the (110) plane. Considering the readiness of removing the surface atoms on (112), (122) and (123) as discussed above, it may be concluded that (112), (122) and (123) planes of pure iron are fast corroding planes and as a result of their rapid corrosion the (110) plane appeared relatively

even and larger in extent. In other words, the (110) plane is the major one to form the large area shiny steps and facets. Their side faces are formed by (112), (122) and (123) in the patterns.

It was difficult to measure the angles between the original surface and the facets developed during corrosion. However, pattern 1 was observed always when the (110) plane was close to the surface of the original grain. The angle between these planes were estimated within several degrees. However, pattern 3 was found rarely, while most of the corroded surfaces showed either pattern 1 or 2.

2. Anodic dissolution of pure iron. The results of the quantitative disintegration studies of pure iron show that there is no significant amount of disintegration of the anode in both hydrochloric and sulfuric acids. In all cases, the average values are less than one percent. This small percentage can be considered within the limits of experimental errors, particularly considering those negative values whose absolute values are compatible with the positive ones. However, it was frequently observed that anodic gas bubbles went down and then up, suggesting that these bubbles stuck to minute iron particles. Upon dissolution of metal the particles (bubbles) went up. Furthermore, when a piece of zone-refined iron was anodically dissolved in concentrated

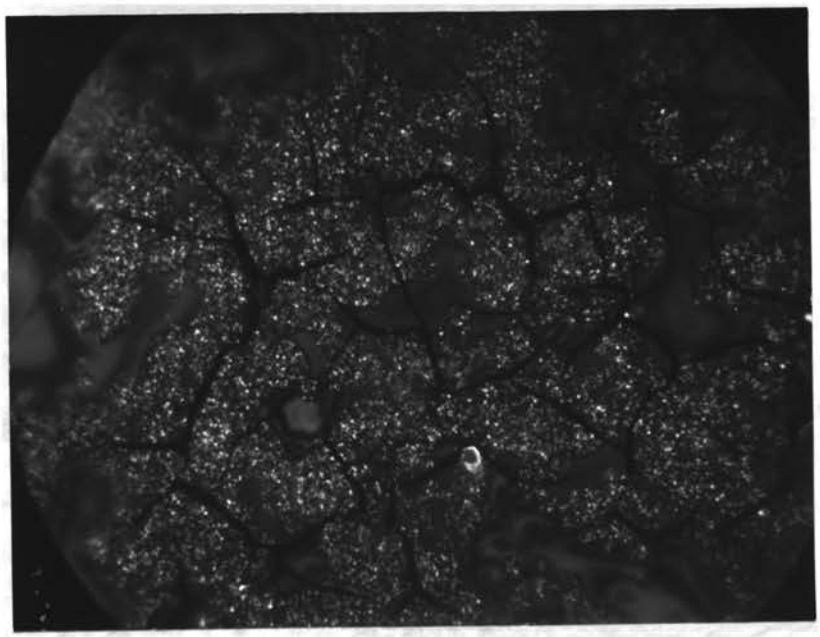

Figure 35. Minute iron particles(white) on a surface film formed upon anodic dissolution of zone-refined iron in conc. HNO_3. x 1430.

nitric acid at a current density of 500 mA/cm^2, the current went down gradually to zero because of the passivation and there were fine black particles on the anodic surface (see Figure 35). These particles were identified as iron by the X-ray patterns.

Nevertheless, one specimen did show about 3.5 percent of anodic disintegration in 3 normal hydrochloric acid. This specimen was cold-rolled and recrystallized at 500°C in vacuo and the grain size was very fine (c.f. the average grain size of zone-refined iron is about 5 mm in diameter). The microscopic pictures of this sample are shown in Figure 36. The size of the particles formed due to disintegration of the anode ranged from about 0.2 to 0.8 mm in diameter (see Figure 37). They are certainly not the same kind of chunks as proposed by March and Schaschl to explain the positive difference effect. They assumed that the particles were very small consisting of only a few atoms. It can be easily noticed that the specimen under discussion has a very uneven grain size (Figure 36) and at some locations the large grains are surrounded by several fine grains and also that the particles (Figure 37) of the disintegrating anode have the same size as the mother-specimen's. Therefore, those particles separating from the anode of pure iron are considered to be the products of grain boundary failure due to rapid dissolution of surrounding finer grains. Anodic dissolu-

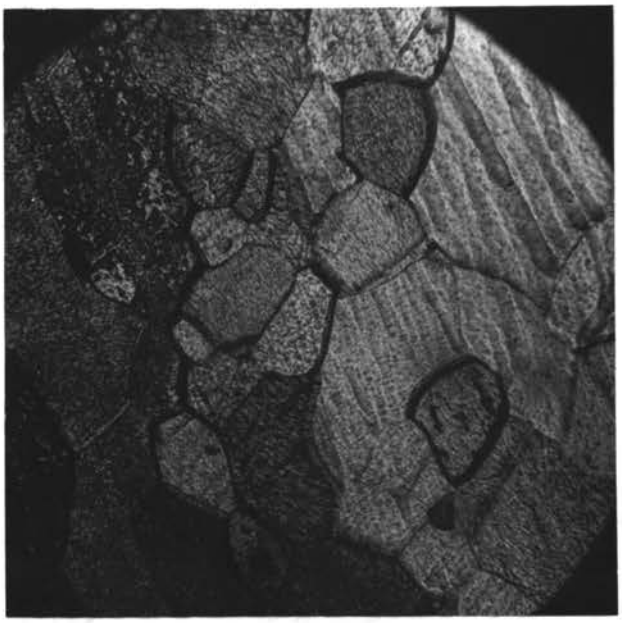

Figure 36. Grain size of a zone-refined iron (recrystallized) sample which yielded disintegration. x 150.

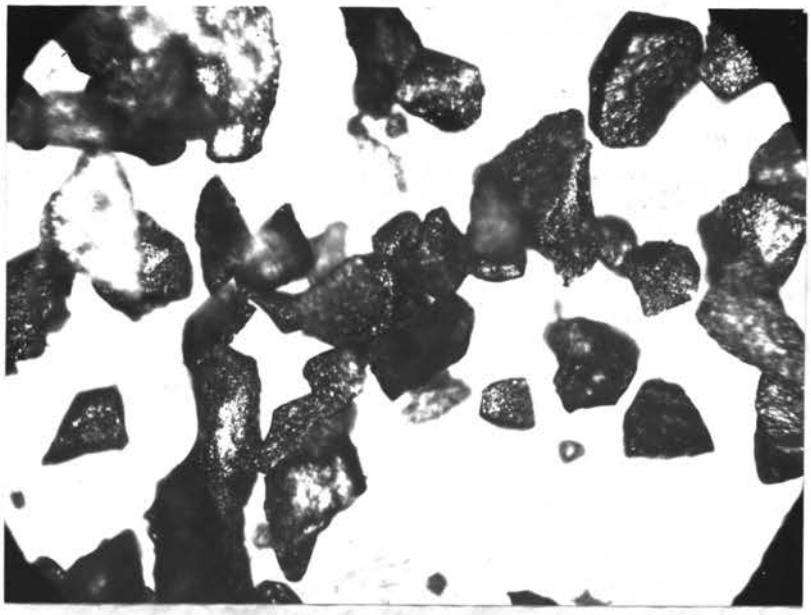

Figure 37. Particles formed due to anodic disintegration of recrystallized zone-refined iron in 3 N HCl. x 150.

tion of pure iron proceeds by dissolving atoms one by one and there is apparently no anodic disintegration.

In order to prove this grain boundary failure and separation of the grains from the anode, electrolytic iron was used which also has an uneven grain size and whose grains are columnar. When the longitudial side of these columnar grains was exposed to the acid, a large amount of disintegration could be observed (see Figures 38 & 39). The particles dropping out of the anode were columnar in shape as in the mother-metal. However, the plane perpendicular to the columnar axis has a relatively even grain size, and when this face was exposed to the acid, there was only a small amount of disintegration. From all the anodic dissolution experiments, the following conclusion can be drawn: (1) anodic dissolution of pure iron is accompanied by disintegration only to a very small extent and (2) disintegration occurs clearly when an uneven grain sized anode of pure iron is dissolved.

Figure 38. Particles formed due to anodic disintegration of electrolytic iron having a fiber-structure(see next Fig.) in 6 N H_2SO_4. x 150.

Figure 39. Columnar structure of electrolytic iron used for anodic dissolution. x 150.

VIII. SUMMARY

1. When pure iron dissolves in acids (such as conc. HCl, 1.5 N HNO_3, 2 N H_2SO_4, 25 % aqeous solution of aqua regia and conc. HF), the corroded surface shows mainly three kinds of corrosion patterns, which consist of step, ledges or facets.

2. The (110) plane of iron is most evenly attacked and appears as the main facet in each of the three patterns.

3. The (112), (122) and (123) planes are also developed during corrosion of iron in acids, but these planes are not large as compared with the (110) plane.

4. The atomic density and coordination number on the surface plane of the iron specimen are of importance in the formation of corrosion patterns: i.e., the higher these figures, the more even and larger the face developed.

5. On anodic dissolution in sulfuric and hydrochloric acids zone-refined iron does not produce any measurable chunk or disintegration effect.

6. Sometimes iron particles fall off because of the grain boundary failure.

APPENDIX

Zone-refined iron

No. 2536 10.7°C

Front		Back	
93.129	106.948	174.200	F = 0.45012
34.822	20.991	153.692	θ = 80.7689°
			a = 2.86574 Å

No. 2537 10.7°C

Front		Back	
91.225	105.063	172.339	F = 0.44983
32.846	19.010	151.807	θ = 80.7641°
			a = 2.86576 Å

No. 2532 20.0°C

Front		Back	
88.655	102.452	169.753	F = 0.45031
30.411	16.610	149.175	θ = 80.7290°
			a = 2.86607 Å

No. 2533 20.0°C

Front		Back	
91.133	104.908	172.165	F = 0.45062
32.868	19.165	151.597	θ = 80.7316°
			a = 2.86605 Å

No. 2610 30.0°C

Front		Back	
92.385	106.237	173.468	F = 0.45060
34.152	20.300	152.801	θ = 80.6874°
			a = 2.86641 Å

No. 2611 30.0°c

Front		Backe	
89.831	103.686	170.970	Θ = 80.6825°
31.594	17.729	150.282	a = 2.86645 Å

No. 2612 40.0°C

Front		Back	
86.882	100.711	168.001	Θ = 80.6477°
28.672	14.853	147.250	a = 2.86674 Å

No. 2613 40.0°C

Front		Back	
86.285	100.037	167.365	Θ = 80.6464°
27.958	14.199	146.607	a = 2.86675 Å

No. 2614 50.0°C

Front		Back	
92.538	106.381	173.807	Θ = 80.5990°
34.329	20.491	152.926	a = 2.86713 Å

No. 2615 50.0°C

Front		Back	
89.163	103.015	170.389	Θ = 80.6143°
30.952	17.196	149.550	a = 2.86701 Å

No. 2534 59.6°C

Front		Back	
			F = 0.45051
84.088	97.905	165.367	θ = 80.5510°
25.873	12.094	144.393	a = 2.86744 Å

No. 2535 59.6°C

Front		Back	
			F = 0.45057
90.580	104.356	171.798	θ = 80.5732°
32.366	18.588	150.876	a = 2.86725 Å

Iron whiskers

No. 2712 15.0°C

Front	Back	
		F = 0.44953
83.933	165.110	θ = 80.7559°
25.513	144.546	a = 2.86407 Å

No. 2713 15.0°C

Front	Back	
		F = 0.44988
82.599	163.769	θ = 80.7455°
24.216	143.198	a = 2.86408 Å

No. 2714 24.7°C

Front	Back	
		F = 0.44978
79.608	160.834	θ = 80.7017°
21.290	140.161	a = 2.86629 Å

No. 2715 24.7°C

Front	Back	F = 0.44963
83.846	165.084	θ = 80.6981°
25.471	143.396	a = 2.86632 Å

No. 2716 24.7°C

Front	Back	F = 0.44998
88.129	169.277	θ = 80.7066°
29.762	148.624	a = 2.86625 Å

No. 2717 34.8°C

Front	Back	F = 0.45018
88.729	169.912	θ = 80.6682°
30.434	149.173	a = 2.86657 Å

No. 2718 34.8°C

Front	Back	F = 0.45020
82.568	163.753	θ = 80.6674°
24.295	143.023	a = 2.86657 Å

No. 2719 34.8°C

Front	Back	F = 0.45003
82.631	163.841	θ = 80.6740°
24.333	143.108	a = 2.86652 Å

No. 2726 45.2°c

Front	Back	F = 0.45036
83.288	164.486	Θ = 80.6257°
25.028	143.671	a = 2.86692 Å

No. 2727 45.2°C

Front	Back	F = 0.45037
82.587	163.781	Θ = 80.6301°
24.335	142.976	a = 2.86688 Å

No. 2728 56.0°C

Front	Back	F =0.45015
84.632	165.880	Θ = 80.5677°
26.341	144.925	a = 2.86740 Å

No. 2729 56.0°C

Front	Back	F = 0.45009
82.282	163.597	Θ = 80.5729
24.010	142.652	a = 2.86735 Å

No. 2730 56.0°C

Front	Back	F = 0.45081
84.415	165.558	Θ = 80.5659°
26.134	144.631	a = 2.86741 Å

No. 2731 64.0°C

Front	Back	F = 0.45043
88.925	170.186	θ = 80.5401°
30.654	149.184	a = 2.86763 Å

No. 2732 64.0°C

Front	Back	F = 0.45045
82.788	164.062	θ = 80.5356°
24.504	143.041	a = 2.86766 Å

Thermally charged samples

T - 1 Hydrogen charged at 500°C.

No. 2604 At 25.0°C

Front		Back	F = 0.45025
86.923	100.750	168.039	θ = 80.6996°
28.593	14.799	147.383	a = 2.86631 Å

No. 2605 At 25.0°C

Front		Back	F = 0.45031
89.486	103.318	170.581	θ = 80.7088°
31.163	17.372	149.948	a = 2.86623 Å

T - 2 Hydrogen charged at 700°C.

No. 2618 at 25.0°C

Front		Back	F = 0.45035
87.408	101.224	168.494	θ = 80.7061°
29.087	15.290	147.857	a = 2.86626 Å

No. 2619 at 25.0°C

Front		Back	
89.545	103.345	170.592	F = 0.45078
31.373	17.568	149.978	Θ = 80.7066°C
			a = 2.86625 Å

T - 3 Hydrogen charged at 800°C.

No. 2616 at 25.0°C

Front		Back	
89.222	103.062	170.287	F = 0.45078
31.050	17.285	149.676	Θ = 80.7090°
			a = 2.86623 Å

No. 2617 at 25.0°C

Front		Back	
85.513	99.312	166.571	F = 0.45068
27.323	13.543	145.973	Θ = 80.7169°
			a = 2.86618 Å

Cathodically charged samples

C - 1 in 10 % H_2SO_4

No. 2631 at 25.0°C

Front		Back	
90.068	103.860	171.186	F = 0.45027
31.766	17.980	150.542	Θ = 80.7046°
			a = 2.86627 Å

No. 2632 at 25.0°C

Front		Back	
86.176	99.995	167.307	F = 0.45017
27.852	14.103	146.681	Θ = 80.7148°
			a = 2.86623 Å

C - 2 in 10 % H_2SO_4 (+ HgCl)

No. 2625 at 24.5°C

Front		Back	
91.382	105.240	182.450	F = 0.45058
33.154	19.288	151.923	Θ = 80.70138°
			a = 2.86619 Å
			(a_{25}=2.86621 Å)

No. 2627 at 24.5°C

Front		Back	
94.349	108.241	175.513	F = 0.45011
36.086	22.213	154.884	Θ = 80.7147°
			a = 2.86618 Å
			(a_{25}= 2.86620 Å)

ANALYSIS OF IRON IN ELECTROLYTE(*)

Washed distilled water (for specime) was joint to the electrolyte for the titration, and whole solution was checked whether total weight loss of the specimen went into solution. First, entire iron in solution was reduced with stannous chlorde and mercuric chloride, then 200 ml. of water, 10 ml. of 1:5 sulfuric acid, 5 ml. of 85 percent phosphoric acid and 6 to 8 drops of indicator (0.2 percent solution of sodium diphenylamine sulfonate in water) were added and titrated slowly with 0.1 N standard dichromate solution, stirring constantly, until the pure green color changed toward a gray-green. Then the dichromate was added very slowly, one drop at a time, until the first tinge of purple or violet-blue appeared.

Sample calculation:

amount of standard solution (0.09857 N $K_2Cr_2O_7$ solution) used for titration was 36.6 ml.

0.09857 x 36.60 x 55.58 = 0.2015 g of iron

BIBLIOGRAPHY

BIBLIOGRAPHY

1. Pfeil, L. B., Proc. Roy. Soc. A112, 182 (1926).

2. Welch, G. E., "Dissolution Rates of Aone-refined Iron and Steel in Hydrochloric and Sulfuric Acids and in Dosium Chloride Solutions", M. S. Thesis, Missouri School of Mines and Metallurgy, Rolla, Missouri (1963).

3. Straumanis, M. E. & Martin, R. L., Corrosion Science 5, 765, (1965).

4. Schaschl, E. & Marsh, G. A., Corrosion 13, 243t (1957).

5. Blake, P. D., Jordan, M. F. & Dumphrey, W. I., in "Hydrogen in Iron and Steel", p 76, Iron and Steel Inst., London, (1961).

6. Smith, D. P., "Hydrogen in Metals", p 44, Univ. of Chicago Press., (1948).

7. Sieverts, A., Kumbhaar, W. & Jurish, E., Z. Physik. Chem. 77, 591, (1911).

8. Martin, E., Arch. Eisenhüttenw. 3, 407, (1929).

9. Armbruster, M. H., J. Am. Chem. Soc. 65, 1043 (1943).

10. Hull, A. W., Phys. Rev. 10, 661 (1917).

11. Davey, W. P., Phys. Rev. 23, 292 (1924).

12. Blake, F. C., Phys. Rev. 26, 60 (1925).

13. Davey, W. P., Z. Krist. 63, 316 (1926).

14. Mayer, G., Z. Krist. 70, 383 (1929).

15. van Arkel, A. E. & Burgers, W. G., Z. Metallkunde 23 149 (1931).

16. Bradley, A. J. & Jay, A. H., Proc. Phys. Soc.(London) 44, 563 (1932).

17. Esser, H. & Müller, G., Arch. Eisenhüttenw. 7, 265 (1933)

18. Owen, E. A. & Yates, E. L., Phil. Mag. 15, 472 (1933).

19. Jette, E. R. & Foote, F., J. Chem. Phys. 3, 605 (1935).

20. Straumanis, M. E. & Ievins, A., Z. Physik. 98, 461 (1936).

21. Montoro, V., Metallurgia ital. 29, 8 (1937).

22. Hanawalt, J. D., Rinn, H. W. & Frevel, L. K., Ind. Eng. Chem., Anal. Ed. 10, 457 (1938).

23. Bergen, H., Ann. Physk. 39, 553 (1941).

24. Lu, S. S. & Chang, Y. L., Proc. Phys. Soc. (London) 53, 517 (1941).

25. Troiano, A. R. & MCGuire, F. T., Tr. A.S.M. 31, 340 (1943).

26. Thomas, D. E., J. Sci. Instr. 25, 440 (1948).

27. Kochanovska, A., Physica 15, 191 (1949).

28. Swanson, H. E., Fuyat, R. K. & Ugrinic, G. M., Nat'l. Bureau of Standards Circular 539, vol. IV, p 3 (1955).

29. Grønvold, F,, Haarldsen, H. & Vihovde, J., Acta Chem. Scand. 8, 1927 (1954).

30. Owen, E. A. & Williams, G. I., J. Sci. Instr. 31, 49 (1954).

31. Sutton, A. L. & Hume-Rothery, W., Phil. Mag. 46, 1295 (1955).

32. Basinski, Z. S., Hume-Rothery, W. & Sutton, A. L., Proc. Roy. Soc. A229, 459 (1955).

33. Gorton, A. T., Bitsianes, G. & Joseph, T. L., Tr. A.I. M.E. 233, 1520 (1965).

34. Heumann, T., Naturwiss. 32, 296 (1944).

35. Wever, F. & Pfarr, B., Mitt. K. W. Inst. Eisenforschg. 15, 137; Stahl u. Eisen 53, 991 (1933).

36. Baukloh, W. & Stromburg, W., Z. Metallkunde 29, 427 (1937).

37. Portevin, A., Chaudron, G. & Moreau, L., Compt. rend. 204, 1252 (1937).

38. Andrews, J. N. & Ubbelohde, A. R., Proc. Roy. Soc. A253, 6 (1959).

39. Tetelman, A. S., Wagner, C. N. J. & Robertson, W. D., Acta Metall. 9, 205 (1961).

40. Lihl, F., Arch. Metallkunde 1, 16 (1946).

41. Rawdon, H. S., Hidnert, P. & Tucker, W. A., Tr. A.S.M. 10, 233 (1926).

42. Plusquellec, J. Azou, P. & Bastien, P., Compt. rend. 244, 1195 (1957).

43. Tetelman, A. S., Wagner, C. N. J. & Robertson, W. D., Acta Metall. 9, 205 (1961).

44. Souder, W. & Hidnert, P., BS. Sci. pap. 21 , 524 (1926 - 27).

45. Ebert, E., Z. Physik 47, 712 (1928).

46. Austin, J. B. & Pierce, R. H. H. Jr., Tr. A. S. M. 22, 447 (1934).

47. Nix, F. C. & MacNair, D., Phys. Rev. 60, 597 (1941).

48. Lehr, P., Compt. rend. 242, 632 (1956).

49. "Metals Hnadsbook" vol. 1, p 1206, 8th. ed., Am. Soc. Metals, (1961).

50. "International Critical Tables" vol. II, p 456, McGraw Hill Book Co. N. Y. (1927).

51. Adcock, F. & Bristow, C. A., Proc. Roy. Soc. A153, 172 (1936).

52. Cleaves, H. E. & Heigel, J. M., J. Research Nat. Bur. Stand. 28, 643 (1942).

53. Ribbeck, F., Z. Physik 38, 772 (1926); 39, 787 (1926).

54. Jeager, F. M., Rosenbohm, E. & Zuithoff, A. J., Recueil des Travaux Chemiques des Pays-Bas 57, 1313 (1938).

55. Pallister, P. R., J. Iron and Steel Inst. 161, 87 (1949).

56. Bäcklund, N. G., Phys. Chem. Solids 20, 1 (1961).

57. Belloc, G., Compt. rend. 136, 500 (1903).

58. Kleine, H., Z. Physik 33, 391 (1925).

59. Franzini, T., Rend. r. ist. Lombardo [2] 64, 709 (1931).

60. Müller, F., Dissertn., Leipzig (Lab. A. Sieverts) (1911), "Gas in Metals, Absorption of Hydrogen etc. and effects on electrical resistivity"; Internal. Z. Metallog. 3, 37 (1913).

61. Johnson, W. H., Proc. Roy. Soc. (London) 23, 168 (1875).

62. Kimura, S., Proc. Roy. Soc. (Edinburgh) 20, 203 (1893).

63. Harding, E. A. & Smith, D. P., J. Am. Chem. Soc. 40, 1508 (1918).

64, Grave, E., Z. Physik. Chem. 77, 513 (1911).

65. Portevin, A., Compt. rend. 204, 1252 (1937).

66. Van Ooijen, D. J. & Fast, J. D., Acta Met. 11, 211 (1963).

67. Speller, F. N., "Corrosion Causes and Prevention", 1st. ed., p 79, McGraw Hill, N. Y. (1926).

68. Engell, H. J., Arch. Eisenhüttenw. 26, 393 (1955).

69. Buck, W. R. & Leidheiser, H. Jr., Z. Elektrochem. 59, 748 (1955).

70. Buck, W. R. & Leidheiser, H. Jr., J. Electrochem. Soc. 104, 474 (1957).

71. Marsh, G. A. & Schaschl, E., J. Electrochem. Soc. 107, 960 (1960).

72. Heffelfinger, R. E., Chase, D. L., Rengstofrff, G. W. P. & Henery, W. M., Analytical Chem. 30, 112 (1958).

73. Brenner, S. S., Acta Met. 4, 62 (1956).

74. Wayman, C.M., J. Appl. Phys. 32, 844 (1961).

75. Martin, J. F., Takacs, R. C., Rapp, R. & Melnick, L. M.,

Tr. A.I.M.E. 230, 107 (1964).

76. Johnson, E. W. & Hill, M. L., Acta Met. 3, 99 (1955).

77. Johnson, E. W. & Hill, M. L., Tr. A.I.M.E. 218, 1104 (1960).

78. Straumanis, M. E., in Clark: "Encyclopedia of X-rays and Gamma Rays", p 735, Reinhold Publishing Corp. N. Y. (1963).

79. Straumanis, M. E., Am. Mineralogist 37, 48 (1952).

80. Straumanis, M. E., Am. Mineralogist 38, 669 (1953).

81. Mellor, J. W., "Higher Mathematics for Studenst of Chemistry and Physics with Special Reference to Practical Work", 4th. ed. p 326, Dover Publications, Inc., (1955).

82. Morlet, J. G., Johnson, H. H. & Troiano, A. R., J. Iron and Steel Inst. 189, 37 (1958).

83. Riad, S. M., "Lattice Parameters, Thermal Expansion Coefficients, Densities, and Perfection in Silver and in the alpha-phase of the Silver-Indium System", Ph.D. dissertation, University of Missouri, Rolla, Missouri (1964).

84. Pauling, L., J. Am. Chem. Soc. 69, 542 (1947).

85. Bearden, J. A., Henins, A., Sauder, C. & Thomsen, J. S., Pys. Rev. 135, A899 (1964).

86. Cohen, E. R. & DuMond, J. W. M., Rev. Modern Phys. 37, 537 (1965).

ACKNOWLEDGEMENT

The author wishes to express his sincere appreciation to Dr. M. E. Straumanis, Research Professor of Materials and Professor of Metallurgical Engineering, for his guidance and assistance during this research work, and to Dr. W. J. James, Professor of Chemistry and Director of the Graduate Center for Materials Research, U. M. R., and to Dr. H. P. Leighly, Associate Professor of Metallurgical Engineering, for their valuable suggestions and discussions in this investigation.

As a foreign student the author appreciates sincerely the generosity and wonderful hospitality of this great American institution which allowed him to study on the campus and is indebted for the financial assistance (from O N R) without which it would have been impossible to pursue this study.

Sincere thanks are due to the various members of the faculty who gave of their time in assisting with this work.

VITA

The author was born on November 14, 1936 in PyongYang, Korea. He received his B.S. in metallurgical engineering in March, 1958 from the College of Engineering, Seoul National University. After his graduation, he worked as a research assistant at the Scientific Research Institute, Seoul, Korea from 1958 to 1961.

He has been enrolled in the Graduate School of the Missouri School of Mines and Metallurgy, sine January, 1962.

In July, 1963, he received the M.S. degree in metallurgical engineering from this school.